5-3-2019

Forest Aboveground Biomass Estimation Using Multi-Source Remote Sensing Data in Temperate Forests

Siqi Li

sli151@syr.edu

FOREST ABOVEGROUND BIOMASS ESTIMATION USING MULTI-SOURCE

REMOTE SENSING DATA IN TEMPERATE FORESTS

by

Siqi Li

A dissertation
submitted in partial fulfillment
of the requirement for the
Doctor of Philosophy Degree
State University of New York
College of Environmental Science and Forestry
Syracuse, New York
May 2019

Department of Environmental Resources Engineering

Approved by:
Lindi J. Quackenbush, Major Professor
Donald J. Leopold, Chair of the Examining Committee
Lindi J. Quackenbush, Department Chair
Gary M. Scott, Director of Division of Engineering
S. Scott Shannon, Dean, The Graduate School

Acknowledgements

I feel deeply grateful for all the people who made this dissertation possible. I would not stand at this point if I did not have support from my committee members, my friends and family.

I would like to first thank my advisor, Dr. Lindi Quackenbush, for leading me to this program and giving me the opportunity to work closely with her. Her passion, enthusiasm and energy for research and teaching are incredible. I have admired her since the first day we met. I am forever grateful to her for everything she has done for me. Secondly, I would like to thank my MPS advisor, Dr. Lianjun Zhang, for his support in my two degrees. I also really appreciate the input from Dr. Stephen Stehman, Dr. Colin Beier, Dr. Jungho Im and Dr. Bahram Salehi in my research.

There are moments that make life change course; getting accepted by ESF is definitely one. However, this was the seed planted by other two important advisors in my life, Dr. Yinghui Zhao and Dr. Zhen Zhen, who had inspired and encouraged me to pursue a Ph.D. degree in US.

I would not be who I am today without the steady and unconditional love of my parents, grandparents, fiancé and many other family members. Their boundless love has given me the confidence to do what I want to do through knowing they were rooting for me. Thanks for allowing me the freedom to pursue my dreams.

Thanks to ESF and Syracuse, I will never forget the wonderful life here!

Table of Contents

List of Tables

List of Figures

Abstract

S. Li. Forest Aboveground Biomass Estimation Using Multi-Source Remote Sensing Data in Temperate Forests, 145 pages, 21 tables, 19 figures, 2019. APA style guide used.

Forests are a crucial part of global ecosystems. Accurately estimating aboveground biomass (AGB) is important in many applications including monitoring carbon stocks, investigating forest degradation, and designing sustainable forest management strategies. Remote sensing techniques have proved to be a cost-effective way to estimate forest AGB with timely and repeated observations. This dissertation investigated the use of multiple remotely sensed datasets for forest AGB estimation in temperate forests.

We compared the performance of Landsat and lidar data—individually and fused—for estimating AGB using multiple regression models (MLR), Random Forest (RF) and Geographically Weight Regression (GWR). Our approach showed MLR performed similarly to GWR and both were better than RF. Integration of lidar and Landsat inputs outperformed either data source alone. However, although lidar provides valuable three-dimensional forest structure information, acquiring comprehensive lidar coverage is often cost prohibitive. Thus we developed a lidar sampling framework to support AGB estimation from Landsat images. We compared two sampling strategies—systematic and classification-based—and found that the systematic sampling selection method was highly dependent on site conditions and had higher model variability. The classification-based lidar sampling strategy was easy to apply and provides a framework that is readily transferable to new study sites.

The performance of Sentinel-2 and Landsat 8 data for quantifying AGB in a temperate forest using RF regression was also tested. We modeled AGB using three datasets: Sentinel-2, Landsat 8, and a pseudo dataset that retained the spatial resolution of Sentinel-2 but only the spectral bands that matched those on Landsat 8. We found that while RF model parameters impact model outcomes, it is more important to focus attention on variable selection. Our results showed that the incorporation of red-edge information increased AGB estimation accuracy by approximately 6%. The additional spatial resolution improved accuracy by approximately 3%. The variable importance ranks in the RF regression model showed that in addition to the red-edge bands, the shortwave infrared bands were important either individually (in the Sentinel-2 model) or in band indices. With the growing availability of remote sensing datasets, developing tools to appropriately and efficiently apply remote sensing data is increasingly important.

Key Words: regression; Random Forest; Geographically Weighed Regression; data integration; systematic sampling; classification-based sampling; forest types;

S. Li

Candidate for the degree of Doctor of Philosophy, May 2019

Lindi J. Quackenbush, Ph.D.

Department of Environmental Resources Engineering

Division of Engineering

State University of New York College of Environmental Science and Forestry,

Syracuse, New York

1. Dissertation Introduction

1.1. Introduction

1.1.1. Background

Forests provide critical resources and are one of the most important ecosystems covering the Earth's land surface. However, human and natural actions have stressed forests across the globe. Disturbance of natural ecosystems can contribute to climate change, decrease biological diversity, disturb hydrological cycles, and cause soil erosion and degradation (Singh et al., 2018). People have recognized the need to protect forest ecosystems and maintain sustainable development (Almeida et al., 2019). Sustainable and effective forest management requires accurate, consistent and timely forest monitoring.

Forest aboveground biomass (AGB) is a fundamental parameter for describing the structure and function of forest ecosystems (Li et al., 2019). AGB has been identified as an essential biodiversity variable to measure ecosystem function (Pettorelli et al., 2016). Many forest ecosystem processes are reflected in changes of AGB value, thus AGB is often used to monitor forest ecosystem processes. Accurate estimation of AGB is indicative of the extent to which forests contribute to the global carbon budget and can reduce uncertainty in understanding the quantity and distribution of terrestrial carbon stocks.

1.1.2. AGB estimation techniques

Forest AGB has been used to address various technical and scientific questions, including estimating forest productivity and monitoring the global carbon cycle over time (Viana et al., 2012). Traditional forest inventories can provide accurate forest AGB estimation by measuring the dry weight of trees or applying measured tree height or diameter at breast height to biomass

allometric equations (Basuki et al., 2009; Djomo et al., 2010; Nam et al., 2016). However, both methods are laborious, time consuming, and practical only for local scale measurements. Such approaches are also complicated by the necessity to gain physical access for field measurements. Remote sensing technologies have long been applied to estimate forest attributes (Cohen and Spies, 1992). With the increasing availability of diverse remotely sensed datasets, studies have explored AGB estimation using medium- and high-spatial resolution optical imagery (Cohen et al., 2003; Meng et al., 2009), radar (Boudreau et al., 2008), and light detection and ranging (lidar) data (Li et al., 2015).

The Landsat satellites have been one of the most popular remote sensing datasets for AGB estimation. With open and free access to the digital data archive, Landsat satellites have provided continuous coverage of most of the globe since the 1980s. Numerous studies have proved the feasibility of Landsat data for AGB estimation (Wang et al., 2018; Zheng et al., 2004). The more recently available Sentinel-2 satellites have similar access with improved spatial, spectral and temporal resolutions and offer great potential to improve forest AGB estimates. The first Sentinel-2 sensor was launched by the European Space Agency in June 2015 with 13 spectral bands. Sentinel-2 includes red-edge bands not available on any of the Landsat sensors. The red-edge bands characterize the sharp increase in vegetation reflectance and collecting data in this portion of the spectrum has been demonstrated to improve the accuracy of AGB estimation (Dang et al., 2019). However, one of the main drawbacks of using passive remote sensing data, such as Landsat or Sentinel, is a well-documented saturation problem. The problem relates to the fact that indices derived from passive sources tend to asymptotically approach a saturation level after reaching a certain biomass density (Chi et al., 2017; Knapp et al., 2018; Lumbierres et al., 2017; O. Mutanga and Skidmore, 2004; Vafaei et al., 2018).

An alternative to passive data sources are the use of active sensors such as lidar and radar. Lidar data can be used to characterize vertical forest information, which is a critical variable for AGB estimation. Many studies have also reported that lidar can estimate AGB without the saturation problem faced by passive sources (Luo et al., 2019; Sun et al., 2019; Zhao and Popescu, 2009). However, compared with passive optical remote sensing data, the cost and volume of lidar data tends to be higher for the same extent. The cost of lidar data acquisition is influenced by factors such as the location, frequency, and point density. Reducing lidar point density or sampling through lidar transects can reduce budget demands as well as keep the data volume manageable. Several studies have investigated the relationship between lidar point density and forest attribute estimation and reported that reliable accuracy can be achieved with relatively low lidar point density (Watt et al., 2014; Singh et al., 2015; Singh et al., 2016). Reducing lidar data coverage has also been explored using different sampling strategies with promising results (Hudak et al., 2002). The challenge is that the optimal lidar transect coverage reported varies across studies with no specifications about the ideal transect design clearly defined. While transects are often selected with equal intervals, some studies used auxiliary information to subjectively select lidar transects. In most situations these factors—e.g. sampling unit, sampling direction, transect coverage and transect interval—cannot be concurrently controlled due to limitations in data, time, or human resources. Exploring the importance of these different factors, as well as the interaction between them, can help people to make better choices in order to optimize AGB estimation.

1.1.3. Remote sensing data fusion

Lidar has proved to be the most powerful single sensor for estimating many forest variables (Gonzalez et al., 2010), such as canopy height (Hyde et al., 2006), biomass (Cao et al.,

2019) and vegetation height (Nie et al., 2018). However, optical sensors have advantages in terms of spatial coverage and availability. Fusion of multiple data types can harness the spectral, spatial, and temporal advantages of different data sources. Data fusion can also improve information interpretation and reduce uncertainty compared to using any source dataset independently (Li et al., 2016; Lu et al., 2019; Solberg et al., 1994). Thus, the fusion of lidar and Landsat has been adopted by many researchers (Xu et al., 2018). Data fusion has been applied to various applications including object detection and delineation (Heinzel et al., 2008; Kim et al., 2010), change detection (Trinder and Salah, 2012), image classification (Hartling et al., 2019), and forest characterization (Vogeler and Cohen, 2016). Multi-sensor fusion has demonstrated better performance than using single sensor data in numerous forest variable estimation studies (Singh et al., 2012; Hyde et al., 2006).

1.1.4. Statistical methods

Statistical models applied to relate field forest attribute observations and remotely sensed data including parametric and non-parametric models. The most frequently used methods for estimating AGB include multiple linear regression models and machine learning algorithms. Linear regression models assume residuals are uncorrelated, which is inappropriate when considering the spatial dependence of forest variables. Machine learning algorithms have the ability to learn and build estimation models from training data. The random forest (RF) algorithm proposed by Breiman (2001) is one of most commonly used machine learning algorithms. It can be applied for both classification and regression and has several distinct advantages. RF can be used to rank and select important predictor variables, generate relationship models between forest attributes and predictor variables, and apply models to map

forest attributes. RF is efficient in dealing with large input datasets while requiring few parameters (Shao et al., 2015; Belgiu and Drăguţ, 2016).

A weakness of multiple linear regression models is that important local variations may not be reflected. Geographically weighted regression (GWR) is an extension of multiple linear regression that allows coefficients for environmental covariates to vary at different locations (Kumar et al., 2012). Localized coefficients of GWR are based on weighting observations around a sample point using a distance decay function. The closer the data point is to the sample point, the greater the weight applied. GWR is a powerful approach for modeling spatially heterogeneous processes. Zhang and Shi (2004) modeled forest growth using GWR and concluded that the GWR model performed better than a traditional ordinary least-squares model. GWR provides useful information about the impact of surrounding environmental factors and neighboring competitors on tree growth variation.

1.2. Hypotheses

This dissertation investigates the use of remotely sensed data in forest aboveground biomass estimation. This study explores the value of lidar and Landsat fusion for estimating AGB using different methods and in different forest conditions. It investigates the potential for developing a protocol for using lidar samples to support AGB estimation using Landsat inputs. The study also explores the utility of the enhanced spectral and spatial characteristics of Sentinel-2 data for AGB estimation. In exploring these broad objectives, the following research hypotheses are addressed in this study:

1. Lidar and Landsat data fusion enhances AGB estimation compared to single source approaches.

2. AGB estimation quality varies with application of multiple linear regression, RF and GWR approaches.

3. Forest type influences the performance of AGB estimation using lidar and Landsat inputs.

4. Lidar sampling can capture the majority of AGB variation explained by full lidar coverage but stability of AGB estimation is influenced by lidar sampling strategy used.

5. The increased spectral and spatial resolution of Sentinel-2 improves AGB estimation outcomes compared to Landsat 8.

This dissertation uses a manuscript format, where Chapters 2, 3 and 4 are presented as independent manuscripts. Research hypotheses 1, 2 and 3 are explored in Chapter 2 of this dissertation. Research hypothesis 4 is explored in Chapter 3 and research hypothesis 5 is explored in Chapter 4 of this dissertation.

1.3. Reference

Almeida, D.R.A.D., Stark, S.C., Shao, G., Schietti, J., Nelson, B.W., Silva, C.A., Gorgens, E.B., Valbuena, R., Papa, D.D.A. & Brancalion, P.H.S. (2019). Optimizing the remote detection of tropical rainforest structure with airborne lidar: leaf area profile sensitivity to pulse density and spatial sampling. *Remote Sensing*, 11(1), 92. https://doi.org/10.3390/rs11010092

Breiman, L. (2001). Random forests. *Machine Learning*, 45(1), 5–32. https://doi.org/10.1023/A:1010933404324

Cao, L., Liu, H., Fu, X., Zhang, Z., Shen, X., & Ruan, H. (2019). Comparison of UAV LiDAR and Digital Aerial Photogrammetry Point Clouds for Estimating Forest Structural Attributes in Subtropical Planted Forests. *Forests*, 10(2), 145. https://doi.org/10.3390/f10020145

Cohen, W. B., & Spies, T. A. (1992). Estimating structural attributes of Douglas-fir/western hemlock forest stands from Landsat and SPOT imagery. *Remote Sensing of Environment*, 41(1), 1–17. https://doi.org/10.1016/0034-4257(92)90056-P

Dang, A. T. N., Nandy, S., Srinet, R., Luong, N. V., Ghosh, S., & Kumar, A. S. (2019). Forest aboveground biomass estimation using machine learning regression algorithm in Yok Don National Park, Vietnam. *Ecological Informatics*, 50, 24–32. https://doi.org/10.1016/j.ecoinf.2018.12.010

Gonzalez, P., Asner, G. P., Battles, J. J., Lefsky, M. A., Waring, K. M., & Palace, M. (2010). Forest carbon densities and uncertainties from Lidar, QuickBird, and field measurements in California. *Remote Sensing of Environment*, 114(7), 1561–1575. https://doi.org/10.1016/j.rse.2010.02.011

Hartling, S., Sagan, V., Sidike, P., Maimaitijiang, M., & Carron, J. (2019). Urban Tree Species Classification Using a WorldView-2/3 and LiDAR Data Fusion Approach and Deep Learning. *Sensors*, 19(6), 1284. https://doi.org/10.3390/s19061284

Heinzel, J. N., Weinacker, H., & Koch, B. (2008). Full automatic detection of tree species based on delineated single tree crowns–a data fusion approach for airborne laser scanning data and aerial photographs. *Proceedings of SilviLaser*, 2008(8th).

Hudak, A. T., Lefsky, M. A., Cohen, W. B., & Berterretche, M. (2002). Integration of lidar and Landsat ETM+ data for estimating and mapping forest canopy height. *Remote Sensing of Environment*, 82(2–3), 397–416. https://doi.org/10.1016/S0034-4257(02)00056-1

Hyde, P., Dubayah, R., Walker, W., Blair, J. B., Hofton, M., & Hunsaker, C. (2006). Mapping forest structure for wildlife habitat analysis using multi-sensor (LiDAR, SAR/InSAR, ETM+, Quickbird) synergy. *Remote Sensing of Environment*, 102(1–2), 63–73. https://doi.org/10.1016/j.rse.2006.01.021

Kim, S.R., Kwak, D.A., Son, Y., Bae, S.W., Kim, C. & Yoo, S. (2010). Estimation of carbon storage based on individual tree detection in Pinus densiflora stands using a fusion of aerial photography and LiDAR data. *Science China Life Sciences*, 53(7), 885–897.https://doi.org/ 10.1007/s11427-010-4017-1

Li, C., Li, Y., & Li, M. (2019). Improving Forest Aboveground Biomass (AGB) Estimation by Incorporating Crown Density and Using Landsat 8 OLI Images of a Subtropical Forest in Western Hunan in Central China. *Forests*, 10(2), 104. https://doi.org/10.3390/f10020104

Li, W., Niu, Z., Chen, H., Li, D., Wu, M., & Zhao, W. (2016). Remote estimation of canopy height and aboveground biomass of maize using high-resolution stereo images from a

low-cost unmanned aerial vehicle system. *Ecological Indicators*, 67, 637–648. https://doi.org/10.1016/j.ecolind.2016.03.036

Lu, N., Zhou, J., Han, Z., Li, D., Cao, Q., Yao, X., Tian, Y., Zhu, Y., Cao, W. & Cheng, T. (2019). Improved estimation of aboveground biomass in wheat from RGB imagery and point cloud data acquired with a low-cost unmanned aerial vehicle system. *Plant Methods*, 15(1), 17.https://doi.org/10.1186/s13007-019-0402-3

Luo, S., Wang, C., Xi, X., Nie, S., Fan, X., Chen, H., Yang, X., Peng, D., Lin, Y. & Zhou, G. (2019). Combining hyperspectral imagery and LiDAR pseudo-waveform for predicting crop LAI, canopy height and above-ground biomass. *Ecological Indicators*, 102, 801–812. https://doi.org/10.1016/j.ecolind.2019.03.011

Nie, S., Wang, C., Xi, X., Luo, S., Li, S., & Tian, J. (2018). Estimating the height of wetland vegetation using airborne discrete-return LiDAR data. *Optik*, 154, 267–274. https://doi.org/ 10.1016/j.ijleo.2017.10.016

Pettorelli, N., Wegmann, M., Skidmore, A., Mücher, S., Dawson, T.P., Fernandez, M., Lucas, R., Schaepman, M.E., Wang, T., O'Connor, B. & Jongman, R.H. (2016). Framing the concept of satellite remote sensing essential biodiversity variables: challenges and future directions. *Remote Sensing in Ecology and Conservation*, 2(3), 122–131.https://doi.org/ 10.1002/rse2.15

Singh, K. K., Vogler, J. B., Shoemaker, D. A., & Meentemeyer, R. K. (2012). LiDAR-Landsat data fusion for large-area assessment of urban land cover: Balancing spatial resolution, data volume and mapping accuracy. *ISPRS Journal of Photogrammetry and Remote Sensing*, 74, 110–121. https://doi.org/10.1016/j.isprsjprs.2012.09.009

Singh, M., Evans, D., Chevance, J.-B., Tan, B. S., Wiggins, N., Kong, L., & Sakhoeun, S. (2018). Evaluating the ability of community-protected forests in Cambodia to prevent deforestation and degradation using temporal remote sensing data. *Ecology and Evolution*, 8(20), 10175–10191. https://doi.org/10.1002/ece3.4492

Solberg, A. H. S., Jain, A. K., & Taxt, T. (1994). Multisource classification of remotely sensed data: fusion of Landt TM and SAR images. *IEEE Transactions on Geoscience and Remote Sensing*, 32(4), 768–778.http://doi.org/10.1109/36.298006

Sun, X., Li, G., Wang, M., & Fan, Z. (2019). Analyzing the Uncertainty of Estimating Forest Aboveground Biomass Using Optical Imagery and Spaceborne LiDAR. *Remote Sensing*, 11(6), 722.https://doi.org/10.3390/rs11060722

Trinder, J. C., & Salah, M. (2012). Aerial images and lidar data fusion for disaster change detection. ISPRS Annals of Photogrammetry, *Remote Sensing and Spatial Information Sciences*, I–4, 227–232. https://doi.org/10.5194/isprsannals-I-4-227-2012

Vogeler, J. C., & Cohen, W. B. (2016). A review of the role of active remote sensing and data fusion for characterizing forest in wildlife habitat models. *Revista de Teledetección,* (45), 1. https://doi.org/10.4995/raet.2016.3981

Wang, M., Sun, R., & Xiao, Z. (2018). Estimation of Forest Canopy Height and Aboveground Biomass from Spaceborne LiDAR and Landsat Imageries in Maryland. *Remote Sensing*, 10(2), 344. https://doi.org/10.3390/rs10020344

Xu, Z., Guan, K., Casler, N., Peng, B., & Wang, S. (2018). A 3D convolutional neural network method for land cover classification using LiDAR and multi-temporal Landsat imagery. *ISPRS Journal of Photogrammetry and Remote Sensing*, 144, 423–434. https://doi.org/10.1016/j.isprsjprs.2018.08.005

Zhao, K., & Popescu, S. (2009). Lidar-based mapping of leaf area index and its use for validating GLOBCARBON satellite LAI product in a temperate forest of the southern USA. *Remote Sensing of Environment*, 113(8), 1628–1645. https://doi.org/10.1016/j.rse.2009.03.006

Zheng, D., Rademacher, J., Chen, J., Crow, T., Bresee, M., Le Moine, J., & Ryu, S.R. (2004). Estimating aboveground biomass using Landsat 7 ETM+ data across a managed landscape in northern Wisconsin, USA. *Remote Sensing of Environment*, 93(3), 402–411. https://doi.org/10.1016/j.rse.2004.08.008

2. Manuscript 1: The influence of forest type and biomass range on forest aboveground biomass estimation from integrated airborne lidar and Landsat data

2.1. Abstract

Quantifying forest aboveground biomass (AGB) is crucial for understanding the role of forests in the global carbon cycle. Light detection and ranging (lidar) data provides accurate measurement of forest structure in the vertical plane; however, since current airborne lidar datasets are often practically limited in terms of spatial coverage lidar data is often supplemented by more extensively distributed passive imagery. We compared the performance of Landsat, lidar, an integration of Landsat and lidar for estimating AGB using multiple regression models (MLR), Random Forest (RF) and Geographically Weight Regression (GWR) in Huntington Wildlife Forest in Central New York State. Our approach showed MLR performed similarly to GWR and both were better than RF. We also explored the performance of AGB estimation from different data sources under different forest type and AGB range conditions. Our study found both factors impacted model accuracy. AGB estimation using Landsat data performed better in hardwood forest compared to softwood forest, which was contrary to using only lidar data. This study demonstrated the importance of forest type and AGB range on AGB estimation and suggests pre-classification of data based on forest type and AGB range may enhance AGB estimation results.

Keywords: Multiple Linear Regression; Random Forest; Geographically Weighed Regression; data integration; forest measurement

2.2.   Introduction

Concerns about global climate change require understanding of the dynamic between atmospheric and terrestrial carbon cycles. Forest ecosystems play an important role in the exchange of carbon between the atmosphere and the land surface. Aboveground biomass (AGB, in Mg ha^{-1}) is the total dry weight of biological material above the ground in an area (Hu et al., 2016). Characterizing aboveground biomass is crucial for providing essential information to advance our understanding of the global carbon cycle and climate change. For example, forest AGB has been used to study deforestation and forest degradation, land cover change, invasive species, and emission of greenhouse gases (Chen et al., 2016; Houghton et al., 2008; Shao et al., 2018; Wulder et al., 2012). Understanding AGB can inform strategic forest management plans and strengthen policy making. Therefore, it is necessary to explore efficient approaches to estimate and monitor AGB distribution.

Forest inventory to quantify AGB traditionally involved either destructive methods or application of allometric equations (Lu, 2006). Destructive methods require cutting, drying and weighing each tree being inventoried (Kankare et al., 2013). Allometric equations are used to compute AGB based on the measurement of either tree height or diameter at breast height (DBH) from each tree (Chave et al., 2014; Clark and Kellner, 2012). Compared with traditional forest inventory, remote sensing technology has the potential to generate AGB using non-destructive, efficient and repetitive techniques with relatively low cost (Dassot et al., 2011; Gonçalves et al., 2017; Lumbierres et al., 2017). For example, Landsat 8 covers the entire globe every 16 days and data is currently available for download at no cost (https://earthexplorer.usgs.gov/). However, remote sensing technology cannot quantify AGB directly. Instead, AGB is estimated based on

statistical models applied to image-derived variables. Consequently, the performance of remote sensing data in estimation of AGB is highly dependent on the characteristics of the data and the performance of the models applied.

As an active remote sensing technology, lidar determines the distance between a sensor and the reflecting surface based on travel time of an emitted laser pulse (Ucar et al., 2018). Multiple echo sensors can detect several returns for one emitted pulse, which allows detection of tree crowns, leaves at different levels, branches and the underlying ground (Jones and Vaughan, 2010). Through this process, lidar enables characterization of three-dimensional forest structure. Lidar has been successfully applied to estimate tree height (Kwak et al., 2007; Popescu et al., 2002), crown dimension (Falkowski et al., 2006), stem counts (Ene et al., 2012), tree leaf area (Roberts et al., 2005), canopy clumping (García et al., 2015), and tree volume (Takagi et al., 2015; Tesfamichael et al., 2010), and it is regarded by many as the most accurate remote sensing approach for AGB estimation (Ahmed et al., 2015; Feng et al., 2017; Hudak et al., 2002; Korhonen et al., 2011; Riaño et al., 2004; Tang et al., 2014). However, despite the appealing accuracy achieved by lidar for local scales, there are practical limitations that prohibit the application of lidar at regional or continental scales (Galidaki et al., 2017; Liu et al., 2017; Ma et al., 2017; Wang et al., 2016). Moreover, although acquisition of lidar data has been increasing steadily over the past decade, lidar collection is often focused on specific areas of interest rather than systematic coverage of large extents.

To address information needs in forests that lack comprehensive or up-to-date lidar or inventory data, optical remote sensing data can be applied. Optical sensors capture spectral responses of forest canopies, which can be used to derive useful information about the physical

and biological characteristics of the vegetation. Compared to lidar data, multispectral optical remote sensing sensors typically have advantages in terms of both spectral and temporal resolutions. For example, with moderate spatial resolution, the sensors onboard the Landsat series of satellites have collected spectral information from visible to thermal wavelengths with a 16-day repeat coverage of the surface of earth since 1984. Landsat data has been successfully applied to estimate forest cover change (Coppin and Bauer, 1994), deforestation and forest degradation (Margono et al., 2012), timber volume (Trotter et al., 1997), and AGB (Powell et al., 2010). However, the data acquired from optical sensor data are often compromised by factors such as clouds and shadow, weather, topography, forest complexity, and saturation effects at low and high biomass levels (Goldbergs et al., 2018; Lu et al., 2012; Ma et al., 2017).

Integration of multiple data sources can harness the spectral, spatial, and temporal advantages of different sources of data as well as overcome shortcomings of any single data source. Data integration has been applied to various areas including object detection and delineation (Heinzel et al., 2008; Kim et al., 2010), change detection (Trinder and Salah, 2012), classification (Dalponte et al., 2008), and decision making (Vogeler and Cohen, 2016). Lidar and multispectral Landsat data can be integrated to extrapolate lidar-based forest attributes to broader scales through the addition of Landsat's multispectral information and repetitive data collection. Singh et al. (2012) found fusing lidar and Thematic Mapper (TM) data achieved land cover classification accuracy of 87.2%, which outperformed Landsat TM or lidar data alone by 8% and 32%, respectively.

In addition to using appropriate data sources, algorithm selection for establishing biomass estimation models is also critical. Multiple linear regression (MLR) is the most commonly used

algorithm for AGB estimation (Deo et al., 2017; Ediriweera et al., 2014; Hyde et al., 2006; Popescu et al., 2004; Zheng et al., 2007). For MLR, plot level (Boudreau et al., 2008; Deo et al., 2017) biomass typically serves as the dependent variable with both lidar (Cao et al., 2014; Li et al., 2017) and Landsat (Karlson et al., 2015; Zheng et al., 2004) derived factors as predictors. Stepwise variable selection is often used in MLR to select the remote sensing derived variables that best represent AGB while avoiding multicollinearity (Moser et al., 2017). Researchers also report using other approaches to estimate AGB such as machine learning (Karlson et al., 2015; Li et al., 2017; Urbazaev et al., 2018) and Geographically Weighted Regression (GWR). The nonparametric machine learning Random Forest (RF) algorithm has received considerable attention due to its ability to handle imbalanced datasets and its insensitivity to noise (Adam et al., 2014; Mutanga et al., 2012). GWR incorporates spatial location of input data into the algorithm and is a powerful tool for addressing spatial heterogeneity (Benitez et al., 2016). Fassnacht et al. (2014) compared the impact of data sources and prediction method on AGB estimation and found data sources had a larger impact on the outcomes than prediction methods. Previous prediction method comparison often uses one data source (Gagliasso et al., 2014; Propastin, 2012; Zhang and Shi, 2004). In this study, we compared prediction methods using both single data source and data integration.

Despite the fact that various remote sensing data have been applied and compared in the field of AGB estimation, the impact of site condition on estimation accuracy has been minimally reported. The goal of this study was to compare the impact of forest type and AGB range on the performance of lidar and Landsat datasets for AGB estimation. This study developed MLR, RF and GWR models for forest AGB estimation using Landsat and lidar data, both independently and in an integrated approach. More specifically, we aimed to: (1) compare model performance

16

of AGB estimation using Landsat data, airborne lidar data and the integration of the two data sources; (2) examine the advantages and drawbacks of models when applied to different forest stand types, i.e., hardwood, softwood and mixed forests; and (3) evaluate the applicability of the models for different AGB ranges.

2.3. Materials and methods

2.3.1. Study area

The study area for the project was the Huntington Wildlife Forest (HWF) in the central Adirondacks in northern New York State, which is managed by the State University of New York College of Environmental Science and Forestry (SUNY-ESF; 43°58'19" N, 74°13'18" W; Figure 2-1). HWF covers approximately 60 km^2 with mountainous topography and an elevation range from 466 m to 859 m. HWF has a mean annual temperature of 4.4°C and mean annual precipitation of 1010 mm (Shepard et al., 1989). HWF contains both undisturbed natural communities and managed forest stands. The forest is composed of hardwood, mixed, and softwood stands with major species being American beech (*Fagus grandifolia*), yellow birch (*Betula alleghaniensis* Britt.), sugar maple (*Acer saccharum* Marshall.), red spruce (*Picea rubens* Sarg.), red maple (*Acer rubrum* L.*)* and hemlock (*Tsuga* spp.).
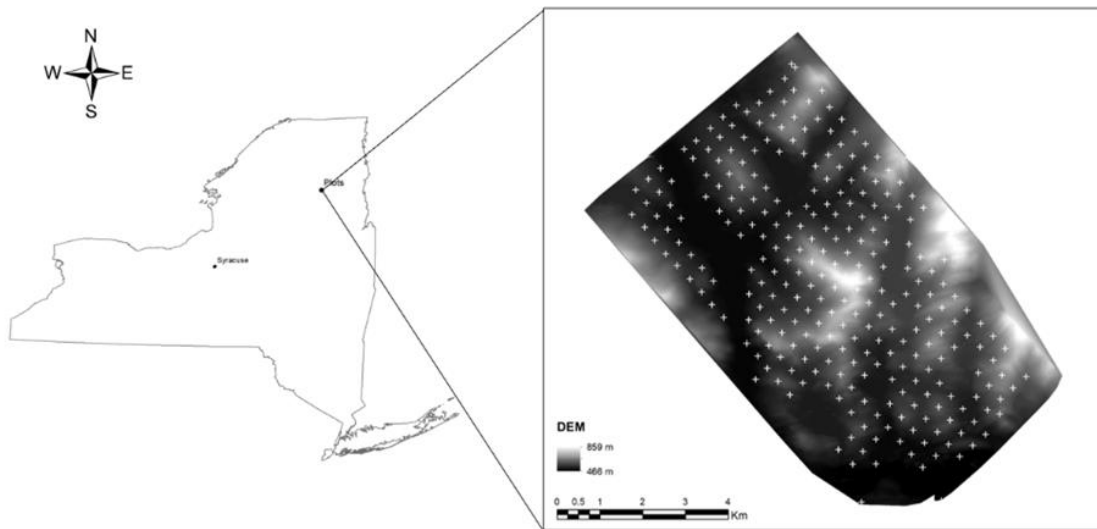
Figure 2-1. Location of Huntington Wildlife Forest in New York State. The figure shows the distribution of 270 forest inventory plots overlaid on a lidar generated DEM.

2.3.2. Field measurements

SUNY ESF maintains continuous forest inventory (CFI) plots within HWF, with comprehensive plot data last collected during the summer of 2011. The center of each CFI plot was located using a global positioning system (GPS) receiver. All trees with diameter at breast height (DBH) of 11.7 cm or greater were measured on a fixed circular plot with radius approximately 16 m. Information recorded for each plot included tree species, DBH, and tree location relative to plot center. Based on the field observations, tree-level AGB was calculated using species-specific DBH allometric equations from Jenkins et al. (Jenkins et al., 2003). Plot-level AGB was then determined by summing the AGB for each tree within a plot and dividing by the plot area. Data from all plots in this study were applied to train the model. Table 2-1 presents a summary of descriptive statistics for plot level AGB in HWF. The unit for plot-level AGB is megagrams per ha (Mg ha^{-1}).

Table 2-1. Summary of descriptive statistics for plot level AGB in HWF (units: Mg ha^{-1}).

Plot Count	Mean	Median	Variance	Minimum	Maximum
270	186.6	186.3	6808.0	0.9	440.3

The United Nations Economic Commission for Europe (UNECE) Food and Agriculture Organization (FAO; UNECE/FAO, 2000) defines mixed forests as stands where neither broadleaved nor coniferous trees account for more than 75% of the tree crown area. Since we collected DBH and used that to determine AGB, we modified the UNECE/FAO approach and defined a plot as hardwood if the total hardwood AGB was more than 75% of total AGB of that plot. Softwood forests were defined as plots with softwood AGB over 75% of total AGB. Mixed forests had neither softwood nor hardwood accounting for more than 75% of the total AGB. Table 2-2 provides a summary of the descriptive statistics for plot level AGB in different forest stand types.

Table 2-2. Summary of descriptive statistics for plot level AGB in different forest stand types (units: Mg ha^{-1}).

	Plot Count	Mean	Median	Variance	Minimum	Maximum
Hardwood	194	182.3	184.5	6693.1	0.9	440.3
Mixed	60	211.9	208.7	5461.0	68.8	390.7
Softwood	16	144.3	133.9	9771.0	9.1	314.7

2.3.3. Lidar data and processing

Airborne lidar data was acquired for HWF on September 10, 2011 (Table 2-3). An ALS60 lidar system was used to simultaneously collect both discrete return point clouds and the waveforms of the returned signals. The lidar sensor was operated at 218.7 kHz at an average flying height of 1770 m above ground with swath width of 542 m and flight line spacing of 407 m. The average point density was more than 10 points/m^2. Raw laser data were post-processed

with Terrasolid's lidar-dedicated TerraScan software (https://www.terrasolid.com/home.php) by Kucera International Inc. All further point-cloud processing tasks were performed with FUSION/IDV software (http://forsys.cfr.washington.edu/fusion/fusionlatest.html).

Table 2-3. ALS60 system settings and raw laser statistics of the lidar data collection for HWF.

Parameter	Value
Scan field of view (FOV)	24°
Outgoing pulse width	4 ns
Flying altitude	1770 m
Swath width	542 m
Flight line spacing	407 m
Footprint diameter	0.3 m
Average point density	>10 pts/m^2
Laser pulse rate	218.7 kHz
Acquisition date	September 10th, 2011

Lidar variables were derived from the lidar points within each inventory plot using the CloudMetrics function in FUSION. Return-based, height-based, and density-based variables were derived (Table 2-4).

Table 2-4. Description of lidar derived variables calculated. Calculation details are described by McGaughey (2019).

Variable name	Description	Variable name	Description
Pt_total	Total number of returns	ht_P25	25th percentile of height
Pt_first	Count of first returns	ht_P30	30th percentile of height
Pt_second	Count of second returns	ht_P40	40th percentile of height
Pt_third	Count of third returns	ht_P50	50th percentile of height
ht_min	height minimum	ht_P60	60th percentile of height
ht_max	height maximum	ht_P70	70th percentile of height
ht_mean	height mean	ht_P75	75th percentile of height
ht_mode	height mode	ht_P80	80th percentile of height
ht_stddev	height standard deviation	ht_P90	90th percentile of height
ht_variance	height variance	ht_P95	95th percentile of height
ht_CV	height coefficient of variation	ht_P99	99th percentile of height
ht_AAD	height absolute deviation from mean	Per_first_5m	Percentage of first returns above 5 m
ht_skewness	height skewness	Per_first_mean	Percentage of first returns above mean
ht_hurtosis	height kurtosis	Per_first_mode	Percentage of first returns above mode
ht_L1	first L moments	Per_all_5m	Percentage of all returns above 5 m
ht_L2	second L moments	Per_all_mean	Percentage of all returns above mean
ht_L3	third L moments	Per_all_mode	Percentage of all returns above mode
ht_L4	fourth L moments	First_abv_mean	First returns above mean
ht_L_kurtosis	L moment kurtosis	First_abv_mode	First returns above mode
ht_L_skewness	L moment skewness	All_abv_mean	All returns above mean
ht_L_CV	L moment coefficient of variation	All_abv_mode	All returns above mode
ht_P01	1st percentile of height	First_returns	Total first returns
ht_P05	5th percentile of height	All_returns	Total all returns
ht_P10	10th percentile of height	Canopy relief ratio	((mean-min)/(max-min))
ht_P20	20th percentile of height		

2.3.4. Landsat data and processing

We selected an orthorectified Landsat 5 TM Level-1 image acquired on June 19, 2011 to estimate AGB (path/row: 15/29). The image was downloaded from the U.S. Geological Survey Earth Explorer web site (https://earthexplorer.usgs.gov/). The image was chosen to minimize both time between Landsat and lidar data acquisitions and cloud cover over the study area. We did not use Landsat 7 data due to the impact of the Scan Line Corrector failure. Although the

Landsat image was collected earlier in the growing season than the lidar images, this was the cloud free image that best coincided with the forest inventory data collection.

Using the metadata associated with the downloaded Landsat imagery, radiometric correction was applied to convert digital numbers into reflectance and mitigate the impact of scene illumination and viewing geometry. Dark object subtraction was applied for atmosphere correction, which was intended to remove the effects of atmosphere scattering and absorption. Both radiometric and atmosphere corrections were performed using ENVI 5.2 (http://www.harrisgeospatial.com/Software-Technology/ENVI). Bands 1–5 (blue (B1), green (B2), red (B3), near infrared (B4), and shortwave infrared (B5)), and band 7 (shortwave infrared (B7)) reflectance values and vegetation indices derived from these bands were used for model variable selection. Five indices commonly used for vegetation analysis were used in the study: Differenced Vegetation Index (DVI), Ratio Vegetation Index (RVI), Normalized Vegetation Difference Index (NDVI), Soil Adjusted Vegetation Index (SAVI) and Modified Soil Adjusted Vegetation Index (MSAVI) (Table 2-5).

Table 2-5. Landsat 5 vegetation indices used in this study: DVI (differenced vegetation index), RVI (ratio vegetation index), NDVI (normalized vegetation difference index), SAVI (soil adjusted vegetation index) and MSAVI (modified soil adjusted vegetation index). Landsat 5 bands B3 (red) and B4 (near-infrared) were applied for index calculation.

Vegetation index	Equation	Source
DVI	$B4 - B3$	Bacour et al. (2006)
RVI	$\dfrac{B4}{B3}$	Jordan (1969)
NDVI	$\dfrac{B4 - B3}{B4 + B3}$	Tucker (1979)
SAVI	$1.5 \times \dfrac{B4 - B3}{B4 + B3 + 0.5}$	Huete (1988)
MASVI	$\dfrac{2 \times B4 + 1 - \sqrt{(2 \times B4 + 1)^2 - 8 \times (B4 - B3)}}{2}$	Qi et al. (1994)

2.3.5. Model establishment and variable selection

This study explored the relationship between forest inventory plot AGB and remote sensing derived variables. The model dependent variable was plot level AGB with Landsat derived variables, lidar derived variables, and variables derived from both datasets applied as predictors. We built three models to estimate AGB using MLR, RF and GWR: (1) Model I: Landsat predictors only; (2) Model II: lidar predictors only; (3) Model III: both Landsat and lidar predictors.

MLR was applied to estimate AGB based on the equation shown below.

$$AGB_i = \beta_0 + \sum_{j=1}^{p} \beta_j X_{ij} + \varepsilon_i \ (i = 1, …, n) \tag{2-1}$$

where β_0 is the intercept, β_j are model coefficients, and X_{ij} represents the remote sensing derived predictors. There are several commonly used variable selection methods when applying MLR: forward selection, backward selection, and stepwise selection. Forward selection starts with the most significant variable in the model and adds the most significant variable among the remaining variables into the model one at a time until none of the remaining variables is statistically significant. Backward selection starts with all variables in the model and removes the least significant variable one by one until all the variables in the model are statistically significant at a chosen level. Both forward and backward selection neglects the interaction among variables, which could result in nonsignificant variables in the model while significant variables are left out. Stepwise selection adds or removes one variable at each step to ensure all variables in the model are significant while none of the variables outside the model are significant to enter the model. Stepwise selection was applied using SAS software

23

(https://www.sas.com/en_us/software/sas9.html) in this study. Our significance level to enter and significance level to stay were both 0.15, which were default values for the software. After performing variable selection, we confirmed that all variables in the model were significant at a 0.10 significance level. We also checked the model variance inflation factor to verify that there was no multicollinearity among independent variables. The predictors selected in MLR were also applied in RF and GWR models.

RF is a non-parametric machine learning algorithm that was implemented using the "RandomForest" package (Liaw and Wiener, 2002) within the R software environment (http://www.R-project.org). RF can be used for regression or classification depending on the type of variable to be estimated. Compared with linear regression techniques, RF has lower bias and avoids overfitting (Boisvenue et al., 2016; Ghosh and Behera, 2018; Gleason and Im, 2012; Tian et al., 2017). RF grows many trees to vote for a result, which makes it insensitive to outliers and noise (Ghosh and Behera, 2018; Gleason and Im, 2012). For each tree, approximately two-thirds of the original data was randomly chosen to build the tree, and the remaining data was used for estimating out-of-bag error and calculating variable importance. In this study, RF was applied to estimate AGB using forest inventory plots as reference data and Landsat derived variables, lidar derived variables, and variables derived from both datasets applied as predictors. Default RF parameters were applied. The default value is 500 for ntree, ⅓ of the total predictors for mtry and 5 for nodesize.

GWR is an extension of standard regression that allows coefficients for environmental covariates to vary at different locations (Kumar et al., 2012). Localized coefficients of GWR are based on weighting observations around a sample point using a distance decay function. The

closer the data point is to the sample point, the greater the weight applied. GWR is a powerful approach for modeling spatially heterogeneous processes. GWR provides useful information about the impact of surrounding environmental factors and neighboring competitors on tree growth variation. In this study, GWR was applied using GWR 4.0 software (https://gwrtools.github.io/gwr4-downloads.html). The bandwidth was selected by minimizing Akaike Information Criterion (AIC)

2.3.6. Validation methods

To assess model performance, we calculated coefficient of determination (R^2), adjusted R^2, AIC, Root Mean Squared Error (RMSE), and Predicted Sum of Squares (PRESS). R^2 is the proportion of dependent variable variation that can be explained by the independent variables in the model and provides information about the goodness of fit of a model. Higher R^2 value are preferable; however, R^2 increases every time a new independent variable is introduced into the model. Therefore, to avoid any bias associated with this issue, we calculated adjusted R^2 because it does not increase as the number of independent variables increases. AIC is a measure of the goodness of fit of an estimated model and provides a means to compare model fit for a given dataset. The PRESS statistic gives a good indication of the predictive power of the fitted model. A small PRESS usually indicates that the model is not overly sensitive to any single data point. For RF and GWR, we applied the same selected variables for each model to keep the comparison between statistical methods consistent.

2.4. Results

2.4.1. Comparison of Landsat, lidar and integration of Landsat and lidar.

Table 2-6 compares the MLR, RF and GWR model results using all 270 hardwood, softwood and mixed forest plots where AGB ranged from 0.85 to 440.27 Mg ha^{-1}. None of the approaches performed well using only Landsat data (Model I), with MLR and GWR having the highest R^2 (0.11); RMSE values were similar across the three Landsat only approaches. Using lidar data only (Model II), MLR had the highest R^2 (0.52) while GWR has the lowest RMSE (55.97 Mg ha^{-1}). Using an integration of lidar and Landsat data (Model III), MLR had the highest R^2 (0.57) and lowest RMSE (55.19 Mg ha^{-1}). MLR had the highest R^2 values for Model I, II and III. Although MLR has slightly higher RMSE value compared with GWR models, the differences were minor. Thus, given that MLR is much easier to apply in most situations, MLR was applied for further analysis.

Table 2-6. Comparison of MLR, RF and GWR for estimating AGB in 270 plots in HWF. Model I uses Landsat data only; Model II uses lidar data only; Model III uses an integration of Landsat and lidar data.

	Predictors	MLR		RF		GWR	
		R^2	RMSE (Mg ha^{-1})	R^2	RMSE (Mg ha^{-1})	R^2	RMSE (Mg ha^{-1})
Model I	B3, B4, B5	0.11	78.49	0.08	78.75	0.11	78.16
Model II	Ht_min; ht_P01; ht_P40; ht_skewness; ht_kurtosis; ht_L2; ht_L_kurtosis	0.52	58.36	0.41	63.05	0.51	55.97
Model III	B4; B5; ht_min; ht_L2; ht_L_CV; ht_P50; Per_first_5m; Per_first_mean	0.57	55.19	0.45	61.17	0.54	55.47

Table 2-7 provides a comparison of model fitting results for Model I, II and III. Model I and II used Landsat and lidar independent variables, respectively. Model III used an integration of Landsat and lidar independent variables. As can be seen, Model II explains 50% of the

variation in AGB and is better than Model I in terms of all of the statistics we considered. Based on this study site, it is clear that lidar data was better than Landsat data in forest AGB estimation when only a single data source is used. However, Model III had better performance than both Model I and Model II, explaining 55% of AGB variation, with significantly decreased AIC, RMSE and PRESS. This demonstrates that integration of Landsat and lidar data could improve AGB estimation compared to using Landsat or lidar data alone.

Table 2-7. Comparison of MLR models for estimating AGB in 270 plots in HWF. Model I uses Landsat data only; Model II uses lidar data only; Model III uses an integration of Landsat and lidar data.

Model	R^2	Adjusted R^2	AIC	RMSE (Mg ha^{-1})	PRESS
I	0.11	0.09	2360	78.49	1707513
II	0.52	0.50	2206	58.36	954298
III	0.57	0.55	2177	55.19	861565

2.4.2. AGB estimation at different forest stand types

Our data was divided into three forest stand types based on the AGB majority in each plot. In contrast to the results reported in Table 2-7 where the three MLR models were applied to all 270 plots, in this step, we applied the three models separately to each forest type group. A summary of the results is shown in Table 2-8. For Model I, adjusted R^2 values from the forest type specific models are higher in hardwood and mixed plots and lower in softwood plots compared with the adjusted R^2 for the pooled model (0.09; Table 2-7). Among the three forest types, hardwood plots have the highest adjusted R^2 for Model I. For Model II and III, adjusted R^2 values from the forest type specific models are higher in softwood and mixed plots and lower in hardwood plots compared to the adjusted R^2 values from the pooled model. The models that used only Landsat data performed best in hardwood plots while the lidar only and integrated Landsat and lidar data models had their best performance in softwood plots.

In all forest stand types, when a single data source was used, the lidar-based model always outperformed the Landsat model. Integration of Landsat and lidar data had the best performance for hardwood and mixed forest AGB estimation; integrating data did not provide improvement over the lidar only model for softwood forest.

Table 2-8. Results of AGB estimation for different forest stand types (hardwood, softwood and mixed) using Landsat only (I), lidar only (II) and integration of Landsat and lidar (III) models.

Stand type	Count	Model	R^2	Adjusted R^2	AIC	RMSE (Mg ha^{-1})	PRESS
Hardwood	194	I	0.17	0.15	1680	75.22	1135975
		II	0.50	0.47	1594	59.34	732410
		III	0.55	0.53	1573	56.14	664276
Softwood	16	I	0.22	0.03	150	97.52	191205
		II	0.97	0.92	110	27.43	123050
		III	0.90	0.70	131	54.42	463699
Mixed	60	I	0.15	0.11	513	69.84	310972
		II	0.60	0.53	480	50.54	180521
		III	0.65	0.58	474	47.79	174537

2.4.3. Model comparison at different forest AGB ranges

To test the impact of different AGB value ranges on model performance we ranked our forest inventory plots by AGB value, and then grouped the data into four subgroups using two methods. The first method had subgroups with an equal number of plots (Table 2-9), the second method distributed the AGB value ranges evenly across the subgroups (Table 2-10). We used comparison of means of pairs of subgroups to determine if the data division meaningfully separated the subgroups. The mean comparison result showed that each data subgroup was significantly different from other subgroups regardless of whether we divided the data by plot count or AGB range.

Both of the methods used to divide the data showed common trends (Figure 2-2) in terms of adjusted R^2, with better performance in the low and high AGB value ranges compared to intermediate AGB values. The Landsat only model had the lowest adjusted R^2 regardless of subgroup. Integration of Landsat and lidar data had the largest adjusted R^2 among the three models, except for subgroup R2. However, in terms of AIC, Model III was better than Model II in only half of the subgroups (N1, N3, R3 and R4). In all other subgroups, although Model III improved Model II both in adjusted R^2 and AIC, the improvement was limited.

Table 2-9. Model comparison on AGB subgroups divided by equal number of plots.

Data	N	AGB range (Mg ha^{-1})	Model	R^2	Adjusted R^2	AIC	RMSE (Mg ha^{-1})	PRESS
N1	67	< 128	I	0.12	0.08	464	31.01	69469
			II	0.55	0.47	432	23.43	43507
			III	0.59	0.52	427	22.48	41545
N2	68	128–186	I	0.03	-0.02	384	16.34	19103
			II	0.23	0.11	380	15.32	17903
			III	0.25	0.12	380	15.24	18352
N3	68	186–242	I	0.02	-0.02	388	16.90	20568
			II	0.15	0.01	391	16.59	21954
			III	0.35	0.23	375	14.63	18759
N4	67	> 242	I	0.09	0.05	500	40.69	119461
			II	0.29	0.17	496	37.92	118620
			III	0.30	0.17	497	37.97	138875

Table 2-10. Model comparison on AGB subgroups divided by equal AGB ranges.

Data	N	AGB range (Mg ha^{-1})	Model	R^2	Adjusted R^2	AIC	RMSE (Mg ha^{-1})	PRESS
R1	55	< 110	I	0.16	0.11	367	27.10	44205
			II	0.60	0.52	338	19.95	26670
			III	0.62	0.53	338	19.77	30782
R2	114	110–210	I	0.05	0.03	753	26.76	84770
			II	0.24	0.18	740	24.62	73815
			III	0.24	0.16	743	24.84	77612
R3	88	210–310	I	0.03	-0.01	595	28.71	76037
			II	0.16	0.06	594	27.71	78874
			III	0.22	0.12	589	26.82	73583
R4	13	> 310	I	0.35	0.13	101	43.19	37214
			II	0.99	0.95	62	10.64	83752
			III	1.00	0.98	43	5.69	14469

(a)   (b)
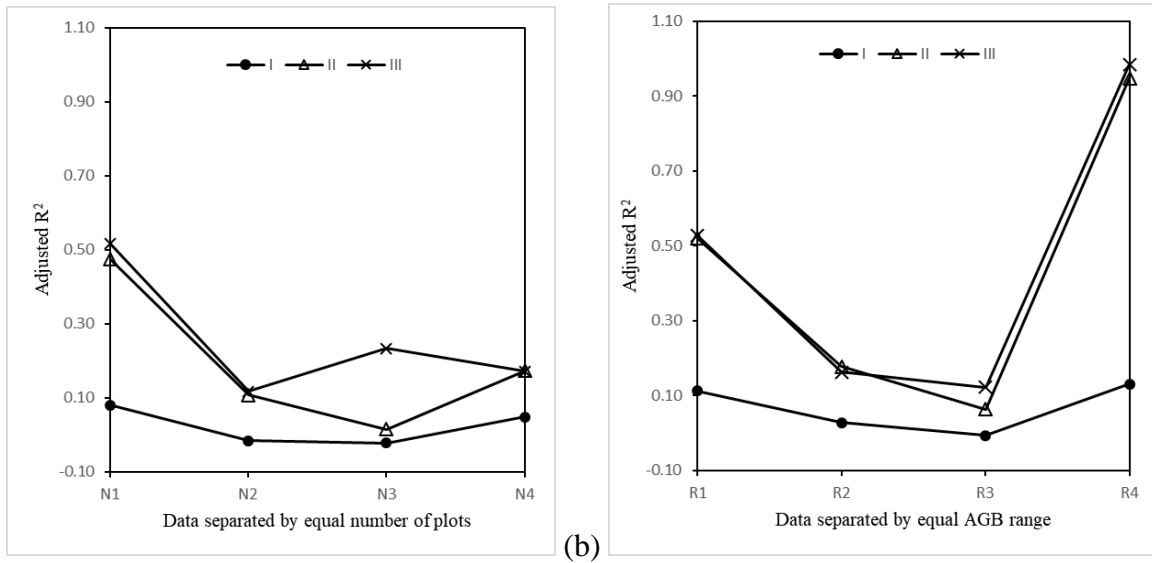
Figure 2-2. Adjusted R^2 values using different model. (a) Subgroups divided by equal number of plots (N1, N2, N3 and N4); (b) subgroup divided by equal AGB value range (R1, R2, R3 and R4).

2.5. Discussion

In this study, we compared the ability of MLR, RF, and GWR approaches in modeling AGB variation. MLR had slightly better performance than GWR, with RF having the weakest performance regardless of input data type. This was contrary to the study by Fassnacht et al.

(2014), who found that RF yielded better performance in a comparison that included stepwise linear regression, support vector machines, Gaussian processes and k-nearest neighbor. Our results were consistent with Li et al. (2014) who compared MLR and RF in biomass estimation on a single study site. Fassnacht et al. (2014) concluded that there is still no general agreement on best practices and that further comparative analysis is needed. There are several possible explanations for the better performance of MLR over RF in our study. One of the advantages of using RF is the ability to handle a large dataset. As stated in earlier studies, RF may result in considerable variance of the estimates when applied to a small number of sample units (Latifi et al., 2012). The second portion of this study suggests that model performance is highly dependent on site conditions. A normality test of the forest inventory plot AGB shows that the data is normally distributed with p values over 0.15 from Anderson-Daring and Shapiro-Wilk normality tests. GWR generally had better model prediction outcomes than MLR, which can be attributed to its capacity to capture spatial autocorrelation and heterogeneity (Gagliasso et al., 2014; Propastin, 2012; Zhang and Shi, 2004). In our study, GWR has similar outcomes with MLR, which can be attributed to the nature of regularly distributed plot locations. Zhang et al. (2009) had found GWR has similar coefficients with MLR in regular plantations. However, there was substantial higher cost in performing GWR in this study.

Using Landsat data, airborne lidar data, and the integration of the two data sources for calculating AGB over different forest types was compared in this study. The models we developed that were based only on Landsat data did not explain AGB variation. Prior studies have found the relationship between AGB and Landsat derived information to be extremely variable (Garcia et al., 2017; Lu, 2006). Avitabile et al. (2012) found that Landsat could be used to produce accurate and detailed estimates of biomass distribution, while Ediriweera et al. (2014)

31

concluded there was no strong relationship between Landsat derived information and ground measured AGB in their study. Lu (2005) found that as sites become more complex, the correlation between AGB and Landsat TM spectral response decreases while the correlation with Landsat TM derived texture information increases. Landsat data is limited by its inherent spatial, spectral and radiometric resolutions. The 30 m ground sampled distance of Landsat data introduces mixed pixels and an inability to deal with in-pixel forest complexity. Multiple land cover types contribute to each pixel value, which made the Landsat data less able to characterize AGB, which is problematic given the impact that forest type has AGB estimation success shown in our study. The moderate spectral resolution of the Landsat sensors also limits the ability to differentiate subtle differences among forest sites. The older Landsat missions were also limited by their 8-bit radiometric resolution. This resolution exacerbates the saturation problem often reported in the literature. Canopy reflectance saturation has been found in sites with complex forest structure and high biomass values (Ediriweera et al., 2014; Lu, 2005; Lu, 2006).

Lidar can overcome the data saturation shortcoming of Landsat by obtaining forest vertical structure information. Lidar is also extremely useful for regions constantly covered by clouds. A number of studies have reported that lidar can obtain more accurate results for AGB estimation than Landsat (Cao et al., 2014; Gleason and Im, 2012; Lu et al., 2012); Garcia et al. (2017) stated that lidar is the most accurate remote sensing technology for biomass estimation. The results from this study showed that the best performance came from the models that relied on integration of lidar and Landsat data, which were slightly better than the models that used only lidar data. Previous studies explored the integration of lidar and Landsat in AGB estimation and these also concluded that this data combination was better than using lidar or Landsat alone

(Babcock et al., 2018; Deo et al., 2017; Ediriweera et al., 2014; Hudak et al., 2002; Hyde et al., 2006; Phua et al., 2017; Yavaşlı, 2016).

Our study showed AGB estimation accuracy can be impacted by site conditions, predictor variables incorporated, and prediction model. Fassnacht et al. (2014) concluded that remote sensing data types the most important factor in their study, followed by prediction method and sample size; however, Fassnacht et al. (2014) did not account for the impact of site conditions in their study and acknowledged that more comprehensive analysis is needed to establish best practices. The impact of remote sensing data source and prediction method was also confirmed by Avitabile et al (2012) who found that adding land cover information could improve model prediction and RF performed better than multiple linear regression. Avitabile et al. (2012) applied the same model to two tropical sites and found the site with a more humid climate had larger errors likely due to the impact of higher rainfall.

The results from this study showed that forest stand-specific models produced better estimations of AGB than the pooled models in hardwood and mixed plots using Landsat data, and better estimations in softwood and mixed plots using lidar or an integration of lidar and Landsat data. Landsat data performed better in AGB estimation of hardwood stands than softwood stands in our study. Similar results have be reported in previous research using Landsat data (Zheng et al., 2004; Zheng et al., 2007). Our study also matched prior work that showed that estimating hardwood AGB is more difficult than softwood when using airborne lidar derived variables (Boudreau et al., 2008; Næsset, 2004; Popescu et al., 2003). Nelson et al. (2017) estimated AGB in the continental US and Mexico for wetland, hardwood, conifer, mixed wood and burn lands. Similar to this study, their results showed lidar derived variables had the best

performance in conifer stands (R^2=0.72, RMSE = 69.29 Mg ha^{-1}), followed by mixed wood (R^2=0.71, RMSE = 50.00 Mg ha^{-1}), and hardwood stands (R^2=0.57, RMSE = 44.49 Mg ha^{-1}). This discrepancy between Landsat and lidar data could be caused by both the different characteristics of data and tree structure. Landsat data is sensitive to forest horizontal expansion while lidar is superior at modeling forest vertical structure. Generally, hardwoods have high canopy cover compared to cone shaped softwood, which increases the detection chance in Landsat images. For softwood trees, the height detected by lidar is more correlated with AGB compare to hardwood trees, since a great amount of the AGB in a hardwood is distributed into lateral branches. Integration of Landsat and lidar data combines the advantages from both datasets and thus tends to have better results than using Landsat or lidar derived variables alone. Since the integrated model in our study tended to use more lidar variables than Landsat variables, the pooled model followed the same pattern as the lidar-only model, that is, performing best in the softwood plots, followed by mixed wood and hardwood.

In this study, we divided plots in two different ways to explore if model performance varied for different AGB ranges. As noted above, when we used all of our available plot data to build the model, we found that an integration of Landsat and lidar data improved AGB estimation compared to the single data models. However, when applied to subgroups, the integration of Landsat and lidar did not always enhance the result. To accurately estimate AGB requires knowledge of the appropriate model application range as well as remote sensing data characteristics. Our results showed that the linear models performed better for low and high AGB values, regardless of how we divided the data. This might be due to the nature of ordinary least square methods, which try to accommodate extreme values, or it could mean that forest structure within plots that have either low or high AGB values are relatively simple and thus

easier to estimate. The extreme low or high AGB levels are from plots with few trees or dense forest, respectively, which may be less influenced by mixed pixel effects. There is a risk of overfitting when dividing data into groups, such as is likely the case for R4, the high AGB group, which has a small number of plots and illustrated particularly high model fit.

2.6. Conclusion

In this study we applied Landsat, lidar, and an integration of Landsat and lidar data for forest AGB estimation. Variables derived from Landsat and lidar data were used as independent variables and AGB value from forest inventory plots was the dependent variable within the models. We compared AGB estimation performance of MLR, RF and GWR approaches and found that MLR had similar results as GWR, with both outperforming RF. We built MLR models using Landsat variables only, lidar variables only and variables from both datasets and tested the application of the models on all inventory plots, on plots with different forest types, and on plots with different AGB ranges. As expected based on prior studies, we found that lidar-based models worked better than Landsat for forest AGB estimation in general. AGB range can impact the outcome of Landsat and lidar data integration, which was better than using either dataset alone in most situations. Our models performed better for low and high AGB values. The best performance for the Landsat models was in application to hardwood stands rather than softwood stands, which was contrary to the lidar models.

Our study showed the importance of understanding site condition when considering the datasets and models to use for AGB estimation. Accurate estimation of AGB requires knowledge of both remote sensing data characteristics and site conditions; no remote sensing dataset appears to be universally best across all site conditions. Our efforts aimed to improve understanding of

35

the interaction between remote sensing data and site conditions, so that we can better select and apply the most suitable dataset in order to enhance model performance. The variation in model performance across forest type or AGB level observed in this study suggests that AGB estimation may be improved through preliminary classification based on forest type or biomass level. While a more comprehensive evaluation of a broader range of sites, particularly softwood plots, is needed to determine if generalizations of data are possible, extension of this study may facilitate more efficient application of both models and datasets.

2.7.   References

Adam, E., Mutanga, O., Abdel-Rahman, E. M., & Ismail, R. (2014). Estimating standing biomass in papyrus (Cyperus papyrus L.) swamp: Exploratory of in situ hyperspectral indices and random forest regression. *International Journal of Remote Sensing*, *35*(2), 693–714. https://doi.org/10.1080/01431161.2013.870676

Ahmed, O. S., Franklin, S. E., Wulder, M. A., & White, J. C. (2015). Characterizing stand-level forest canopy cover and height using Landsat time series, samples of airborne LiDAR, and the Random Forest algorithm. *ISPRS Journal of Photogrammetry and Remote Sensing*, *101*, 89–101. https://doi.org/10.1016/j.isprsjprs.2014.11.007

Avitabile, V., Baccini, A., Friedl, M. A., & Schmullius, C. (2012). Capabilities and limitations of Landsat and land cover data for aboveground woody biomass estimation of Uganda. *Remote Sensing of Environment*, *117*, 366–380. https://doi.org/10.1016/j.rse.2011.10.012

Babcock, C., Finley, A.O., Andersen, H.E., Pattison, R., Cook, B.D., Morton, D.C., Alonzo, M., Nelson, R., Gregoire, T., Ene, L. & Gobakken, T. (2018). Geostatistical estimation of forest biomass in interior Alaska combining Landsat-derived tree cover, sampled airborne lidar and field observations. *Remote Sensing of Environment*, *212*, 212–230. https://doi.org/10.1016/j.rse.2018.04.044

Bacour, C., Bréon, F.-M., & Maignan, F. (2006). Normalization of the directional effects in NOAA–AVHRR reflectance measurements for an improved monitoring of vegetation cycles. *Remote Sensing of Environment*, *102*(3–4), 402–413. https://doi.org/10.1016/j.rse.2006.03.006

Benitez, F. L., Anderson, L. O., & Formaggio, A. R. (2016). Evaluation of geostatistical techniques to estimate the spatial distribution of aboveground biomass in the Amazon

rainforest using high-resolution remote sensing data. *Acta Amazonica*, *46*(2), 151–160. https://doi.org/ 10.1590/1809-4392201501254

Boisvenue, C., Smiley, B. P., White, J. C., Kurz, W. A., & Wulder, M. A. (2016). Integration of Landsat time series and field plots for forest productivity estimates in decision support models. *Forest Ecology and Management*, *376*, 284–297. https://doi.org/10.1016/j.foreco.2016.06.022

Boudreau, J., Nelson, R., Margolis, H., Beaudoin, A., Guindon, L., & Kimes, D. (2008). Regional aboveground forest biomass using airborne and spaceborne LiDAR in Québec. *Remote Sensing of Environment*, *112*(10), 3876–3890. https://doi.org/10.1016/j.rse.2008.06.003

Cao, L., Coops, N. C., Hermosilla, T., Innes, J., Dai, J., & She, G. (2014). Using small-footprint discrete and full-waveform airborne LiDAR metrics to estimate total biomass and biomass components in subtropical forests. *Remote Sensing*, *6*(8), 7110–7135. https://doi.org/10.3390/rs6087110

Chave, J., Réjou-Méchain, M., Búrquez, A., Chidumayo, E., Colgan, M.S., Delitti, W.B., Duque, A., Eid, T., Fearnside, P.M., Goodman, R.C. & Henry, M. (2014). Improved allometric models to estimate the aboveground biomass of tropical trees. *Global Change Biology*, *20*(10), 3177–3190. https://doi.org/10.1111/gcb.12629

Chen, Q., McRoberts, R. E., Wang, C., & Radtke, P. J. (2016). Forest aboveground biomass mapping and estimation across multiple spatial scales using model-based inference. *Remote Sensing of Environment*, *184*, 350–360. https://doi.org/10.1016/j.rse.2016.07.023

Clark, D. B., & Kellner, J. R. (2012). Tropical forest biomass estimation and the fallacy of misplaced concreteness. *Journal of Vegetation Science*, *23*(6), 1191–1196. https://doi.org/10.1111/j.1654-1103.2012.01471.x

Coppin, P. R., & Bauer, M. E. (1994). Processing of multitemporal Landsat TM imagery to optimize extraction of forest cover change features. *IEEE Transactions on Geoscience and Remote Sensing*, *32*(4), 918–927. https://doi.org/10.1109/36.298020

Dalponte, M., Bruzzone, L., & Gianelle, D. (2008). Fusion of Hyperspectral and LIDAR Remote Sensing Data for Classification of Complex Forest Areas. *IEEE Transactions on Geoscience and Remote Sensing*, *46*(5), 1416–1427. https://doi.org/10.1109/TGRS.2008.916480

Dassot, M., Constant, T., & Fournier, M. (2011). The use of terrestrial LiDAR technology in forest science: application fields, benefits and challenges. *Annals of Forest Science*, *68*(5), 959–974. https://doi.org/ 10.1007/s13595-011-0102-2

Deo, R. K., Russell, M. B., Domke, G. M., Andersen, H.-E., Cohen, W. B., & Woodall, C. W. (2017). Evaluating Site-Specific and Generic Spatial Models of Aboveground Forest Biomass Based on Landsat Time-Series and LiDAR Strip Samples in the Eastern USA. *Remote Sensing*, *9*(6), 598. https://doi.org/10.3390/rs9060598.

Ediriweera, S., Pathirana, S., Danaher, T., & Nichols, D. (2014). Estimating above-ground biomass by fusion of LiDAR and multispectral data in subtropical woody plant communities in topographically complex terrain in North-eastern Australia. *Journal of Forestry Research*, *25*(4), 761–771. https://doi.org/10.1007/s11676-014-0485-7

Ene, L., Næsset, E., & Gobakken, T. (2012). Single tree detection in heterogeneous boreal forests using airborne laser scanning and area-based stem number estimates.

International Journal of Remote Sensing, *33*(16), 5171–5193. https://doi.org/10.1080/01431161.2012.657363

Falkowski, M. J., Smith, A. M. ., Hudak, A. T., Gessler, P. E., Vierling, L. A., & Crookston, N. L. (2006). Automated estimation of individual conifer tree height and crown diameter via two-dimensional spatial wavelet analysis of lidar data. *Canadian Journal of Remote Sensing*, *32*(2), 153–161. https://doi.org/10.5589/m06-005

Fassnacht, F., Hartig, F., Latifi, H., Berger, C., Hernández, J., Corvalán, P., & Koch, B. (2014). Importance of sample size, data type and prediction method for remote sensing-based estimations of aboveground forest biomass. *Remote Sensing of Environment*, *154*, 102–114. https://doi.org/10.1016/j.rse.2014.07.028

Feng, Y., Lu, D., Chen, Q., Keller, M., Moran, E., dos-Santos, M.N., Bolfe, E.L. & Batistella, M. (2017). Examining effective use of data sources and modeling algorithms for improving biomass estimation in a moist tropical forest of the Brazilian Amazon. *International Journal of Digital Earth*, *10*(10), 996–1016. https://doi.org/10.1016/j.rse.2014.07.028

Gagliasso, D., Hummel, S., & Temesgen, H. (2014). A Comparison of Selected Parametric and Non-Parametric Imputation Methods for Estimating Forest Biomass and Basal Area. *Open Journal of Forestry*, *04*(01), 42–48. https://doi.org/10.4236/ojf.2014.41008

Galidaki, G., Zianis, D., Gitas, I., Radoglou, K., Karathanassi, V., Tsakiri–Strati, M., Woodhouse, I. & Mallinis, G. (2017). Vegetation biomass estimation with remote sensing: focus on forest and other wooded land over the Mediterranean ecosystem. *International Journal of Remote Sensing*, *38*(7), 1940–1966. https://doi.org/10.1080/01431161.2016.1266113

García, M., Gajardo, J., Riaño, D., Zhao, K., Martín, P., & Ustin, S. (2015). Canopy clumping appraisal using terrestrial and airborne laser scanning. *Remote Sensing of Environment*, *161*, 78–88. https://doi.org/10.1016/j.rse.2015.01.030

Garcia, M., Saatchi, S., Casas, A., Koltunov, A., Ustin, S., Ramirez, C., Garcia-Gutierrez, J., & Balzter, H. (2017). Quantifying biomass consumption and carbon release from the California Rim fire by integrating airborne LiDAR and Landsat OLI data. *Journal of Geophysical Research: Biogeosciences*, *122*(2), 340–353. https://doi.org/10.1002/2015JG003315

Ghosh, S. M., & Behera, M. D. (2018). Aboveground biomass estimation using multi-sensor data synergy and machine learning algorithms in a dense tropical forest. *Applied Geography*, *96*(May), 29–40. https://doi.org/10.1016/j.apgeog.2018.05.011

Gleason, C. J., & Im, J. (2012). Forest biomass estimation from airborne LiDAR data using machine learning approaches. *Remote Sensing of Environment*, *125*, 80–91. https://doi.org/10.1016/j.rse.2012.07.006

Goldbergs, G., Levick, S. R., Lawes, M., & Edwards, A. (2018). Hierarchical integration of individual tree and area-based approaches for savanna biomass uncertainty estimation from airborne LiDAR. *Remote Sensing of Environment*, *205*, 141–150. https://doi.org/10.1016/j.rse.2017.11.010

Gonçalves, F., Treuhaft, R., Law, B., Almeida, A., Walker, W., Baccini, A., dos Santos, J. & Graça, P. (2017). Estimating Aboveground Biomass in Tropical Forests: Field Methods and Error Analysis for the Calibration of Remote Sensing Observations. *Remote Sensing*, *9*(1), 47. https://doi.org/10.3390/rs9010047

Heinzel, J. N., Weinacker, H., & Koch, B. (2008). Full automatic detection of tree species based on delineated single tree crowns - a data fusion approach for airborne laser scanning data and aerial photographs. *Proceedings of SilviLaser, 2008(8th).*

Houghton, R. A., Lawrence, K. T., Hackler, J. L., & Brown, S. (2008). The spatial distribution of forest biomass in the Brazilian Amazon: a comparison of estimates.. *Global Change Biology*, *7*(7), 731–746. https://doi.org/10.1111/j.1365-2486.2001.00426.x

Hu, T., Su, Y., Xue, B., Liu, J., Zhao, X., Fang, J., & Guo, Q. (2016). Mapping Global Forest Aboveground Biomass with Spaceborne LiDAR, Optical Imagery, and Forest Inventory Data. *Remote Sensing*, *8*(12), 565. https://doi.org/10.3390/rs8070565

Hudak, A. T., Lefsky, M. A., Cohen, W. B., & Berterretche, M. (2002). Integration of lidar and Landsat ETM+ data for estimating and mapping forest canopy height. *Remote Sensing of Environment*, *82*(2–3), 397–416. https://doi.org/10.1016/S0034-4257(02)00056-1

Huete, A. R. (1988). A soil-adjusted vegetation index (SAVI). *Remote Sensing of Environment*, *25*(3), 295–309. https://doi.org/10.1016/0034-4257(88)90106-X

Hyde, P., Dubayah, R., Walker, W., Blair, J. B., Hofton, M., & Hunsaker, C. (2006). Mapping forest structure for wildlife habitat analysis using multi-sensor (LiDAR, SAR/InSAR, ETM+, Quickbird) synergy. *Remote Sensing of Environment*, *102*(1–2), 63–73. https://doi.org/10.1016/j.rse.2006.01.021

Jenkins, J. C., Chojnacky, D. C., Heath, L. S., & Birdsey, R. A. (2003). National-scale biomass estimators for United States tree species. *Forest Science*, *49*(1), 12–35. https://doi.org/10.1093/forestscience/49.1.12

Jones, H. G., & Vaughan, R. A. (2010). *Remote sensing of vegetation: principles, techniques, and applications*. Oxford ; New York: Oxford University Press.

Jordan, C. F. (1969). Derivation of leaf-area index from quality of light on the forest floor. *Ecology*, *50*(4), 663–666. https://doi.org/10.2307/1936256

Kankare, V., Vastaranta, M., Holopainen, M., Räty, M., Yu, X., Hyyppä, J., Hyyppä, H., Alho, P. & Viitala, R. (2013). Retrieval of Forest Aboveground Biomass and Stem Volume with Airborne Scanning LiDAR. *Remote Sensing*, *5*(5), 2257–2274. https://doi.org/10.3390/rs5052257

Karlson, M., Ostwald, M., Reese, H., Sanou, J., Tankoano, B., & Mattsson, E. (2015). Mapping tree canopy cover and aboveground biomass in Sudano-Sahelian woodlands using Landsat 8 and random forest. *Remote Sensing*, *7*(8), 10017–10041. https://doi.org/10.3390/rs70810017

Kim, S.R., Kwak, D.A., Lee, W.K., Son, Y., Bae, S.W., Kim, C., & Yoo, S. (2010). Estimation of carbon storage based on individual tree detection in Pinus densiflora stands using a fusion of aerial photography and LiDAR data. *Science China Life Sciences*, *53*(7), 885–897. https://doi.org/ 10.1007/s11427-010-4017-1

Korhonen, L., Korpela, I., Heiskanen, J., & Maltamo, M. (2011). Airborne discrete-return LIDAR data in the estimation of vertical canopy cover, angular canopy closure and leaf area index. *Remote Sensing of Environment*, *115*(4), 1065–1080. https://doi.org/10.1016/j.rse.2010.12.011

Kumar, S., Lal, R., & Liu, D. (2012). A geographically weighted regression kriging approach for mapping soil organic carbon stock. *Geoderma*, *189*, 627–634. https://doi.org/10.1016/j.geoderma.2012.05.022

Kwak, D.A., Lee, W.K., Lee, J.H., Biging, G. S., & Gong, P. (2007). Detection of individual trees and estimation of tree height using LiDAR data. *Journal of Forest Research*, *12*(6), 425–434. https://doi.org/10.1007/s10310-007-0041-9

Latifi, H., Fassnacht, F., & Koch, B. (2012). Forest structure modeling with combined airborne hyperspectral and LiDAR data. *Remote Sensing of Environment*, 121, 10-25. https://doi.org/10.1016/j.rse.2012.01.015

Li, A., Dhakal, S., Glenn, N., Spaete, L., Shinneman, D., Pilliod, D., Arkle, R. & McIlroy, S. (2017). Lidar aboveground vegetation biomass estimates in shrublands: Prediction, uncertainties and application to coarser scales. *Remote Sensing*, *9*(9). https://doi.org/10.3390/rs9090903

Li, M., Im, J., Quackenbush, L. J., & Liu, T. (2014). Forest biomass and carbon stock quantification using airborne LiDAR data: A case study over Huntington Wildlife Forest in the Adirondack Park. *IEEE Journal of Selected Topics in Applied Earth Observations and Remote Sensing*, *7*(7), 3143–3156. https://doi.org/ 10.1109/JSTARS.2014.2304642

Liaw, A., & Wiener, M. (2002). Classification and Regression by randomForest. *R News*, *2*(3), 18–22. http://CRAN.R-project.org/doc/Rnews/

Liu, L., Coops, N. C., Aven, N. W., & Pang, Y. (2017). Mapping urban tree species using integrated airborne hyperspectral and LiDAR remote sensing data. *Remote Sensing of Environment*, *200*, 170–182. https://doi.org/10.1016/j.rse.2017.08.010

Lu, D. (2005). Aboveground biomass estimation using Landsat TM data in the Brazilian Amazon. *International Journal of Remote Sensing*, *26*(12), 2509–2525. https://doi.org/10.1080/01431160500142145

Lu, D. (2006). The potential and challenge of remote sensing-based biomass estimation. *International Journal of Remote Sensing*, *27*(7), 1297–1328. https://doi.org/10.1080/01431160500486732

Lu, D., Chen, Q., Wang, G., Moran, E., Batistella, M., Zhang, M., Vaglio Laurin, G. & Saah, D.. (2012). Aboveground Forest Biomass Estimation with Landsat and LiDAR Data and Uncertainty Analysis of the Estimates. *International Journal of Forestry Research*, *2012*, 1–16. https://doi.org/10.1155/2012/436537

Lumbierres, M., Méndez, P., Bustamante, J., Soriguer, R., & Santamaría, L. (2017). Modeling Biomass Production in Seasonal Wetlands Using MODIS NDVI Land Surface Phenology. *Remote Sensing*, *9*(4), 392. https://doi.org/10.3390/rs9040392

Ma, J., Xiao, X., Qin, Y., Chen, B., Hu, Y., Li, X., & Zhao, B. (2017). Estimating aboveground biomass of broadleaf, needleleaf, and mixed forests in Northeastern China through analysis of 25-m ALOS/PALSAR mosaic data. *Forest Ecology and Management*, *389*, 199–210. https://doi.org/10.1016/j.foreco.2016.12.020

Margono, B.A., Turubanova, S., Zhuravleva, I., Potapov, P., Tyukavina, A., Baccini, A., Goetz, S. & Hansen, M.C. (2012). Mapping and monitoring deforestation and forest degradation in Sumatra (Indonesia) using Landsat time series data sets from 1990 to 2010. *Environmental Research Letters*, *7*(3), 034010. https://doi.org/10.1088/1748-9326/7/3/034010

McGaughey, R. J. (2019, February 21). *FUSION/LDV: Software for LIDAR Data Analysis and Visualization*. Retrieved from http://forsys.cfr.washington.edu/Software/FUSION/FUSION_manual.pdf

Moser, P., Vibrans, A.C., McRoberts, R.E., Næsset, E., Gobakken, T., Chirici, G., Mura, M. & Marchetti, M. (2017). Methods for variable selection in LiDAR-assisted forest inventories. *Forestry*, *90*(1), 112–124. https://doi.org/10.1093/forestry/cpw041

Mutanga, O., Adam, E., & Cho, M. A. (2012). High density biomass estimation for wetland vegetation using worldview-2 imagery and random forest regression algorithm. *International Journal of Applied Earth Observation and Geoinformation*, *18*(1), 399–406. https://doi.org/10.1016/j.jag.2012.03.012

Næsset, E. (2004). Practical large-scale forest stand inventory using a small-footprint airborne scanning laser. *Scandinavian Journal of Forest Research*, *19*(2), 164–179. https://doi.org/10.1080/02827580310019257

Nelson, R., Margolis, H., Montesano, P., Sun, G., Cook, B., Corp, L., Andersen, H.E., Pellat, F.P., Fickel, T., Kauffman, J. & Prisley, S. (2017). Lidar-based estimates of aboveground biomass in the continental US and Mexico using ground, airborne, and satellite observations. *Remote Sensing of Environment*, *188*, 127–140. https://doi.org/10.1016/j.rse.2016.10.038

Phua, M.H., Johari, S.A., Wong, O.C., Ioki, K., Mahali, M., Nilus, R., Coomes, D.A., Maycock, C.R. & Hashim, M. (2017). Synergistic use of Landsat 8 OLI image and airborne LiDAR data for above-ground biomass estimation in tropical lowland rainforests. *Forest Ecology and Management*, *406*, 163–171. https://doi.org/10.1016/j.foreco.2017.10.007

Popescu, S. C., Wynne, R. H., & Nelson, R. F. (2002). Estimating plot-level tree heights with lidar: local filtering with a canopy-height based variable window size. *Computers and Electronics in Agriculture*, *37*(1–3), 71–95. https://doi.org/10.1016/S0168-1699(02)00121-7

Popescu, S. C., Wynne, R. H., & Nelson, R. F. (2003). Measuring individual tree crown diameter with lidar and assessing its influence on estimating forest volume and biomass. *Canadian Journal of Remote Sensing*, *29*(5), 564–577. https://doi.org/10.5589/m03-027

Popescu, S. C., Wynne, R. H., & Scrivani, J. A. (2004). Fusion of small-footprint lidar and multispectral data to estimate plot-level volume and biomass in deciduous and pine forests in Virginia, USA. *Forest Science*, *50*(4), 551–565. https://doi.org/10.1016/S0168-1699(02)00121-7

Powell, S. L., Cohen, W. B., Healey, S. P., Kennedy, R. E., Moisen, G. G., Pierce, K. B., & Ohmann, J. L. (2010). Quantification of live aboveground forest biomass dynamics with Landsat time-series and field inventory data: A comparison of empirical modeling approaches. *Remote Sensing of Environment*, *114*(5), 1053–1068. https://doi.org/10.1016/j.rse.2009.12.018

Propastin, P. (2012). Modifying geographically weighted regression for estimating aboveground biomass in tropical rainforests by multispectral remote sensing data. *International Journal of Applied Earth Observation and Geoinformation*, *18*, 82–90. https://doi.org/10.1016/j.jag.2011.12.013

Qi, J., Chehbouni, A., Huete, A., Kerr, Y., & Sorooshian, S. (1994). A modified soil adjusted vegetation index. *Remote Sensing of Environment*, *48*(2), 119–126. https://doi.org/10.1016/0034-4257(94)90134-1

R Development Core Team. (2008). (2019, February 21). *R: A Language and Environment for Statistical Computing*. Retrieved from http://www.R-project.org

Riaño, D., Valladares, F., Condés, S., & Chuvieco, E. (2004). Estimation of leaf area index and covered ground from airborne laser scanner (Lidar) in two contrasting forests.

Agricultural and Forest Meteorology, *124*(3–4), 269–275. https://doi.org/10.1016/j.agrformet.2004.02.005

Roberts, S. D., Dean, T. J., Evans, D. L., McCombs, J. W., Harrington, R. L., & Glass, P. A. (2005). Estimating individual tree leaf area in loblolly pine plantations using LiDAR-derived measurements of height and crown dimensions. *Forest Ecology and Management*, *213*(1–3), 54–70. https://doi.org/10.1016/j.foreco.2005.03.025

Shao, G., Shao, G., Gallion, J., Saunders, M. R., Frankenberger, J. R., & Fei, S. (2018). Improving Lidar-based aboveground biomass estimation of temperate hardwood forests with varying site productivity. *Remote Sensing of Environment*, *204*, 872–882. https://doi.org/10.1016/j.rse.2017.09.011

Shepard, J. P., Mitchell, M. J., Scott, T. J., Zhang, Y. M., & Raynal, D. J. (1989). Measurements of wet and dry deposition in a Northern Hardwood forest. *Water, Air, and Soil Pollution*, *48*(1), 225–238. https://doi.org/10.1007/BF00282380

Singh, K. K., Vogler, J. B., Shoemaker, D. A., & Meentemeyer, R. K. (2012). LiDAR-Landsat data fusion for large-area assessment of urban land cover: Balancing spatial resolution, data volume and mapping accuracy. *ISPRS Journal of Photogrammetry and Remote Sensing*, *74*, 110–121. https://doi.org/10.1016/j.isprsjprs.2012.09.009

Takagi, K., Yone, Y., Takahashi, H., Sakai, R., Hojyo, H., Kamiura, T., Nomura, M., Liang, N., Fukazawa, T., Miya, H. & Yoshida, T. (2015). Forest biomass and volume estimation using airborne LiDAR in a cool-temperate forest of northern Hokkaido, Japan. *Ecological Informatics*, *26*, 54–60. https://doi.org/10.1016/j.ecoinf.2015.01.005

Tang, H., Brolly, M., Zhao, F., Strahler, A.H., Schaaf, C.L., Ganguly, S., Zhang, G. & Dubayah, R. (2014). Deriving and validating Leaf Area Index (LAI) at multiple spatial scales

through lidar remote sensing: A case study in Sierra National Forest, CA. *Remote Sensing of Environment*, *143*, 131–141. https://doi.org/10.1016/j.rse.2013.12.007

Terrasolid Home. (n.d.). Retrieved March 25, 2018, from https://www.terrasolid.com/home.php

Tesfamichael, S. G., van Aardt, J. A. N., & Ahmed, F. (2010). Estimating plot-level tree height and volume of Eucalyptus grandis plantations using small-footprint, discrete return lidar data. *Progress in Physical Geography*, *34*(4), 515–540. https://doi.org/10.1177/0309133310365596

Tian, X., Yan, M., van der Tol, C., Li, Z., Su, Z., Chen, E., Li, X., Li, L., Wang, X., Pan, X. & Gao, L. (2017). Modeling forest above-ground biomass dynamics using multi-source data and incorporated models: A case study over the qilian mountains. *Agricultural and Forest Meteorology*, *246*(May), 1–14. https://doi.org/10.1016/j.agrformet.2017.05.026

Trinder, J. C., & Salah, M. (2012). Aerial images and LiDAR data fusion for disaster change detection. *ISPRS Annals of Photogrammetry, Remote Sensing and Spatial Information Sciences*, *I–4*, 227–232. https://doi.org/10.5194/isprsannals-I-4-227-2012

Trotter, C. M., Dymond, J. R., & Goulding, C. J. (1997). Estimation of timber volume in a coniferous plantation forest using Landsat TM. *International Journal of Remote Sensing*, *18*(10), 2209–2223. https://doi.org/10.1080/014311697217846

Tucker, C. J. (1979). Red and photographic infrared linear combinations for monitoring vegetation. *Remote Sensing of Environment*, *8*(2), 127–150. https://doi.org/10.1016/0034-4257(79)90013-0

Ucar, Z., Bettinger, P., Merry, K., Akbulut, R., & Siry, J. (2018). Estimation of urban woody vegetation cover using multispectral imagery and LiDAR. *Urban Forestry & Urban Greening*, *29*, 248–260. https://doi.org/10.1016/j.ufug.2017.12.001

UNECE/FAO, F. (2000). Forest resources of Europe, CIS, North America, Australia, Japan and New Zealand (industrialized temperate/boreal countries): UN-ECE/FAO contribution to the global forest resources Assessment 2000. United Nations Economic Commission for Europe. *Food and Agricultural Organization*.

Urbazaev, M., Thiel, C., Cremer, F., Dubayah, R., Migliavacca, M., Reichstein, M., & Schmullius, C. (2018). Estimation of forest aboveground biomass and uncertainties by integration of field measurements, airborne LiDAR, and SAR and optical satellite data in Mexico. *Carbon Balance and Management*, *13*(1), 5. https://doi.org/10.1186/s13021-018-0093-5

Vogeler, J. C., & Cohen, W. B. (2016). A review of the role of active remote sensing and data fusion for characterizing forest in wildlife habitat models. *Revista de Teledetección*, (45), 1. https://doi.org/10.4995/raet.2016.3981

Wang, Q., Pang, Y., Li, Z., Sun, G., Chen, E., & Ni-Meister, W. (2016). The Potential of Forest Biomass Inversion Based on Vegetation Indices Using Multi-Angle CHRIS/PROBA Data. *Remote Sensing*, *8*(12), 891. https://doi.org/10.3390/rs8110891

Wulder, M.A., White, J.C., Nelson, R.F., Næsset, E., Ørka, H.O., Coops, N.C., Hilker, T., Bater, C.W. & Gobakken, T. (2012). Lidar sampling for large-area forest characterization: A review. *Remote Sensing of Environment*, *121*, 196–209. https://doi.org/10.1016/j.rse.2012.02.001

Yavaşlı, D. D. (2016). Estimation of above ground forest biomass at Muğla using ICESat/GLAS and Landsat data. *Remote Sensing Applications: Society and Environment*, *4*, 211–218. https://doi.org/10.1016/j.rsase.2016.11.004

Zhang, L., & Shi, H. (2004). Local modeling of tree growth by geographically weighted regression. *Forest Science*, *50*(2), 225–244. https://doi.org/10.1093/forestscience/50.2.225

Zheng, D., Rademacher, J., Chen, J., Crow, T., Bresee, M., Le Moine, J., & Ryu, S.R. (2004). Estimating aboveground biomass using Landsat 7 ETM+ data across a managed landscape in northern Wisconsin, USA. *Remote Sensing of Environment*, *93*(3), 402–411. https://doi.org/10.1016/j.rse.2004.08.008

Zheng, G., Chen, J. M., Tian, Q. J., Ju, W. M., & Xia, X. Q. (2007). Combining remote sensing imagery and forest age inventory for biomass mapping. *Journal of Environmental Management*, *85*(3), 616–623. https://doi.org/10.1016/J.JENVMAN.2006.07.015

Zhang, L., Ma, Z., & Guo, L. (2009). An evaluation of spatial autocorrelation and heterogeneity in the residuals of six regression models. Forest Science, 55(6), 533-548. https://doi.org/10.1093/forestscience/55.6.533

3. Manuscript 2: Airborne lidar sampling strategies to enhance forest aboveground biomass estimation from Landsat imagery

3.1. Abstract

Accurately estimating aboveground biomass (AGB) is important in many applications including monitoring carbon stocks, investigating deforestation and forest degradation, and designing sustainable forest management strategies. Although lidar provides critical three-dimensional forest structure information for estimating AGB, acquiring comprehensive lidar coverage is often cost prohibitive. This project focused on developing a lidar sampling framework to support AGB estimation from Landsat images. Two sampling strategies, systematic and classification-based, were tested and compared. Analysis was performed over a temperate forest study site in northern New York State and the process was then validated at a similar site located in central New York State. Our results demonstrated that while inclusion of lidar data using systematic or classification-based sampling supports AGB estimation, the systematic sampling selection method was highly dependent on site conditions and had higher accuracy variability. The classification-based lidar sampling strategy was easy to apply and provides a framework that is readily transferable to new study sites.

Keywords: systematic sampling; classification-based sampling; forest types; data fusion; regression; Random Forest

3.2. Introduction

3.2.1. Remote sensing forest AGB estimation

Forest ecosystem management requires comprehensive, timely and accurate monitoring efforts (Matasci et al., 2018). Above ground biomass (AGB) is an important indicator in

monitoring the change of forest carbon stocks. Airborne lidar has been successfully applied to estimate forest biophysical parameters and has proved to provide accurate AGB estimation in many studies (Chen et al., 2012; Maltamo et al., 2006), particularly when used in coordination with data from passive sensors. Commonly used remote sensing data sources, such as Landsat (Lu et al., 2012), Moderate Resolution Imaging Spectroradiometer (MODIS; Zhang et al., 2014) and radar (Baghdadi et al., 2015), tend to reach a saturation point that limits their effectiveness in estimating higher AGB levels (Knapp et al., 2018). The saturation level of radar varies with the bands applied. For example, the X- and C-band backscatters saturate at low biomass levels (30–50 Mg ha^{-1}; Zhang et al., 2014) and L-band saturation ranges from 40–150 Mg ha^{-1} (Mitchard et al., 2009). Lidar does not suffer from this saturation problem and thus is able to more accurately estimate AGB (Hajj et al., 2017). However, lidar acquisitions are often practically limited by cost or data volume. Although the increasing availability of unmanned aerial vehicles (UAVs) is providing new avenues for data collection, the cost and effort to acquire lidar data are still higher than passive sensors like Landsat, MODIS, or Sentinel. Moreover, acquiring full coverage lidar is often infeasible for large area studies due to the data volume. Kelly and Di Tommaso (2015) provide an example of a 5-hectare forest stand that can be covered by a 300 byte Landsat Thematic Mapper (TM) image or a 50 Mb 10 pulse/m^2 lidar dataset. These cost and data limitations inhibit the widespread and ready availability of lidar data.

3.2.2. Lidar and Landsat fusion

Sensors like those onboard the Landsat satellites can provide extensive forest coverage with low cost but offer limited capacity for vertical characterization. Conversely, lidar can provide accurate measurements of forest attributes in the vertical plane; however, as mentioned above, lidar acquisitions are often limited in horizontal extent due to issues with cost and data

volume. Additionally, lidar cannot capture all necessary forest attributes. For example, Erdody and Moskal (2010) discuss the limitation of lidar data in discerning tree species. To mitigate the weaknesses of each data type, fusion of lidar and Landsat has been proposed and explored for AGB estimation (Ediriweera et al., 2014; Lu et al., 2012). The advantages of lidar and Landsat data fusion are twofold: (1) the synergistic usage of advantages from both datasets, and (2) with appropriate sampling, full lidar coverage is not required.

3.2.3. Lidar sampling

Researchers have applied lidar sampling to mitigate the limitations associated with managing cost and data volume. Instead of collecting full-coverage data, lidar sampling can significantly reduce the time and effort needed for data collection, organization and processing. Lidar samples supply detailed information on specific locations that can be used to calibrate models to derive forest attributes for other regions (Ørka et al., 2012). Studies have demonstrated that lidar sampling can provide estimates for biomass (Ene et al., 2016; Næsset et al., 2009) or forest height (Hudak et al., 2002). Researchers have used numerous statistical methods to extrapolate forest biophysical parameters beyond lidar samples to represent a broader area of interest. For example, Boudreau et al. (2008) used intermediate samples of airborne lidar data to extrapolate AGB estimates from plot-level forest inventory data to a broader spaceborne lidar coverage. In a two-stage method, they first developed a lidar-based biomass equation to relate plot-level biomass and airborne lidar derived variables and then applied the equation to estimate biomass throughout the airborne lidar coverage. The second stage developed a regression equation between the lidar derived biomass and spaceborne ICESat Geoscience Laser Altimer System (GLAS) metrics in order to extrapolate the limited lidar biomass estimates to the broader GLAS coverage.

54

There are two approaches to reduce lidar data volume—thinning lidar density and reducing lidar extent—that have proved to have minimal impact on accuracy estimation of biophysical parameters compared with using full lidar data coverage. For example, Holmgren, (2004) reduced laser density from 4.3 to 0.1 pulses/m^2 and observed minimal change in errors for estimation of mean tree height, basal area, and stem volume. This was also confirmed by Maltamo et al., (2006) who reported that simulated point density reduction had no effect on volume estimation accuracy. Instead of using full lidar data coverage, Chen and Hay (2011) sampled 17.6% of total lidar extent and achieved similar accuracies as the full lidar data in estimating canopy height.

Decisions regarding lidar sample locations are critical. Countless lidar samples can be generated with similar data collecting efforts but may generate different analysis outcomes. It is preferable to use lidar samples that best characterize the study area in order to achieve similar outcomes as comprehensive lidar coverage. Sampling methods used to reduce lidar coverage generally fall into two categories: systematic sampling and classification-based sampling. In systematic lidar sampling, data is collected based on a designated sampling unit and distance interval. The distribution of sampling units may be point, strip, or grid based. Tsui et al. (2013) sampled lidar data using a grid pattern in which horizontal and vertical lines had distance intervals of 1000 m. Hudak et al. (2002) sampled lidar data using both strip and point patterns with distance intervals of 250 m, 500 m, 1000 m, and 2000 m. Systematic sampling is easy to design and apply, but it might fail to represent the full data range, especially if only a small portion of data is sampled. Classification-based sampling can help compensate for this situation by better representing all value ranges. In classification-based sampling, a classification map is created and then applied to assist lidar sample selection. Chen and Hay (2011) aimed to model

forest canopy height from lidar samples that were selected by combining pseudo-height classification from QuickBird imagery with several other inputs in a rule-based model. The rules included non-overlapping transects, covering all height classes, and selecting pseudo-height histograms with the highest correlation to the pseudo-height histogram derived from all data. Previous studies have considered both systematic sampling and classification-based sampling though there has not been a comparison of these two strategies.

3.2.4. Objectives

The overall aim of this study was to deepen our understanding of lidar sampling for AGB estimation. While the value of lidar sampling has been well documented and various lidar sampling strategies have been proposed, there are no widely accepted protocols for cost-effective lidar sampling for AGB estimation. Additionally, while forest type has long been recognized as a factor in AGB estimation, prior studies have not documented the use of forest type classification for lidar sampling selection within this field. This paper presents a methodological framework to map AGB in temperate forests by combining ground-based inventory data, comprehensive Landsat data and lidar samples acquired using a variety of methods. We particularly focused on: (1) assessing whether lidar samples can substitute for comprehensive lidar data collection, (2) characterizing the differences in AGB estimation based on systematic and classification-based sampling lidar sampling strategies, and (3) providing a protocol for lidar sampling acquisition, implementation, and evaluation.

3.3. Data and methods

3.3.1. Study areas

3.3.1.1. Main study area: Huntington Wildlife Forest

Our main study area is the Huntington Wildlife Forest (Huntington) in the central Adirondack Park in northern New York State. The Huntington property provided a location for evaluating the value of different lidar sampling procedures and developing a sampling protocol. Huntington is managed by the State University of New York College of Environmental Science and Forestry (SUNY-ESF; 43°58'19" N, 74°13'18" W; Figure 3-1). Huntington covers approximately 60 km^2 area with mountainous topography ranging in elevation from 466 m to 859 m above mean sea level. Huntington has a mean annual temperature of 4.4°C and mean annual precipitation of 1010 mm (Shepard et al., 1989). Huntington contains both undisturbed natural communities and managed forest stands with major species being American beech (*Fagus grandifolia*), yellow birch (*Betula alleghaniensis Britt.*), sugar maple (*Acer saccharum Marshall.*), red spruce (*Picea rubens Sarg.*), red maple (*Acer rubrum L.*) and hemlock (*Tsuga spp.*).
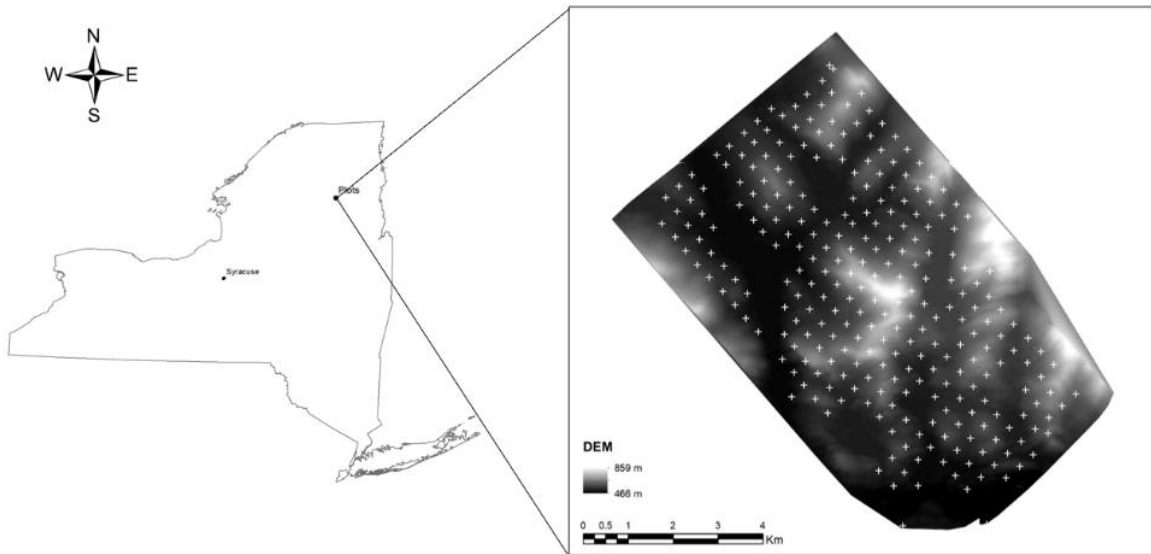
Figure 3-1. Location of Huntington Wildlife Forest in New York State. The figure shows the distribution of 270 forest inventory plots overlaid on a lidar generated digital elevation model.

3.3.1.2. Test study area: Heiberg Memorial Forest

Our test study area is the Heiberg Memorial Forest (Heiberg) south of Syracuse in central New York State. Heiberg is also managed by SUNY ESF (42°47'12" N, 76°05'37" W; Figure 3-2). Heiberg provided an independent site for testing the lidar sampling protocol developed at Huntington. Heiberg covers approximately 16 km^2 with elevation ranging from 383 m to 625 m above mean sea level. The majority of Heiberg is conifer plantations (6.64 km^2, 42%), Allegheny hardwoods (5.65 km^2, 36%) or open areas (2.39 km^2, 15%). Predominant conifer species include Norway spruce (*Picea abies*), hemlock (*Tsuga*), white pine (*Pinus strobus*) and eastern larch (*Larix laricina*). Deciduous tree species mainly include maple (*Acer*), ash (*Fraxinus L.*), beech (*Betula*), and basswood (*T. americana*).
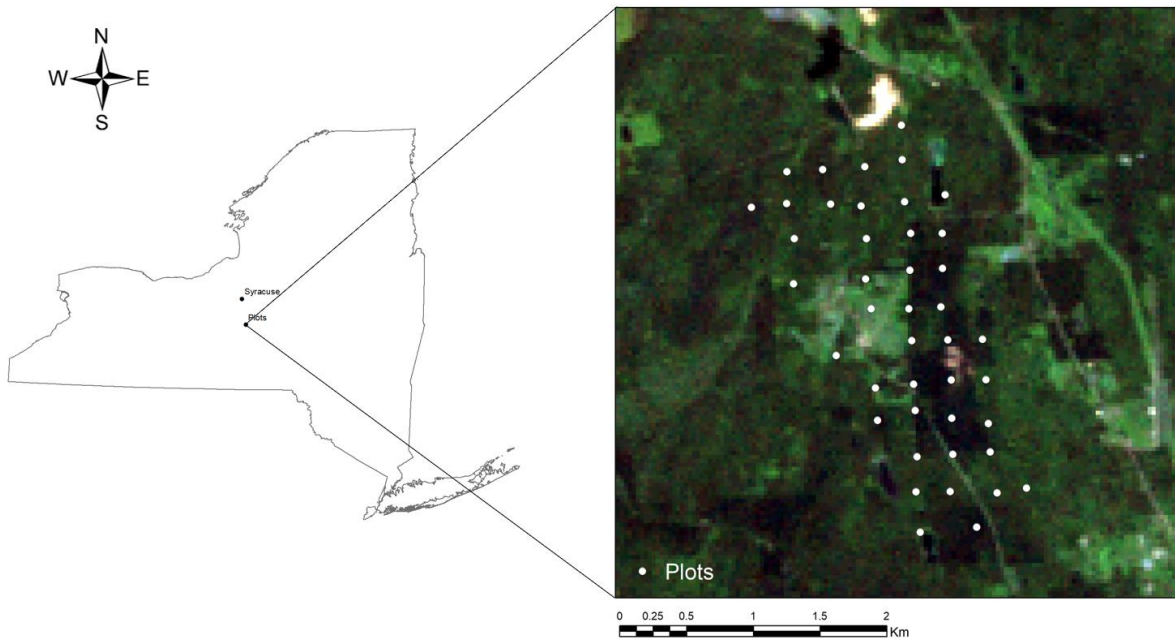
Figure 3-2. Location of Heiberg Memorial Forest in New York State. The forest inventory plots (white dots) are overlaid on a true color Landsat 5 image composite.

3.3.2. Field inventory data

SUNY ESF maintains continuous forest inventory (CFI) plots within Huntington and Heiberg forests, with comprehensive data collection during the summer of 2011 and 2010, respectively. The CFI plots are approximately 405 m^2 circular regions, with the center of each plot located using a global positioning system receiver. All trees in the plot with diameter at breast height (DBH) of 11.7 cm or greater were measured in Huntington and 9.1 cm or greater were measured in Heiberg. Information recorded for each tree included tree species, DBH, and location relative to the plot center.

Based on the field observations, tree-level AGB was calculated using species-specific DBH allometric equations from Jenkins et al. (2003). Plot-level AGB was calculated as the average AGB per unit area within each plot in megagrams per hectare (Mg ha^{-1}). This was

calculated by dividing the tree-level AGB total by the plot area. Table 3-1 presents plot-level AGB descriptive statistics for Huntington and Heiberg forests.

The United Nations Economic Commission for Europe (UNECE) Food and Agriculture Organization (FAO; UNECE/FAO, 2000) defines a stand as mixed forest where neither broadleaved nor coniferous trees account for more than 75% of the tree crown area. We adapted the UNECE/FAO approach and defined a plot as hardwood if the hardwood AGB within the plot was over 75% of the total AGB. Softwood plots were similarly defined when at least 75% of the total AGB was softwood AGB. Mixed forest plots had neither softwood nor hardwood accounting for more than 75% of the total AGB. Table 3-1 provides descriptive statistics for plot level AGB in hardwood, softwood, and mixed plots in Huntington and Heiberg forests.

Table 3-1. Plot level AGB descriptive statistics for all plots and plots grouped by forest type (hardwood, softwood, and mixed) in Huntington and Heiberg forests (units: Mg ha^{-1}).

Study area	Forest type	Plot count	Mean	Median	Variance	Min	Max
Huntington	Total	270	186.6	186.3	6808.0	0.9	440.3
	Hardwood	194	182.3	184.5	6693.1	0.9	440.3
	Mixed	60	211.9	208.7	5461.0	68.8	390.7
	Softwood	16	144.3	133.9	9771.0	9.1	314.7
Heiberg	Total	43	212.6	215.9	9672.9	2.0	375.8
	Hardwood	31	220.8	249.7	9699.2	2.0	375.8
	Mixed	9	220.3	249.0	7846.7	76.4	323.9
	Softwood	3	104.9	59.5	7548.8	50.1	205.1

3.3.3. Lidar data and processing

Airborne lidar data was acquired for Huntington and Heiberg on September 10, 2011 and August 10, 2010, respectively. ALS60 lidar systems were used to simultaneously collect both discrete return point clouds and the waveforms of the returned signals. Characteristics of the lidar data collections for Huntington and Heiberg are summarized in Table 3-2. Raw laser data was post-processed by Kucera International using Terrasolid's TerraScan software

(https://www.terrasolid.com/home.php). All further point-cloud processing tasks were performed within FUSION software (http://forsys.cfr.washington.edu/fusion/fusionlatest.html).

Table 3-2. ALS60 system settings and raw laser statistics of the lidar data collection for Huntington and Heiberg forests.

Study site	Huntington	Heiberg
Scan field of view (FOV)	24°	28°
Outgoing pulse width	4 ns	4 ns
Flying altitude	540 m	487 m
Swath width	~542 m	~554 m
Average point density	>10 pts/m^2	>7 pts/m^2
Laser pulse rate	218.7 kHz	183.8 kHz
Acquisition date	September 10, 2011	August 10, 2010

Lidar variables were derived from the lidar points within each inventory plot using the CloudMetrics function in FUSION. Return-based, height-based, and density-based variables were derived (Table 3-3).

Table 3-3. Description of lidar derived variables calculated. Calculation details are described by McGaughey (2019).

Variable name	Description	Variable name	Description
Pt_total	Total number of returns	ht_P50	50th percentile of height
Pt_first	Count of first returns	ht_P60	60th percentile of height
Pt_second	Count of second returns	ht_P70	70th percentile of height
Pt_third	Count of third returns	ht_P75	75th percentile of height
ht_min	height minimum	ht_P80	80th percentile of height
ht_max	height maximum	ht_P90	90th percentile of height
ht_mean	height mean	ht_P95	95th percentile of height
ht_mode	height mode	ht_P99	99th percentile of height
ht_stddev	height standard deviation	Per_first_5m	Percentage of first returns above 5 m
ht_variance	height variance	Per_first_mean	Percentage of first returns above mean
ht_CV	height coefficient of variation	Per_first_mode	Percentage of first returns above mode
ht_skewness	height skewness	Per_all_5m	Percentage of all returns above 5 m
ht_hurtosis	height kurtosis	Per_all_mean	Percentage of all returns above mean
ht_AAD	height absolute deviation from mean	Per_all_mode	Percentage of all returns above mode
ht_P01	1st percentile of height	First_abv_mean	First returns above mean
ht_P05	5th percentile of height	First_abv_mode	First returns above mode
ht_P10	10th percentile of height	All_abv_mean	All returns above mean
ht_P20	20th percentile of height	All_abv_mode	All returns above mode
ht_P25	25th percentile of height	First_returns	Total first returns
ht_P30	30th percentile of height	All_returns	Total all returns
ht_P40	40th percentile of height	Canopy relief ratio	((mean-min)/(max-min))

3.3.4. Landsat data and processing

We selected orthorectified Landsat TM Level-1 images acquired on June 19, 2011 (path/row: 15/29) and July 18, 2010 (path/row: 15/30) that covered the Huntington and Heiberg forest areas, respectively. The images were downloaded from the U.S. Geological Survey Earth Explorer (https://earthexplorer.usgs.gov/). Although the Landsat images were collected earlier in the growing season than the lidar datasets, they were the cloud-free images that best coincided with the forest inventory data collection.

Using the metadata associated with the downloaded Landsat images, radiometric correction was applied to convert digital numbers into reflectance aiming to mitigate the impact

of scene illumination and viewing geometry. Dark object subtraction was applied for atmosphere correction, which was intended to remove the effects of atmosphere scattering and absorption. Radiometric and atmosphere correction were both performed using ENVI 5.2 (https://www.harrisgeospatial.com/). Landsat bands 1–5 and 7 (blue, green, red, near infrared, and two shortwave infrared), reflectance values and vegetation indices calculated from these bands were used for model variable selection. Five commonly used vegetation indices were applied in this study: Differenced Vegetation Index (DVI), Ratio Vegetation Index (RVI), Normalized Vegetation Difference Index (NDVI), Soil Adjusted Vegetation Index (SAVI) and Modified Soil Adjusted Vegetation Index (MSAVI) (Table 3-4).

Table 3-4. Landsat TM vegetation indices used in this study: DVI (differenced vegetation index), RVI (ratio vegetation index), NDVI (normalized vegetation difference index), SAVI (soil adjusted vegetation index) and MSAVI (modified soil adjusted vegetation index). Landsat 5 red (B3) and near-infrared (B4) bands were used for index calculation.

Vegetation index	Equation	Source
DVI	$B4 - B3$	Bacour et al. (2006) (Bacour, Bréon, & Maignan, 2006)
RVI	$\dfrac{B4}{B3}$	Jordan (1969) (Jordan, 1969)
NDVI	$\dfrac{B4 - B3}{B4 + B3}$	Tucker (1979) (Tucker, 1979)
SAVI	$1.5 \times \dfrac{B4 - B3}{B4 + B3 + 0.5}$	Huete (1988) (Huete, 1988)
MASVI	$\dfrac{2 \times B4 + 1 - \sqrt{(2 \times B4 + 1)^2 - 8 \times (B4 - B3)}}{2}$	Qi et al. (1994) (Qi, Chehbouni, Huete, Kerr, & Sorooshian, 1994)

3.3.5. Lidar and Landsat fusion procedure

3.3.5.1. Overview

We used AGB data developed from full lidar coverage as a baseline to see if Landsat-based AGB models that used lidar samples could achieve accuracies that approached that of models that used the more expensive full lidar coverage. We also sought to determine how accuracy varied with sampling strategy and if there was a way to establish a protocol to guide lidar sample collection. The work flow for this study is shown in Figure 3-3. The baseline for comparison in our study was an AGB model developed from the comprehensive lidar data coverage. Forest inventory plot and lidar data were applied to build a first stage regression model that was then used to estimate AGB for the Huntington study area. The impact of different lidar sampling strategies was explored using second stage regression models, which established a relationship between samples of the lidar estimated AGB values and Landsat derived variables. Two categories of lidar sampling strategies were explored: systematic sampling and classification-based sampling. The classification-based sampling approach was based on a Random Forest (RF) forest type classification. To assess the accuracy of different sampling strategies, Landsat estimated AGB values generated from second stage regression models were validated using plot and lidar estimated AGB values using root mean square error (RMSE) and relative root mean square error (RRMSE).
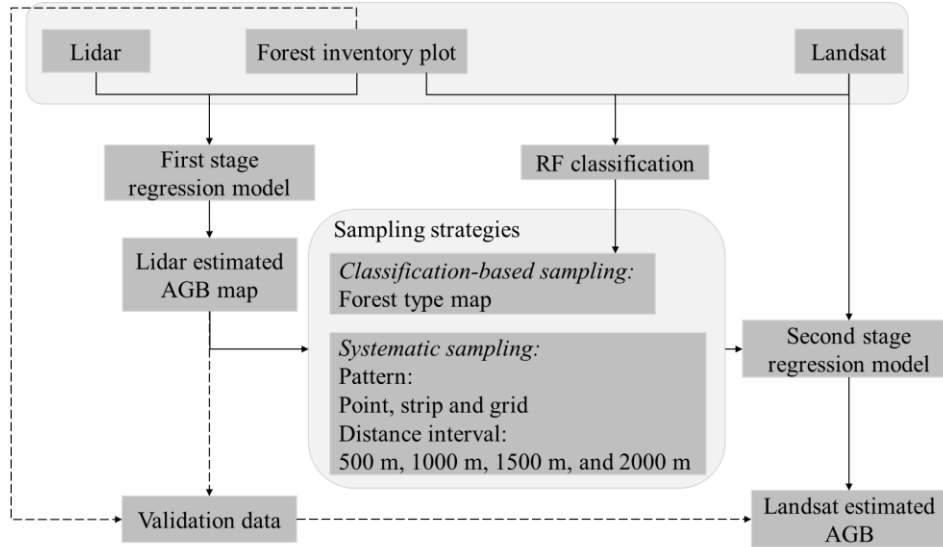
Figure 3-3. Flowchart of the research process including data, sampling strategies, methods and results.

3.3.5.2. Regression and variable selection

This study explored the relationship between AGB and remote sensing derived variables using regression models based on the equation below:

$$AGB_i = \beta_0 + \sum_{j=1}^{p} \beta_j X_{ij} + \varepsilon_i (i = 1, ..., n) \tag{3-1}$$

where β_0 is the intercept, β_j are model coefficients, and X_{ij} represents the remote sensing derived predictors. As discussed in the prior section, regression models were built in two distinct steps within the work flow (Figure 3-3). In the first stage regression model, the dependent variable was AGB for the 270 plots within the Huntington area and the predictors were selected from lidar derived variables using the forward variable selection method. Similar to prior studies (Ali et al., 2019; Van Vinh et al., 2019), using the natural logarithm of both dependent and predictor variables was found to achieve better performance for the first stage regression model. The second component of the analysis applied equation 3-1 to develop regression models for a

series of different sampling strategies (described in the next section). Shown as second stage regression models in Figure 3-3, these models used a sample of the lidar estimated AGB values as the dependent variable and Landsat variables as predictors without variable selection. All variables were used to facilitate comparison by ensuring all second stage regression models had the same predictors.

There are several commonly used variable selection methods when applying multiple linear regression: forward, backward, and stepwise selection. Forward selection starts with the most significant variable in the model and sequentially adds the next most significant variable into the model until none of the remaining variables are significant. Backward selection starts with all variables in the model and successively removes the least significant variable until all the variables in the model are significant at a chosen level. Stepwise selection adds or removes one variable at each step to ensure all variables in the model are significant while no variable outside the model is significant enough to enter the model. Forward selection was applied when building the first stage regression model because it supported easy application of the following procedures.

3.3.5.3. Lidar sampling strategies

Two sampling strategies were adopted in this study: systematic and classification-based sampling. In systematic sampling, combinations of three sampling patterns (point, strip, and grid) and four sampling intervals (500 m, 1000 m, 1500 m, and 2000 m) were applied to acquire twelve systematic lidar samples (Figure 3-4). A northwest-southeast alignment was applied to be consistent with the airplane flight path used during the lidar acquisition. The classification-based sampling used the same sampling pattern and amount of data as the best performing systematic

sampling strategy. However, instead of using a pre-defined distance interval, the classification-based sampling selected data based on the forest type distribution within the samples.

Based on the 542 m lidar data acquisition swath width, a 500×500 m square area was chosen as the basic sampling unit at Huntington. However, given the smaller forest extent of our test site, for the Heiberg area, a 200×200 m square area was chosen as the basic sampling unit. By reducing the basic sampling unit at Heiberg, we kept the overall area percentage sampled consistent with the Huntington analysis.
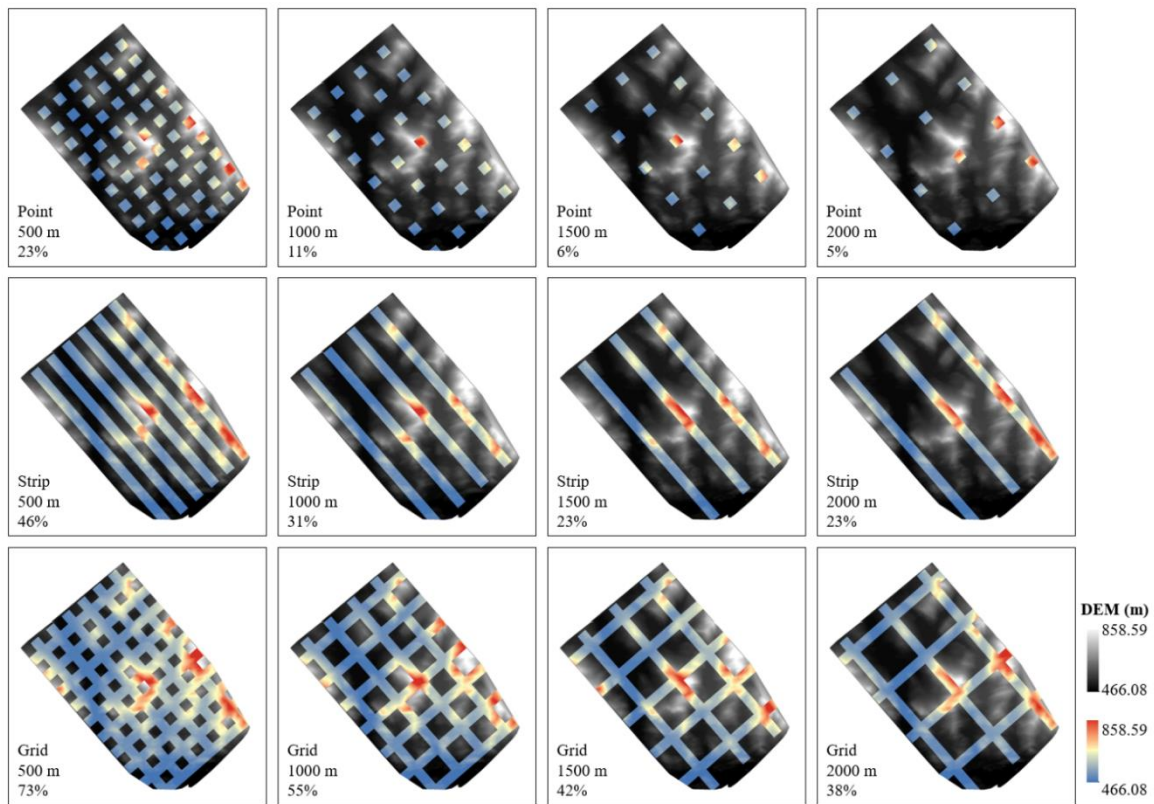
Figure 3-4. Distribution of lidar samples generated from twelve systematic lidar sampling strategies. Each sampling strategy had a unique combination of sampling pattern, distance interval, and percentage of sampled area as indicated in the lower left corner of each panel. Sampled area is shown in color on top of the greyscale digital elevation model.

3.3.5.4. RF classification of forest type for classification-based sampling

RF is a non-parametric machine learning algorithm that was implemented in this study using the "RandomForest" package (Liaw and Wiener, 2002) within the R software environment (http://www.R-project.org). RF can be used for regression or classification depending on the type of variable to be estimated. Compared with linear regression techniques, RF has lower bias and avoids overfitting (Boisvenue et al., 2016; Ghosh and Behera, 2018; Gleason and Im, 2012; Tian et al., 2017). RF grows many trees to vote for a result, which makes it insensitive to outliers and noise (Ghosh and Behera, 2018; Gleason and Im, 2012). For each tree, approximately two-thirds of the original data was randomly chosen to build the tree, and the remaining data was used for estimating out-of-bag error and calculating variable importance. In this study, RF was applied to develop a forest type classification map using forest inventory plots as reference data and Landsat derived variables as predictors. Default RF parameters were applied: 500 for ntree, square foot of the total predictors for mtry, and 1 for nodesize.

3.3.5.5. Chi-square test for selecting classification-based samples

For the classification-based sampling, there is a need to identify a sample that represents the overall distribution of forests within the study site. There are multiple approaches that can be used to explore the relationship between a sample and the population. The chi-square goodness of fit test is used to determine whether an observed categorical variable frequency distribution differs from an expected distribution.

$$\chi^2 = \sum \frac{(O_i - E_i)^2}{E_i}$$

$$E_i = Np_i$$

(3-2)

where O_i is the observed frequency, E_i is the expected frequency, N is total number of observations, and p_i is percentage of type i in the expected distribution. The similarity between observed and expected distribution can be reflected from χ^2 value. Smaller χ^2 value indicates more similar distributions. In this study, forest type distribution from the sampled area was our observed distribution and forest type distribution from the whole study area was our expected distribution. We divided study site into multiple non-overlapping strips. Using this method, we calculated the χ^2 value between the whole study area and each strip based on forest type distribution. Smaller χ^2 values correspond to strips forest type composition that was more similar to the whole study site.

3.3.5.6. Accuracy assessment for second stage regression models

Second stage regression models were assessed using model fitting R^2. In addition, the Landsat AGB estimations generated from second stage regression models were compared to plot and lidar estimated AGB with accuracy reported using RMSE and RRMSE. The plot estimated AGB was calculated from ground inventory plots and the lidar estimated AGB was the estimated AGB value generated by applying the first stage regression model to the whole area. Plot estimated AGB was considered the best estimate of actual AGB. Therefore, plot tested RMSE was given more importance in terms of model comparison.

$$RMSE = \sqrt{\frac{1}{m}\sum_{k=1}^{m}(AGB_{Landsat,k} - AGB_{ref,k})^2} \tag{3-3}$$

$$RRMSE = \frac{RMSE}{\frac{1}{m}\sum_{k=1}^{m}(AGB_{ref,k})} \tag{3-4}$$

where $AGB_{Landsat,k}$ is Landsat derived AGB from second stage regression models, $AGB_{ref,k}$ is plot or lidar derived AGB, m is the number of validation data (k = 1, 2, …, m).

3.4. Results

3.4.1. Full lidar coverage AGB estimation

All 270 forest inventory plots in Huntington were used when establishing the relationship between plot AGB and the lidar derived variables using the first stage regression model. The regression equation for the final model selected is shown in Equation 3-5. This equation shows the two variables selected through the forward variable selection process: ht_P90 (90th percentile of lidar point heights) and Per_first_mean (percentage of first returns above mean return height within each plot). The model has an R^2 of 0.58, RMSE of 67.9 Mg ha^{-1}, and RRMSE of 36.4%. Figure 3-5 shows a scatter plot illustrating the relationship between the field-based plot AGB and the lidar estimated AGB for the Huntington site.

$$AGB_{plot} = e^{-4.41 + 2.61 \times \ln(ht\_P90) + 0.39 \times ln\,(Per\_first\_mean)} \tag{3-5}$$
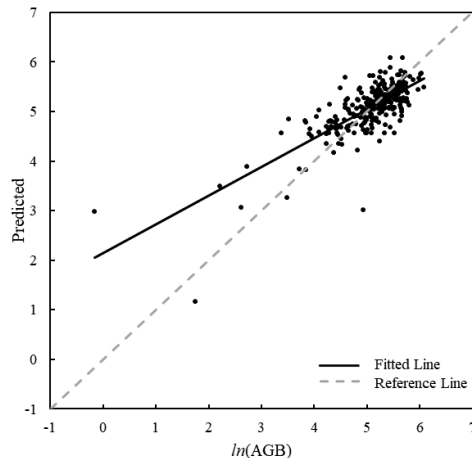
Figure 3-5. Scatter plot between plot and lidar estimated AGB at the Huntington Wildlife Forest.

Raster layers of ht_P90 and Per_first_mean covering the whole area were created from the lidar point data. A cell size of 30 m was adopted for both raster layers to be consistent with the Landsat spatial resolution. The two raster layers were then applied in Equation 3-5 to generate a lidar estimated AGB map for Huntington (Figure 3-6).
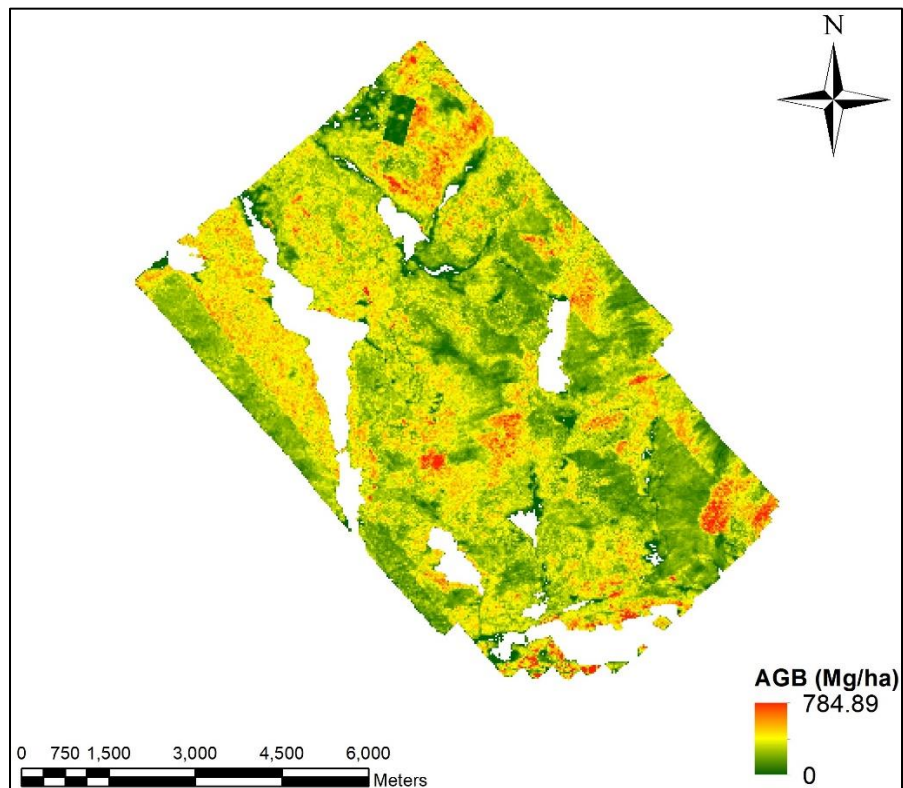
Figure 3-6. Lidar estimated AGB distribution map calculated using Equation 3-5 and the lidar derived ht_P90 and Per_first_mean raster layers. Lidar estimated AGB value at Huntington ranged from 0 to 784.89 Mg/ha. Water areas were masked out.

3.4.2. Systematic sampling AGB estimation for the Huntington area

We used the AGB data developed from the full lidar coverage using Equation 3-5 as a baseline to see if the Landsat based AGB model using lidar samples can achieve accuracies that approached that of the more expensive full lidar coverage AGB estimation. Several second stage

regression models were built for each sampling strategy. The model for each sampling strategy was evaluated by looking at the model fitting R^2, RMSE and RRMSE values calculated using both the field-based plot AGB and the lidar estimated AGB as references (Table 3-5). The number of pixels applied for building the regression models is also summarized in Table 3-5.

The first stage regression model shown in Equation 3-5 that used the full lidar coverage had an R^2 of 0.58. Of the systematic sampling strategies, point sampling at a sample interval of 1500 m showed the highest R^2 at 0.41. The point pattern generally outperformed the strip and grid patterns with higher R^2 values at sample intervals of 1000 m, 1500 m, and 2000 m. None of the twelve systematic sampling strategies explored matched the RMSE and RRMSE values for AGB derived from the full lidar coverage. Using the full lidar coverage, the RMSE was 67.9 Mg ha^{-1} and RRMSE was 36.4% using the field-derived plot observations as a reference. Plot-based RMSE and RRMSE for the systematic sampling strategies ranged from 84.2–93.9 Mg ha^{-1} and 45.1%–50.3%, respectively, while the lidar based RMSE and RRMSE ranged 70.5–81.1 Mg ha^{-1} and 40.9%–47.0%, respectively. The strip sampling strategies had the lowest average RMSE and RRMSE values, but they also had the highest variation among different distance intervals. Strip sampling at 1500 m had the lowest plot and lidar based RMSE and RRMSE values among all systematic sampling strategies.

Table 3-5. Evaluation of the second stage regression models developed for the twelve systematic sampling strategies developed from combinations of three sampling patterns (grid, point, strip) and four distance intervals (500 m, 1000 m, 1500 m, 2000 m). Models were evaluated based on model fitting R^2, and plot and lidar AGB based RMSE and RRMSE values.

Sampling strategy		Model fitting		Model testing			
				Plot based reference		Lidar based reference	
		Pixel Count	R^2	RMSE (Mg ha^{-1})	RRMSE (%)	RMSE (Mg ha^{-1})	RRMSE (%)
Point	500 m	14772	0.20	89.3	47.8	71.7	41.6
	1000 m	6880	0.30	92.8	49.7	76.5	44.4
	1500 m	3906	0.41	93.9	50.3	81.1	47.0
	2000 m	3268	0.31	90.1	48.3	74.3	43.1
Strip	500 m	29743	0.24	89.7	48.1	72.2	41.9
	1000 m	19727	0.23	92.5	49.6	74.6	43.3
	1500 m	15335	0.19	84.2	45.1	70.5	40.9
	2000 m	15193	0.14	87.3	46.8	70.8	41.0
Grid	500 m	45962	0.22	89.3	47.9	71.9	41.7
	1000 m	34185	0.24	91.0	48.8	73.3	42.5
	1500 m	27316	0.22	88.7	47.5	72.1	41.8
	2000 m	24735	0.19	91.8	49.2	73.4	42.6

Overall, although the point sampling generally had higher R^2 values, the strip sampling approach had smaller RMSE and RRMSE values when assessed using the field-based AGB values. Strip sampling also matches the nature of airplane flight paths, which renders it easy to adopt from a practical viewpoint. Therefore, strip pattern was applied for further analysis.

The location of the starting point for the systematic sampling determines the location of all subsequent samples. To evaluate the sensitivity of the AGB estimates to this starting point and examine the stability of systematic sampling, we tested five different starting points for the strip sampling using a 1500 m interval. Figure 3-7 illustrates the arrangement of the five systematic strip sampling layouts with 500 m swath width and a distance interval of 1500 m.
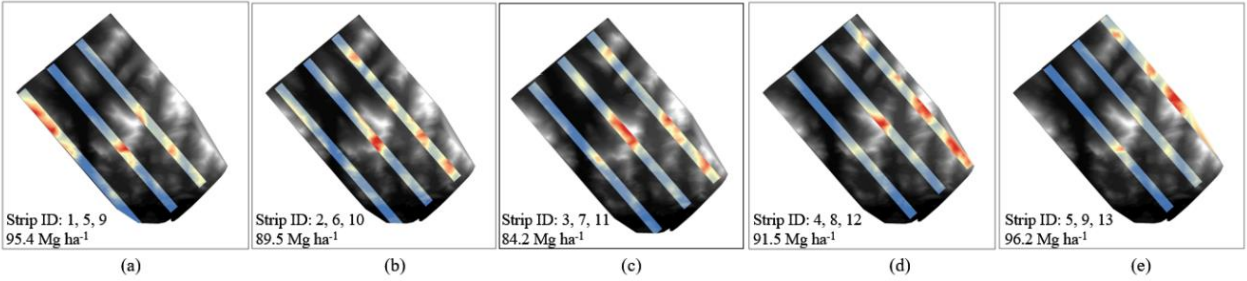
Figure 3-7. Possible outcomes using strip sampling pattern at the distance interval of 1500 m. The sampled strip ID and plot based RMSE values are listed in the lower left corner of each part of the figure.

Given the variability shown in these five alternatives, we also explored the variability based on random selection of 3 of the 13 non-overlapping strips available for this property. This led to a total of 286 combinations, with plot based RMSE values summarized in Figure 3-8. The plot based RMSE values that came from randomly selecting 3 strips ranged from 80.1–102.0 Mg ha^{-1}.
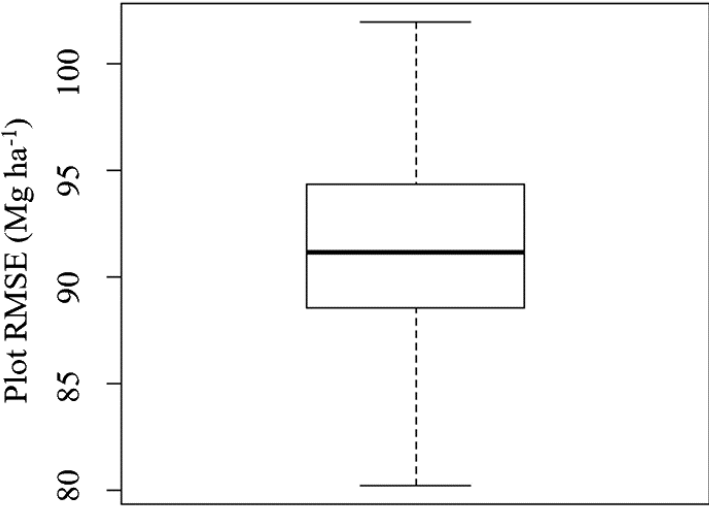
Figure 3-8. The boxplot summarizing plot based RMSE values from 286 possible sampling outcomes that were generated by randomly selecting 3 of the 13 total strips on the Huntington site.

3.4.3. Classification-based sampling AGB estimation for the Huntington area

The second sampling approach explored used a classification-based framework. We used a strip sampling structure at distance interval of 1500 m to select three strips of the forest type map generated from the Landsat data using a RF classification. The forest type classification map identified three classes: hardwood, mixed, and softwood forests. As with the systematic sampling, the Huntington study site was covered with 13, 500m wide non-overlapping strips. The distribution of strips and strip ID are shown in Figure 3-9.
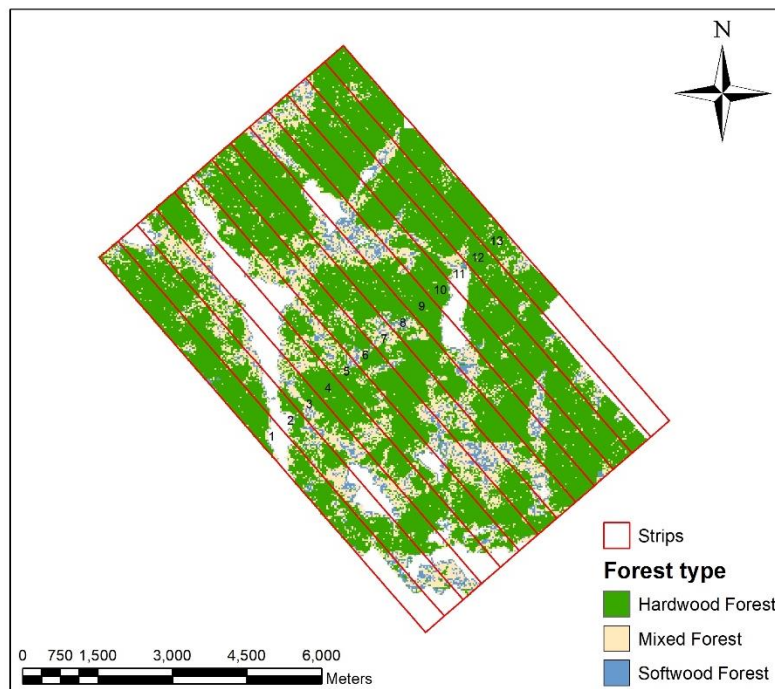
Figure 3-9. RF forest type classification of the Huntington site. Classification used Landsat derived variables as predictors and plot inventory information as a reference. Strips (with ID labeled) used for sampling are overlaid on top of the classification map.

In order to select strips that best represented the entire study site, the frequency of each forest type was summarized within each strip and in the full dataset and Chi-square goodness of fit values were calculated. Strips with smaller chi-square values had a forest class distribution

that was closer to the full data than strips with larger chi-square values. Strips 6, 7, 8 had the smallest chi-square values (Figure 3-10), thus were selected to provide the classification-based lidar sample.
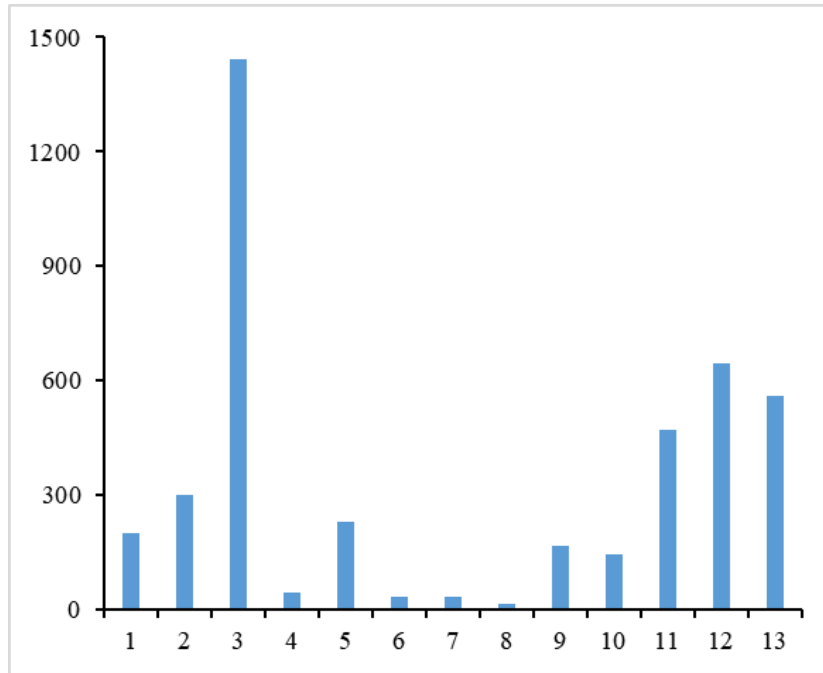
Figure 3-10. Chi-square values between the full coverage and each strip in terms of forest type frequency. X axis is strip name and Y axis is chi-square goodness of fit value.

Lidar estimated AGB within strips 6, 7, and 8 was used to build a regression model with Landsat derived variables as predictors. The model results are shown in Table 3-6. The R^2 for the classification-based sampling is generally higher than any of the twelve systematic sampling strategies and the plot and lidar tested RMSE and RRMSE values are generally smaller. Overall, the classification-based sampling outperformed 75% of the systematic sampling strategies.

Table 3-6. Results of the classification-based sampling model at the Huntington site.

Sampling strategy	Model fitting		Model testing			
			Plot based reference		Lidar based reference	
	Pixel Count	R^2	RMSE (Mg ha^{-1})	RRMSE (%)	RMSE (Mg ha^{-1})	RRMSE (%)
Strip 6, 7, 8	16446	0.26	87.4	47.0	70.9	41.0

3.4.4. Testing classification-based sampling for the Heiberg data

A first stage regression model was built between plot AGB for all 43 Heiberg forest inventory plots and lidar derived variables following the same procedure as in the Huntington site. The regression model is shown in Equation 3-6. The two lidar variables identified through the forward selection process were the 95th percentile of lidar point heights (ht_P95) and the percentage of first returns above 5 m (Per_first_5m). The model had R^2 of 0.74, RMSE of 91.4 Mg ha^{-1}, and RRMSE of 42.6%. Raster layers for ht_P95 and Per_first_5m were created from the Heiberg lidar points with pixel size of 30 m. The two raster layers were applied to Equation 3-6 to acquire lidar estimation of AGB for Heiberg.

$$AGB_{plot} = e^{1.05 + 0.08 \times ht\_P95 + 0.03 \times Per\_first\_5m}$$
(3-6)

To test the transferability of the classification-based sampling method, we applied the procedure developed at Huntington to the Heiberg study area. The forest type classification map with three forest classes (hardwood, mixed, and softwood forests) was produced using RF based on forest inventory plot and Landsat data. The Heiberg site was smaller than the Huntington site, hence was divided into seven, 200 m wide strips along the flight path used to acquire the lidar data. Chi-square values were calculated between full data and each strip based on the distributions of forest type classes. As shown in Figure 3-11, strip 2, 4, 7 had the smallest chi-

square values hence lidar estimated AGB values in those strips were used as the dependent variable and Landsat variables were used as predictors in the regression model.
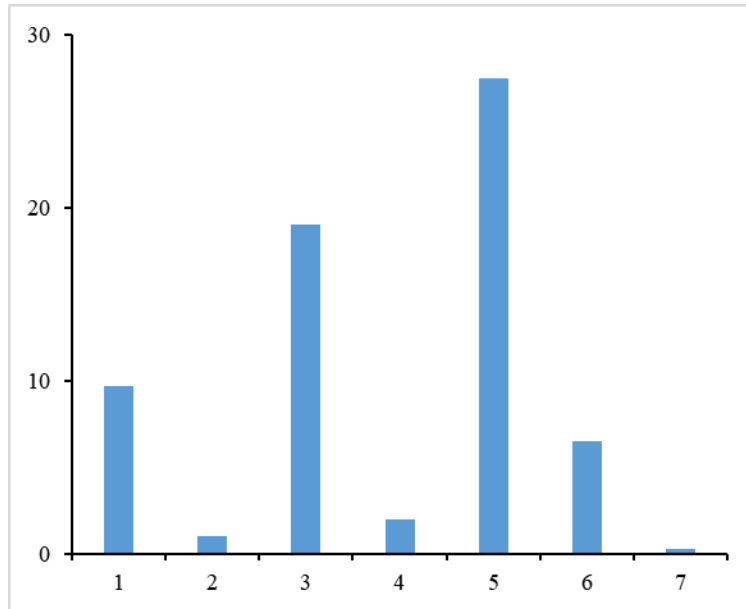
Figure 3-11. Chi-square values between all data and each strip. X axis is strip name and Y axis is chi-square value.

The regression model built using the sample strips was then applied to the Landsat data covering the Heiberg study area to acquire AGB estimates. Landsat AGB estimates were tested using plot and lidar estimated AGB values (Table 3-7). Compared with using full lidar coverage, the classification-based sampling decreased R^2 value from 0.74 to 0.40. Plot and lidar tested RMSE and RRMSE values also increased.

Table 3-7. Results of the classification-based sampling model at the Heiberg site.

Sampling strategy	Model fitting		Model testing			
			Plot based reference		Lidar based reference	
	Pixel Count	R^2	RMSE (Mg ha^{-1})	RRMSE (%)	RMSE (Mg ha^{-1})	RRMSE (%)
Strip 2, 4, 7	2097	0.40	108.18	50.4	136.0	63.4

3.5. Discussion

In this study we aimed to determine if samples of lidar data could be combined with forest inventory data and Landsat imagery to produce viable wall-to-wall maps of AGB. In particular, this study aimed to assess the stability of sampling techniques in order to develop a strategy to identify lidar samples that could be fused with Landsat data to estimate AGB without substantially compromising accuracy when compared to a full lidar based model. In our study, both systematic sampling and classification-based sampling were compared to AGB derived from full lidar coverage. For our main Huntington site, when compared to having full lidar coverage, the RMSE from systematic strip sampling and classification-based sampling both had higher RMSE (by 24% or more). One possible factor to consider in reducing this difference may relate to the proportion of data sampled (Hopkinson et al., 2016; Luo et al., 2016; Saarela et al., 2015). In both sampling approaches, we limited samples to under 25% of the study area. Chen et al. (2012) compared the fusion of QuickBird imagery and different sized lidar samples and concluded that model performance for estimating forest canopy heights increased with lidar sampled area.

Another weakness for the sampling based approach lies in the use of multiple regression models (Feng et al., 2017; Li et al., 2015). In contrast to the AGB estimation based on full lidar coverage that used one regression model, in the sampling-based fusing approach, we used two regression models. By adding the second regression model, we introduced additional uncertainties from both Landsat data and the second statistical model (Skowronski et al., 2014).

Multiple studies have performed lidar sampling, with the strips being the most commonly used sampling pattern among the studies (Chen & Hay, 2011; Hilker, Wulder, & Coops, 2008;

79

Hudak et al., 2002; Tsui et al., 2013). Sampling using data strips is consistent with the nature of airplane flight planning, which makes it a good compromise between ease of use, lower cost, and accuracy. The problem faced when using systematic sampling is inconsistency. Chen and Hay (2011) stated that different lidar transects would generate different results, which is consistent with our outcomes as reported in Table 3-5, which showed the variability in the AGB estimates from the twelve systematic sampling strategies. Systematic sampling using strips at 1500 m intervals showed better performance in terms of RMSE than the other systematic sampling strategies at Huntington study area tested with plot and lidar estimated AGB.

Systematic sampling strategy outcomes are highly connected with site conditions, modeling technique and the use of auxiliary data (Almeida et al., 2019; Cao et al., 2019). Our study demonstrated that even with consistency in terms of modeling technique and auxiliary data inputs, RMSE values varied substantially (Figure 3-7) when we used different starting points to sample three strips at a constant distance interval. These RMSE values varied from outperforming all other systematic sampling strategies in Table 3-5 being the worst sampling strategy. From a practical standpoint, it would be almost impossible to discern which systematic strategy would return a good outcome since you cannot typically explore multiple systematic sampling combinations and would not be considering sampling if the full lidar coverage was available. In our study, there was no general trend in terms of the changes in accuracy with variation in systematic sampling intervals and sampling pattern. This variability may have been linked to differences in forest condition in different regions. Gregoire et al. (2010) recommended considering the AGB gradient during the sampling stage. Although Chen and Hay (2011) got similar performance from N-S and E-W direction lidar samplings, this might be attributed to the forest ecosystem in their study site which was complex and had no general trend in any direction.

If there was a general trend shown in a site, as might be the case for plantation areas, considering sampling direction is highly recommended. Our study supported prior work that demonstrated that systematic sampling is easy to apply, but the instability of the outputs suggests it has lower transferability for AGB estimation at other sites.

We applied classification-based sampling with the goal of using readily available Landsat data to select samples for acquiring lidar data that were representative of the entire study area. Land cover is an important factor in modeling AGB (Zheng et al., 2004; Zheng et al., 2007) and it is easy to overlook some forest types especially over large and heterogeneously distributed areas. Zheng et al. (2007) showed that developing individual regression models for each forest type could improve model accuracy. In general, hardwoods have high canopy cover resulting in more horizontal expansion compared to softwood (Zheng et al., 2004). Selecting lidar strips based on forest type classification result could avoid over or under representation of certain forest types. The classification-based sampling outperformed 75% of the systematic sampling strategies in Huntington study area, and more importantly, provided a means to plan lidar acquisition that was lacking in the systematic sampling approach. Adopting this method to our test Heiberg area, the classification-based sampling also worked effectively, with R^2 and RMSE values acquired from the classification-based sampling only moderately impacted when compared to the full lidar coverage model. The classification-based sampling method provides a means to substantially reduce lidar acquisition without a major compromise in accuracy while providing a preprocessing step to guide application in new study areas. The need to perform the classification does require additional analysis; however, the random nature of systematic sampling can lead to substantial, and unknown a priori, sample variability that potentially decreases transferability of this approach.

81

3.6.   Conclusion

The framework in this study provides an approach to obtain wall-to-wall estimates of AGB by merging lidar samples with Landsat imagery and forest inventory data. We focused on the AGB estimation accuracy based on systematic and classification-based lidar sampling strategies. While systematic lidar sampling can achieve promising AGB estimates and is easy to implement, there was high model outcome variability among systematic sampling strategies. Moreover, the results attained from systematic sampling strategies were highly dependent on site condition, which provides challenges in planning lidar acquisitions. Classification-based lidar sampling provides a planning framework that is more readily transferable to new sites by guiding selection of lidar samples representative of the study site. Fusion of lidar samples and Landsat had lower accuracies in AGB estimation compared with full lidar coverage, which can be exacerbated by the uncertainties introduced by the addition of Landsat data and the use of a second regression model. This study methodically compared different lidar sampling approaches to support AGB estimation. We anticipate the results of this study could facilitate cost-effective lidar data collection for use in future studies.

3.7. Reference

Ali, A., Lin, S.L., He, J.K., Kong, F.M., Yu, J.H., & Jiang, H.S. (2019). Tree crown complementarity links positive functional diversity and aboveground biomass along large-scale ecological gradients in tropical forests. *Science of The Total Environment*, 656, 45–54. https://doi.org/10.1016/j.scitotenv.2018.11.342

Almeida, D.R.A.D., Stark, S.C., Shao, G., Schietti, J., Nelson, B.W., Silva, C.A., Gorgens, E.B., Valbuena, R., Papa, D.D.A. & Brancalion, P.H.S. (2019). Optimizing the remote detection of tropical rainforest structure with airborne lidar: leaf area profile sensitivity to pulse density and spatial sampling. *Remote Sensing*, 11(1), 92. https://doi.org/10.3390/rs11010092

Bacour, C., Bréon, F.M., & Maignan, F. (2006). Normalization of the directional effects in NOAA–AVHRR reflectance measurements for an improved monitoring of vegetation cycles. *Remote Sensing of Environment*, 102(3–4), 402–413.https://doi.org/10.1016/j.rse.2006.03.006

Baghdadi, N., Le Maire, G., Bailly, J.S., Osé, K., Nouvellon, Y., Zribi, M., Lemos, C. & Hakamada, R. (2015). Evaluation of ALOS/PALSAR L-band data for the estimation of Eucalyptus plantations aboveground biomass in Brazil. IEEE Journal of Selected Topics in Applied Earth Observations and Remote Sensing, 8(8), 3802–3811. https://doi.org/10.1109/JSTARS.2014.2353661

Boisvenue, C., Smiley, B. P., White, J. C., Kurz, W. A., & Wulder, M. A. (2016). Integration of Landsat time series and field plots for forest productivity estimates in decision support models. *Forest Ecology and Management*, 376, 284–297. https://doi.org/10.1016/j.foreco.2016.06.022

Boudreau, J., Nelson, R., Margolis, H., Beaudoin, A., Guindon, L., & Kimes, D. (2008). Regional aboveground forest biomass using airborne and spaceborne LiDAR in Québec. *Remote Sensing of Environment*, 112(10), 3876–3890. https://doi.org/10.1016/j.rse.2008.06.003

Cao, L., Coops, N. C., Sun, Y., Ruan, H., Wang, G., Dai, J., & She, G. (2019). Estimating canopy structure and biomass in bamboo forests using airborne LiDAR data. *ISPRS Journal of Photogrammetry and Remote Sensing*, 148, 114–129. https://doi.org/10.1016/j.isprsjprs.2018.12.006

Chen, G., & Hay, G. J. (2011). An airborne lidar sampling strategy to model forest canopy height from Quickbird imagery and GEOBIA. *Remote Sensing of Environment*, 115(6), 1532–1542. https://doi.org/10.1016/j.rse.2011.02.012

Chen, G., Hay, G. J., & St-Onge, B. (2012). A GEOBIA framework to estimate forest parameters from lidar transects, Quickbird imagery and machine learning: A case study in Quebec, Canada. *International Journal of Applied Earth Observation and Geoinformation*, 15, 28–37. https://doi.org/10.1016/j.jag.2011.05.010

Chen, Q., Laurin, G. V., Battles, J. J., & Saah, D. (2012). Integration of airborne lidar and vegetation types derived from aerial photography for mapping aboveground live biomass. *Remote Sensing of Environment*, 121, 108–117.https://doi.org/10.1016/j.rse.2012.01.021

Ediriweera, S., Pathirana, S., Danaher, T., & Nichols, D. (2014). Estimating above-ground biomass by fusion of LiDAR and multispectral data in subtropical woody plant communities in topographically complex terrain in North-eastern Australia. *Journal of Forestry Research*, 25(4), 761–771. https://doi.org/10.1007/s11676-014-0485-7

Ene, L.T., Næsset, E., Gobakken, T., Mauya, E.W., Bollandsås, O.M., Gregoire, T.G., Ståhl, G. & Zahabu, E. (2016). Large-scale estimation of aboveground biomass in miombo woodlands using airborne laser scanning and national forest inventory data. *Remote Sensing of Environment*, 186, 626–636.https://doi.org/10.1016/j.rse.2016.09.006

Erdody, T. L., & Moskal, L. M. (2010). Fusion of LiDAR and imagery for estimating forest canopy fuels. *Remote Sensing of Environment*, 114(4), 725–737.https://doi.org/10.1016/j.rse.2009.11.002

Feng, Y., Lu, D., Chen, Q., Keller, M., Moran, E., dos-Santos, M.N., Bolfe, E.L. & Batistella, M. (2017). Examining effective use of data sources and modeling algorithms for improving biomass estimation in a moist tropical forest of the Brazilian Amazon. *International Journal of Digital Earth*, 10(10), 996–1016. https://doi.org/10.1080/17538947.2017.1301581

Ghosh, S. M., & Behera, M. D. (2018). Aboveground biomass estimation using multi-sensor data synergy and machine learning algorithms in a dense tropical forest. *Applied Geography*, 96(May), 29–40. https://doi.org/10.1016/j.apgeog.2018.05.011

Gleason, C. J., & Im, J. (2012). Forest biomass estimation from airborne LiDAR data using machine learning approaches. *Remote Sensing of Environment*, 125, 80–91. https://doi.org/10.1016/j.rse.2012.07.006

Gregoire, T. G., Ståhl, G., Næsset, E., Gobakken, T., Nelson, R., & Holm, S. (2010). Model-assisted estimation of biomass in a LiDAR sample survey in Hedmark County, Norway. *Canadian Journal of Forest Research*, 41(1), 83–95. https://doi.org/10.1139/X10-195

Hajj, M., Baghdadi, N., Fayad, I., Vieilledent, G., Bailly, J.-S., & Minh, D. (2017). Interest of Integrating Spaceborne LiDAR Data to Improve the Estimation of Biomass in High Biomass Forested Areas. *Remote Sensing*, 9(3), 213. https://doi.org/10.3390/rs9030213

Hilker, T., Wulder, M. A., & Coops, N. C. (2008). Update of forest inventory data with lidar and high spatial resolution satellite imagery. *Canadian Journal of Remote Sensing*, 34(1), 5–12. https://doi.org/10.5589/m08-004

Holmgren, J. (2004). Prediction of tree height, basal area and stem volume in forest stands using airborne laser scanning. *Scandinavian Journal of Forest Research*, 19(6), 543–553. https://doi.org/10.1080/02827580410019472

Hopkinson, C., Chasmer, L., Gynan, C., Mahoney, C., & Sitar, M. (2016). Multisensor and multispectral lidar characterization and classification of a forest environment. *Canadian Journal of Remote Sensing*, 42(5), 501–520. https://doi.org/10.1080/07038992.2016.1196584

Hudak, A. T., Lefsky, M. A., Cohen, W. B., & Berterretche, M. (2002). Integration of lidar and Landsat ETM+ data for estimating and mapping forest canopy height. *Remote Sensing of Environment*, 82(2–3), 397–416. https://doi.org/10.1016/S0034-4257(02)00056-1

Huete, A. R. (1988). A soil-adjusted vegetation index (SAVI). *Remote Sensing of Environment*, 25(3), 295–309. https://doi.org/10.1016/0034-4257(88)90106-X

Jenkins, J. C., Chojnacky, D. C., Heath, L. S., & Birdsey, R. A. (2003). National-scale biomass estimators for United States tree species. *Forest Science*, 49(1), 12–35. https://doi.org/10.1093/forestscience/49.1.12

Jordan, C. F. (1969). Derivation of leaf-area index from quality of light on the forest floor. *Ecology*, 50(4), 663–666. https://doi.org/10.2307/1936256

Knapp, N., Huth, A., Kugler, F., Papathanassiou, K., Condit, R., Hubbell, S. P., & Fischer, R. (2018). Model-assisted estimation of tropical forest biomass change: A comparison of approaches. *Remote Sensing*, 10(5), 1–23. https://doi.org/10.3390/rs10050731

Li, W., Niu, Z., Liang, X., Li, Z., Huang, N., Gao, S., Wang, C. & Muhammad, S. (2015). Geostatistical modeling using LiDAR-derived prior knowledge with SPOT-6 data to estimate temperate forest canopy cover and above-ground biomass via stratified random sampling. *International Journal of Applied Earth Observation and Geoinformation*, 41, 88–98. https://doi.org/10.1016/j.jag.2015.04.020

Liaw, A., & Wiener, M. (2002). Classification and Regression by randomForest. *R News*, 2(3), 18–22. http://CRAN.R-project.org/doc/Rnews/

Lu, D., Chen, Q., Wang, G., Moran, E., Batistella, M., Zhang, M., Vaglio Laurin, G. & Saah, D. (2012). Aboveground Forest Biomass Estimation with Landsat and LiDAR Data and Uncertainty Analysis of the Estimates. *International Journal of Forestry Research*, 2012, 1–16. https://doi.org/10.1155/2012/436537

Luo, S., Chen, J. M., Wang, C., Xi, X., Zeng, H., Peng, D., & Li, D. (2016). Effects of LiDAR point density, sampling size and height threshold on estimation accuracy of crop biophysical parameters. *Optics Express*, 24(11), 11578–11593. https://doi.org/10.1364/OE.24.011578

Maltamo, M., Eerikäinen, K., Packalén, P., & Hyyppä, J. (2006). Estimation of stem volume using laser scanning-based canopy height metrics. *Forestry*, 79(2), 217–229. https://doi.org/10.1093/forestry/cpl007

Matasci, G., Hermosilla, T., Wulder, M.A., White, J.C., Coops, N.C., Hobart, G.W. & Zald, H.S. (2018). Large-area mapping of Canadian boreal forest cover, height, biomass and other

structural attributes using Landsat composites and lidar plots. *Remote Sensing of Environment*, 209, 90–106. https://doi.org/10.1016/j.rse.2017.12.020

McGaughey, R. J. (2019, February 21). FUSION/LDV: Software for LIDAR Data Analysis and Visualization. Retrieved from http://forsys.cfr.washington.edu/Software/FUSION/FUSION_manual.pdf

Mitchard, E.T., Saatchi, S.S., Woodhouse, I.H., Nangendo, G., Ribeiro, N.S., Williams, M., Ryan, C.M., Lewis, S.L., Feldpausch, T.R. & Meir, P. (2009). Using satellite radar backscatter to predict above-ground woody biomass: A consistent relationship across four different African landscapes. *Geophysical Research Letters*, 36(23). https://doi.org/10.1029/2009GL040692

Næsset, E., Gobakken, T., & Nelson, R. (2009). Sampling and mapping forest volume and biomass using airborne LIDARs. In: McRoberts, Ronald E.; Reams, Gregory A.; Van Deusen, Paul C.; McWilliams, William H., Eds. Proceedings of the Eighth Annual Forest Inventory and Analysis Symposium; 2006 October 16-19; Monterey, CA. Gen. Tech. Report WO-79. Washington, DC: US Department of Agriculture, Forest Service. 297-301., 79.

Ørka, H. O., Wulder, M. A., Gobakken, T., & Næsset, E. (2012). Subalpine zone delineation using LiDAR and Landsat imagery. *Remote Sensing of Environment*, 119, 11–20. https://doi.org/10.1016/j.rse.2011.11.023

Qi, J., Chehbouni, A., Huete, A., Kerr, Y., & Sorooshian, S. (1994). A modified soil adjusted vegetation index. *Remote Sensing of Environment*, 48(2), 119–126. https://doi.org/10.1016/0034-4257(94)90134-1

Saarela, S., Grafström, A., Ståhl, G., Kangas, A., Holopainen, M., Tuominen, S., Nordkvist, K. & Hyyppä, J. (2015). Model-assisted estimation of growing stock volume using different combinations of LiDAR and Landsat data as auxiliary information. *Remote Sensing of Environment*, 158, 431–440. https://doi.org/10.1016/j.rse.2014.11.020

Shepard, J. P., Mitchell, M. J., Scott, T. J., Zhang, Y. M., & Raynal, D. J. (1989). Measurements of wet and dry deposition in a Northern Hardwood forest. *Water, Air, and Soil Pollution*, 48(1), 225–238. https://doi.org/10.1007/BF00282380

Skowronski, N. S., Clark, K. L., Gallagher, M., Birdsey, R. A., & Hom, J. L. (2014). Airborne laser scanner-assisted estimation of aboveground biomass change in a temperate oak–pine forest. *Remote Sensing of Environment*, 151, 166–174. https://doi.org/10.1016/j.rse.2013.12.015

Tian, X., Yan, M., van der Tol, C., Li, Z., Su, Z., Chen, E., Li, X., Li, L., Wang, X., Pan, X. & Gao, L. (2017). Modeling forest above-ground biomass dynamics using multi-source data and incorporated models: A case study over the qilian mountains. *Agricultural and Forest Meteorology*, 246, 1–14. https://doi.org/10.1016/j.agrformet.2017.05.026

Tsui, O. W., Coops, N. C., Wulder, M. A., & Marshall, P. L. (2013). Integrating airborne LiDAR and space-borne radar via multivariate kriging to estimate above-ground biomass. *Remote Sensing of Environment*, 139, 340–352. https://doi.org/10.1016/j.rse.2013.08.012

Tucker, C. J. (1979). Red and photographic infrared linear combinations for monitoring vegetation. *Remote Sensing of Environment*, 8(2), 127–150. https://doi.org/10.1016/0034-4257(79)90013-0

UNECE/FAO, F. (2000). Forest resources of Europe, CIS, North America, Australia, Japan and New Zealand (industrialized temperate/boreal countries): UN-ECE/FAO contribution to

the global forest resources Assessment 2000. United Nations Economic Commission for Europe. Food and Agricultural Organization.

Van Vinh, T., Marchand, C., Linh, T. V. K., Vinh, D. D., & Allenbach, M. (2019). Allometric models to estimate above-ground biomass and carbon stocks in Rhizophora apiculata tropical managed mangrove forests (Southern Viet Nam). *Forest Ecology and Management*, 434, 131–141. https://doi.org/10.1016/j.foreco.2018.12.017

Zhang, Y., Liang, S., & Sun, G. (2014). Forest biomass mapping of northeastern China using GLAS and MODIS data. *IEEE Journal of Selected Topics in Applied Earth Observations and Remote Sensing*, 7(1), 140–152.https://doi.org/ 10.1109/JSTARS.2013.2256883

Zheng, D., Rademacher, J., Chen, J., Crow, T., Bresee, M., Le Moine, J., & Ryu, S.-R. (2004). Estimating aboveground biomass using Landsat 7 ETM+ data across a managed landscape in northern Wisconsin, USA. *Remote Sensing of Environment*, 93(3), 402–411. https://doi.org/10.1016/j.rse.2004.08.008

Zheng, G., Chen, J. M., Tian, Q. J., Ju, W. M., & Xia, X. Q. (2007). Combining remote sensing imagery and forest age inventory for biomass mapping. *Journal of Environmental Management*, 85(3), 616–623. https://doi.org/10.1016/J.JENVMAN.2006.07.015

4. Manuscript 3: Evaluating the performance of Sentinel-2 and Landsat inputs to estimate aboveground biomass in temperate forests

4.1. Abstract

Quantifying forest aboveground biomass (AGB) is helpful for assessing carbon emission and sequestration and can reduce uncertainty in monitoring global carbon cycles and climate change. Remote sensing techniques have proved to be a cost-effective way to estimate forest AGB with timely and repeated observations. We compared the performance of Sentinel-2 and Landsat 8 data for quantifying AGB in a temperate forest using Random Forest (RF) regression. These missions are similar, but Sentinel-2 has higher spatial resolution and collects data from the red-edge region of the electromagnetic spectrum. We modeled AGB using three datasets: Sentinel-2, Landsat 8, and a pseudo dataset that retained the spatial resolution of Sentinel-2 but included only the spectral bands that matched those on Landsat 8. We found that while the RF model parameter values can impact model outcomes, it is more important to focus attention on variable selection. Our results showed that the incorporation of red-edge information—Sentinel-2 compared to the pseudo dataset—increased AGB estimation accuracy by approximately 6%. The additional spatial resolution—comparing the pseudo dataset to Landsat 8—improved accuracy by approximately 3%. The variable importance ranks in the RF regression model showed that in addition to the red-edge bands, the shortwave infrared bands were important either individually (in the Sentinel-2 model) or in band indices.

Keywords: Random Forest regression, red-edge bands, spatial resolution

4.2.   Introduction

Forest ecosystems serve as a carbon reservoir and provide the primary source of carbon transmission from the terrestrial environment to the atmosphere. Hence, they play a critical role in both the global carbon cycle and climate change. Deforestation and forest degradation have resulted in unforeseeable and inconsistent carbon emission that magnifies the challenge of monitoring global carbon cycle and climate change. Forest aboveground biomass (AGB) reveals information about forest structure and condition, soil nutrition allocation and productivity, thus it is useful for assessing carbon emission and sequestration. To reduce the uncertainty in monitoring global carbon cycle and climate change, it is crucial to develop a robust and cost-effective approach to estimate forest AGB that can be implemented repeatedly in a timely manner.

AGB acquisition techniques can be classified into two groups: (1) field-based measurements, which typically include destructive sampling and application of nondestructive allometric equations based on measurements of tree height or diameter at breast height (DBH), and (2) remotely sensed methods, which use terrestrial, airborne, or spaceborne remote sensing data to indirectly estimate AGB. Field measurements on regional or broader scales are not feasible due to constraints on time and other resources. With remote sensing technology, it is possible to obtain measurements from most locations, even those that are inaccessible for human. Another advantage of remote sensing is that it allows information to be attained quickly across significant extents. Remote sensing has proved to be an effective alternative for field measurements for monitoring forests at various scales with timely and repeated updates (Gonzalez et al., 2010; Liu et al., 2017; Powell et al., 2010).

The Landsat satellites have been one of the most popular remote sensing datasets for AGB estimation. With open and free access to the digital dataset archive, Landsat datasets provides continuity covering much of the globe since the 1980s. Numerous studies have proved the feasibility of Landsat data in AGB estimation (Wang et al., 2018; Zheng et al., 2004). These studies rely on both direct analysis of Landsat data as well as incorporation of indices derived from spectral bands. The normalized difference vegetation index (NDVI) is the most widely applied vegetation index extracted from Landsat data (Zhang et al., 2016). NDVI used red and near infrared portions of the electromagnetic spectrum for assessing biophysical properties, which is based around the fact that vegetation chlorophyll pigments have high absorption in the red and high reflectance in the near infrared. However, the main drawback of using NDVI and other vegetation indices is a well-documented saturation problem in that the indices asymptotically approach a saturation level after reaching a certain biomass density (Chi et al., 2017; Knapp et al., 2018; Lumbierres et al., 2017; Mutanga and Skidmore, 2004; Vafaei et al., 2018). Because of this, NDVI tends to underestimate forest biomass in dense or complex forests (Kelsey and Neff, 2014). In response to the limitations of Landsat data, several studies have underscored the need for new remote sensing data (Cao et al., 2014; Liu et al., 2017) as well as algorithms (Avitabile et al., 2012; Zhu and Liu, 2015) to accurately estimate AGB.

A newer moderate resolution remote sensing platform is Sentinel-2, which is a system of two satellites launched in 2015 and 2017 by the European Space Agency (ESA). Sentinel-2 aims to ensure continuity of high-resolution, multispectral images with a high revisit frequency. The Sentinel satellites build from the technology and experience acquired from the long standing moderate spatial resolution Landsat and Satellite Pour l'Observation de la Terre (SPOT) families. Compared with most of the publically available optical datasets, e.g. MODIS and Landsat,

Sentinel-2 provides better spectral, spatial and temporal resolutions. These enhanced characteristics have led Sentinel-2 to outperform Landsat 8 for applications such as land use and land cover classification (Forkuor et al., 2018; Schuster et al., 2012). A distinguishing characteristic of Sentinel-2 data is the inclusion of three red-edge bands. The red-edge region lies between the red and near infrared portions of the electromagnetic spectrum. This is the region where a sharp increase in vegetation reflectance takes place due to the combined effects of strong chlorophyll absorption in red wavelengths and leaf internal scattering in the near infrared wavelengths (Filella and Penuelas, 1994; Horler et al., 1983). Red edge bands have been applied in estimation of canopy and leaf chlorophyll concentration (Delegido et al., 2011; Frampton et al., 2013), leaf area index (LAI) (Delegido et al., 2011; Frampton et al., 2013; Richter et al., 2012; Sibanda et al., 2018), canopy cover (Korhonen et al., 2017), land use and land cover (Forkuor et al., 2018), growing stock volume (Chrysafis et al., 2017; Mura et al., 2018; Puliti et al., 2018), and AGB (Ghosh and Behera, 2018; Laurin et al., 2018; Pandit et al., 2018; Vafaei et al., 2018). Estimating LAI is one of the most popular applications of red edge bands. Several studies have shown that red-edge bands are strongly correlated with LAI and inclusion of red edge vegetation indices can improve LAI estimation accuracy (Korhonen et al., 2017; Mura et al., 2018; Sibanda et al., 2018). The Sentinel-2 red edge bands have also been shown to increase accuracy of Landsat 8 data for image classification (Forkuor et al., 2018).

Sentinel data has been applied to AGB estimation in tropical (Ghosh and Behera, 2018), sub-tropical (Pandit et al., 2018; Vafaei et al., 2018), and Mediterranean (Laurin et al., 2018) forests with promising results. Metrics extracted from Sentinel-2 and Landsat 8 data can be correlated to field inventoried biomass values using statistical models. Random forest (Breiman, 2001) is a non-parametric machine learning technique that has been widely applied to estimate

forest attributes (Hudak et al., 2012). Compared with commonly used statistical regression models, RF is not confined by assumptions of underlying data distributions (Immitzer et al, 2012). Additionally, RF has gained attention in the remote sensing field due to its potential to deal with many predictor variables, capture non-linear relationships, and provide variable importance information. In contrast to parametric methods, RF is also relatively insensitive to problems with small sample size (Immitzer et al., 2012). While RF has more traditionally been applied for classification rather than regression analysis (Adam et al., 2012; Ramoelo et al., 2015), the application of RF in AGB estimation holds great potential compared to other statistical methods (Verrelst et al., 2012).

The overall aim of this study is to explore the application of Sentinel-2 data in AGB estimation with a focus on understanding the potential improvement Sentinel-2 data offers over Landsat 8 imagery for deriving temperate forest AGB. We particularly seek to determine whether the new Sentinel-2 red edge bands can provide improved accuracy in forest AGB estimation and examine whether NDVI is the most appropriate vegetation index when these new bands are available. In order to achieve these aims, this study will: (1) identify the most useful Sentinel-2 bands and band combinations for AGB estimation, and (2) compare the predictive ability of Sentinel-2 and Landsat 8 for AGB estimation.

4.3. Data and materials

4.3.1. Study area

The study area was the Heiberg Memorial Forest (HMF) in Tully, New York, which is managed by the State University of New York College of Environmental Science and Forestry (SUNY-ESF; 42°47'12" N, 76°05'37" W; Figure 4-1. Location of Heiberg Memorial Forest in

New York State. The left and right images show the distribution of 37 plots in Compartment 78 and the 60 plots in Compartment 96, respectively, overlaid on a true color Sentinel-2 image composite at 10 m spatial resolution.). HMF provides educational and research resources representative of forest ecosystems in the northeastern United States for studies including forest management, wildlife management, watershed management, and soil science. HMF covers an area of approximately 16 km^2 with an elevation range of 383–625 m above mean sea level. The majority of HMF is covered with conifer plantations (6.64 km^2, 42%), Allegheny hardwoods (5.65 km^2, 36%) or open areas (2.39 km^2, 15%). Conifer species predominantly consist of Norway spruce (*Picea abies*), hemlock (*Tsuga*) species, white pine (*Pinus strobus*), and eastern larch (*Larix laricina*). Major deciduous tree genera including maple (*Acer*), ash (*Fraxinus* L.), beech (*Betula*), and basswood (*T. americana*). HMF is divided into multiple compartments serving as basic forest management units.
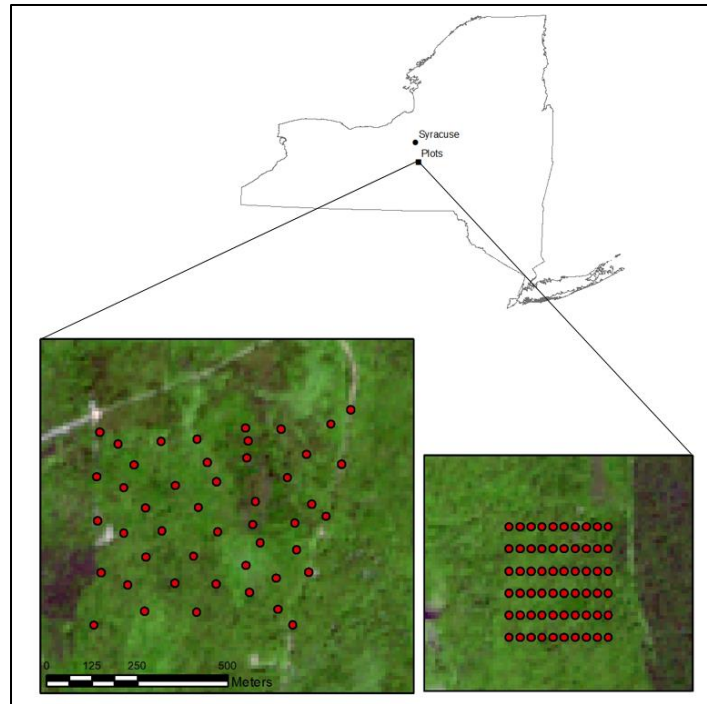
Figure 4-1. Location of Heiberg Memorial Forest in New York State. The left and right images show the distribution of 37 plots in Compartment 78 and the 60 plots in Compartment 96, respectively, overlaid on a true color Sentinel-2 image composite at 10 m spatial resolution.

4.3.2.   Data acquisition and preprocessing

4.3.2.1. Field inventory data

HMF forest inventory data from Compartment 78 and Compartment 96 was used in this study. Both compartments contain over 85% deciduous trees, predominately sugar maple (*Acer saccharum*). Compartment 78 was inventoried during April 2017 with 37 randomly distributed plots. Compartment 96 was inventoried during July 2016 with 60 plots set up in a 30.5 m × 61 m grid pattern. For both compartments, the inventories were done using a basal area factor 10 prism. The prism was held over the plot center. Any tree stem that was only partially offset when viewed through the wedge was counted as in the plots; all others were not counted. Counted trees with diameter at breast height (DBH) over approximately 2.5 cm were subsequently measured.

97

Species and DBH were recorded for each measured tree. Based on the field observations, tree-level AGB was estimated using species-specific DBH allometric equations from Jenkins et al. (2003). Plot-level AGB per area was then calculated in megagrams per hectare (Mg ha^{-1}). Descriptive statistics of plot-level AGB is shown in Table 4-1.

Table 4-1. Summary of descriptive statistics for plot level AGB in HMF (units: Mg ha^{-1})

Plot	Plot Count	Mean	Median	Variance	Minimum	Maximum
Overall	97	214.6	221.5	6808.0	32.5	357.5
Compartment 78	37	188.8	200.6	5224.8	32.5	295.7
Compartment 96	60	230.4	230.6	4280.8	88.5	357.5

4.3.2.2. Remote sensing data acquisition and pre-processing

For this study, data from Sentinel-2A (acquired on June 10, 2016) and Landsat 8 (acquired on June 16, 2016) were used to estimate forest AGB. The dates were chosen to minimize the time gap between the Sentinel-2A and Landsat data acquisitions. Both images were cloud free over the HMF area.

A Sentinel-2A Level-1C (L1C) image covering the entire study area was downloaded from the Copernicus Open Access Hub (https://scihub.copernicus.eu/dhus/#/home). The Sentinel-2A image was delivered in 100×100 km^2 tiles in UTM/WGS84 coordinates. The Level-1C product provides geometrically and radiometrically corrected Top-of-Atmosphere (TOA) reflectance measurements per pixel. Sentinel-2 Toolbox (https://sentinel.esa.int/web/sentinel/toolboxes/sentinel-2) and Sen2Cor plugin (http://step.esa.int/main/third-party-plugins-2/sen2cor/) were applied for data processing. The Sentinel-2 Toolbox includes a collection of features such as image display and navigation, layer management, band arithmetic, and region-of-interest definition. Sen2Cor performs atmospheric

correction by converting Sentinel-2 Level 1C data to a Level 2A product by converting pixel values from Top-of-Atmosphere reflectance to Bottom-of-Atmosphere reflectance. To be consistent for further analysis, all bands were resampled to 10 m pixel size using the nearest sampling method. Plots were overlaid on the Sentinel-2A data and then pixel values over each plot were extracted for further analysis.

An orthorectified Landsat 8 Operational Land Imager (OLI) image (path/row: 15/30) was downloaded from the United States Geological Survey Earth Explorer website (https://earthexplorer.usgs.gov/). Radiometric correction and atmosphere correction were performed using ENVI 5.2 (http://www.harrisgeospatial.com/Software-Technology/ENVI). Using the metadata associated with the downloaded image, we applied radiometric correction to convert raw digital numbers into reflectance and remove the impact of scene illumination and viewing geometry. Dark object subtraction was applied for atmosphere correction, which is intended to remove the effects of atmosphere scattering and absorption. Spectral values from pixels corresponding to plot locations were extracted for analysis.

4.3.3. Remote sensing data comparison

The ESA Sentinel-2 satellite system provides optical images with more spectral bands and finer spatial resolution than Landsat 8. The Sentinel-2 Multispectral Instrument (MSI) that is onboard the Sentinel-2A and Sentinel-2B satellites acquires data in 13 spectral bands: four bands at 10 m, six bands at 20 m, and three bands at 60 m (https://earth.esa.int/web/sentinel/user-guides/sentinel-2-msi/overview). Landsat 8 has 9 spectral bands: eight bands at 30 m and one band at 15 m (https://landsat.usgs.gov/). Table 4-2 summarizes the Sentinel-2 and Landsat 8 band designations. Bands that have similar wavelength ranges are in the same row.

Ten Sentinel-2 spectral bands were applied for data analysis: three visible bands (S2, S3, S4), three red edge bands (S5, S6, S7), two near-infrared (NIR) bands (S8, S8a) and two shortwave infrared (SWIR) bands (S11, S12). Six Landsat 8 bands were applied in the analysis: three visible bands (L2, L3, L4), one NIR band (L5) and two SWIR bands (L6, L7). Compared to Landsat 8, Sentinel 2 has finer spatial resolution as well as three additional red edge bands. A simple comparison between Sentinel-2 and Landsat 8 data may not discern whether differences are due to the finer spatial resolution or red edge bands. Therefore, we generated a pseudo dataset by reducing the Sentinel-2 dataset to use only bands that matched the spectral range of the Landsat 8 bands while retaining the Sentinel-2 spatial resolution. Sentinel-2 bands S2, S3, S4, S8a, S11, S12 in the pseudo dataset spectrally match Landsat 8 bands L2, L3, L4, L5, L6, and L7, respectively. To distinguish the sets of bands during analysis, we referred to this subset of Sentinel-2 bands using labels P1–P6. Table 4-2 showed the spectral range and corresponding label for the three different datasets used in the analysis. Sentinel-2 and the pseudo dataset have the same spatial resolution, but the Sentinel-2 dataset has three more red edge bands and one more NIR band. The pseudo dataset has similar band spectral ranges as Landsat 8, but with finer spatial resolution.

Table 4-2. Band designations for Sentinel-2, pseudo dataset (i.e. relabeled Sentinel-2 bands), and Landsat 8. Bands with similar spectral range are in the same row. Band labels in bold are those applied in this study. NIR: near infrared; SWIR: shortwave infrared.

	Sentinel-2 MSI			Pseudo dataset	Landsat 8 OLI		
	Band	Wavelength (nm)	Pixel size (m)	Band	Band	Wavelength (nm)	Pixel size (m)
Coastal aerosol	S1	433–453	60		L1	435–451	30
Blue	**S2**	458–523	10	**P1**	**L2**	452–512	30
Green	**S3**	543–578	10	**P2**	**L3**	533–590	30
Red	**S4**	650–680	10	**P3**	**L4**	636–673	30
Red edge 1	**S5**	698–713	20				
Red edge 2	**S6**	733–748	20				
Red edge 3	**S7**	773–793	20				
NIR	**S8**	785—900	10				
NIR	**S8a**	855–875	20	**P4**	**L5**	851–879	30
Water vapor	S9	935–955	60				
Cirrus	S10	1360–1390	60		L9	1363–1384	30
SWIR 1	**S11**	1565–1655	20	**P5**	**L6**	1566–1651	30
SWIR 2	**S12**	2100–2280	20	**P6**	**L7**	2107–2294	30
Panchromatic					L8	503–676	15

4.3.4. Statistical analysis

4.3.4.1. Random forest

RF is a non-parametric machine learning algorithm that was implemented in this study using the "RandomForest" package (Liaw and Wiener, 2002) within the R software environment (R Development Core Team, 2008). RF can be used for regression or classification depending on the type of variable to be estimated. Compared with simple regression techniques, RF has lower bias and avoids overfitting problems (Boisvenue et al., 2016; Ghosh and Behera, 2018; Gleason and Im, 2012; Tian et al., 2017). RF grows many trees that are combined through voting to generate a result, which makes it insensitive to outliers and noise (Ghosh and Behera, 2018; Gleason and Im, 2012). For each tree, approximately two-thirds of the original data was chosen

randomly to build the tree, and the remaining data was used for estimating out-of-bag (OOB) error and calculating variable importance. Three parameters need to be optimized in the RF algorithm: ntree, mtry, and nodesize. Ntree defines the number of trees to grow. The default and most commonly used ntree value is 500. The ntree values should be large enough to get all possible results represented several times. At each node of the tree, a subset of variables was selected. Mtry is used to control the number of variables at each node. The default value of mtry depends on whether RF is applied for regression or classification. When RF is used for regression, the default value is one-third of the number of variables. When RF is used for classification, the default value is the square root of the number of variables. Nodesize represents the minimum size of nodes, which controls tree extent. The default value of nodesize is one for classification and five for regression.

In this study, we used field derived AGB values as the response variable and remote sensing derived information as predictor variables in the RF algorithm. To find the ntree and mtry value that can best predict AGB, the two parameters were optimized based on the root mean square error (RMSE) using all plot data. To determine the most suitable RF parameters, we tested ntree values from 500 to 9500 at intervals of 1000 and mtry from 1 to 20 with an increment of one. The default nodesize of five was applied throughout the study.

4.3.4.2. Vegetation indices

The normalized difference vegetation index (NDVI) has been widely applied in AGB estimation. Previous studies have demonstrated that NDVI provides a useful input for modeling AGB (Zhu and Liu, 2015). NDVI was originally proposed by Rouse et al. (1974) as:

$$NDVI = \frac{\rho_{NIR} - \rho_{Red}}{\rho_{NIR} + \rho_{Red}}$$
(4-1)

102

where ρ_{NIR} and ρ_{Red} represent the reflectance from the near infrared and red bands, respectively. While NDVI is commonly applied to vegetation-focused studies, an index can be calculated by generating the normalized difference of any pair of bands. In this study, we calculated normalized difference indices (NDI) using all pairs of bands within the Sentinel-2 and Landsat 8 datasets to determine if other band combinations—particularly using the new red edge bands—provided greater utility in AGB estimation. The general equation applied is:

$$NDI = \frac{\rho_{B_i} - \rho_{B_j}}{\rho_{B_i} + \rho_{B_j}} \ (i > j)$$

(4-2)

where ρ_{B_i} represents the reflectance from band *i*. To avoid including values with the same absolute value, we defined that B_i has higher wavelength than B_j. For the Sentinel-2 data, 10 bands (S2, S3, S4, S5, S6, S7, S8, S8A, S11, and S12) were applied in the NDI equation, which resulted in 45 different combinations. With the reduction in bands for the pseudo dataset, six bands (P1, P2, P3, P4, P5, and P6) were applied resulting in 15 NDIs. Fifteen NDIs were also calculated using the six Landsat 8 bands (L2, L3, L4, L5, L6, and L7). These NDIs and the reflectance values of the individual bands were applied to RF regression analysis.

4.3.4.3. Variable importance and selection

Variable importance can be quantified using mean decrease in accuracy (MDA) in RF. MDA is calculated based on permuting one variable while keeping other variables constant. The evaluation process first calculates differences of OOB data prediction errors with and without permutation of one variable in each tree. Then, the OOB data prediction errors among all trees are averaged and normalized to obtain the MDA for that variable (Breiman, 2001). This process is repeated for all variables.

After ranking the predictors with MDA, the challenge was to minimize the number of predictors while keeping the predictive power as strong as with using all predictors (Ismail and Mutanga, 2010). There are several commonly used variable selection methods: forward selection, backward selection, and stepwise selection. Forward selection starts with the most significant variable in the model and adds the most significant variable among the remaining variables into the model one at a time until none of the remaining variables is significant. Backward selection starts with all variables in the model and removes the least significant variable one by one until all the variables in the model are significant at a chosen level. Stepwise selection adds or removes one variable at each step to ensure all variables in the model are significant while none of the variables outside the model are significant to enter the model. MDA is frequently used for RF variable selection (Belgiu and Drăguţ, 2016; Karlson et al., 2015; Rhee and Im, 2017). A backward selection method was implemented in this study. This method starts with all predictors in the model and then progressively eliminates the variable with the least MDA. At each iteration, the model applied default RF parameters. The smallest subset of variables with lowest RMSE value was then selected to build a reduced model for AGB estimation. A reduced model was developed for each dataset. To test the performance of reduced models, they were compared with full model that used all predictors from the same dataset.

4.4. Results

4.4.1. Optimization of random forest regression models

RF regression was applied to five models in this study. Three of the models used pixel values corresponding to the exact plot locations from the Sentinel-2, pseudo dataset, and Landsat 8. The other two models used mean pixel values of a 3×3 window centered on each plot

location from the Sentinel-2 and pseudo datasets, which have finer spatial resolution than Landsat. The neighborhood mean models were used to explore the pixel size mismatch between Sentinel-2 and Landsat 8. In all models the dependent variable is AGB from all plots while the predictor variables include band values and NDIs calculated from two-band combinations. Table 4-3 shows the total number of predictor variables applied for variable selection in each model, which is the sum of the number of bands and NDIs.

For each model, we tracked the change of RMSE with variation in ntree (500 to 9500) and mtry (1 to 20) values (Figure 4-2). The optimal ntree and mtry values for the five models are listed in Table 4-3. In our analysis, the optimal ntree value was 500 for all of the five models, which matched the RF default value. The optimal mtry values for the three pixel-based models were close to the default value (1/3 of the number of predictor variables). However, the models based on neighborhood mean values did not follow the same trend and had smaller optimal mtry values.

The choice of ntree and mtry values did impact the random forest regression results. Within each of the five models, the RMSE values acquired with ntree of 500 have more variation than those with ntree of 9500. In the first three models (Figure 4-2(a), (b), and (c)), the RMSE values decrease as mtry moved from 1 to the default value and increased once mtry went past the default value. In the model using the Sentinel-2 neighborhood mean value (Figure 4-2(d)), the RMSE values steadily increased with mtry value. In the model using the pseudo dataset neighborhood mean value, the RMSE values briefly decreased and then followed an overall increasing trend as mtry increased. The neighborhood mean models allowed exploration of whether the plot data was better represented by pixel values (Figure 4-2(a) and (b)) or

105

neighborhood mean (Figure 4-2(d) and (e)). Our results found that the models that used pixel values had smaller RMSE values than the corresponding models used neighborhood mean values and followed a similar trend as the Landsat 8 model. Therefore, the pixel-based models were applied for identifying important predictors.

Table 4-3. Summary of parameters for the five models tested in this study. Three models used pixel values extracted from Sentinel-2, pseudo dataset and Landsat 8. Two models used 3×3 neighborhood mean extracted from the Sentinel-2 and pseudo dataset.

	Data	Number of predictors	Optimal ntree	Optimal mtry	Default mtry
Single pixel	Sentinel-2	55	500	20	18
	Pseudo dataset	21	500	8	7
	Landsat 8	21	500	7	7
Neighbor mean	Sentinel-2	55	500	8	18
	Pseudo dataset	21	500	4	7
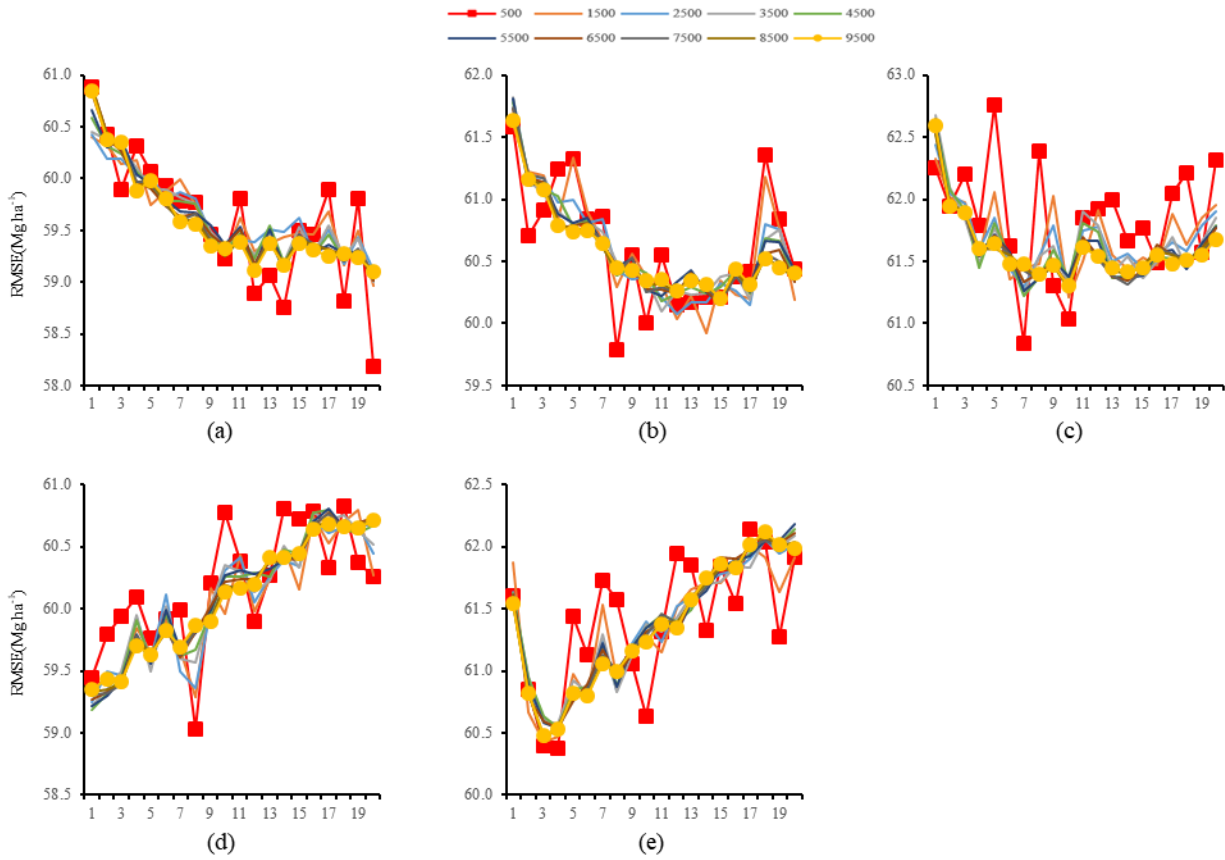
Figure 4-2. Random forest ntree and mtry optimization results from five models: (a) pixel value from Sentinel-2; (b) pixel value from the pseudo dataset; (c) pixel value from Landsat 8; (d) neighborhood mean from Sentinel-2; (e) neighborhood mean from the pseudo dataset.

4.4.2. Identifying the best single band and NDI

In each of the RF regression models, all predictors were ranked using MDA. The predictors evaluated in the model included the band values and NDIs. Predictors with higher MDA values are more important in the RF regression AGB estimation model.

Figure 4-3 shows the ranked importance of predictors in the RF regression model that used the Sentinel-2 pixel values. This model used the optimal ntree (500) and mtry (20) values with 55 predictors. For clarity, Figure 4-3 only shows the most important half of the predictors. Red edge bands (S5, S6 and S7), NIR narrow (S8A), and SWIR bands contributed to the

estimation of AGB. However, the most important predictor was the NDI combination of S7 and S3, which are red edge and green bands, respectively. The most important single band was S12, the SWIR2 band. The traditional NIR-red NDVI input (B8A and B4) ranked 48th of 55 predictors.

Figure 4-3. Variable importance in AGB estimation from Sentinel-2 pixel values using RF regression. The model was developed using ntree of 500 and mtry of 20. Higher MAD values indicate greater variable importance. This figure shows the most important 28 predictors. The remaining 27 predictors had MAD below 2.1%.

Figure 4-4 shows predictor importance measured in terms of MDA in the pseudo dataset model. This RF regression model used optimal ntree of 500 and mtry of 7 with 21 predictors. Predictors from the combination of SWIR (P5 and P6) and NIR (P4) regions contributed most to the model. The most important single band was the NIR band, which ranked 4th in variable importance. In this model, the traditional NDVI ranked 10th among the 21 predictors.
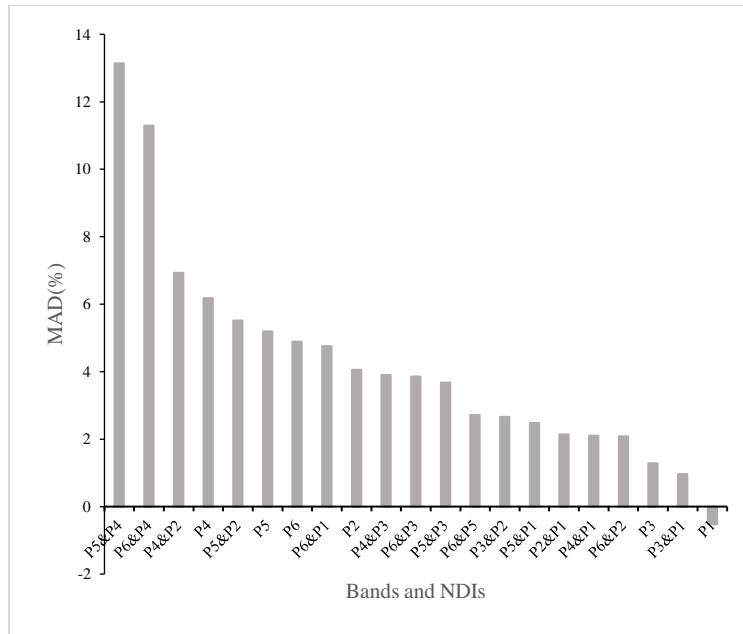
Figure 4-4. Variable importance in AGB estimation from the pseudo dataset pixel values using RF regression. The model was developed using 500 ntree and 8 mtry. Higher MAD values indicate greater variable importance.

Figure 4-5 shows predictor importance measured in terms of MDA in the Landsat 8 model. This RF regression model used optimal ntree of 500 and mtry of 8 with 21 predictors. The most important predictor in this model was the NIR band (L5) followed by the blue band (L2). The most important band combination used SWIR (L6) and NIR (L5). NDVI ranked 17th among the 21 predictors.
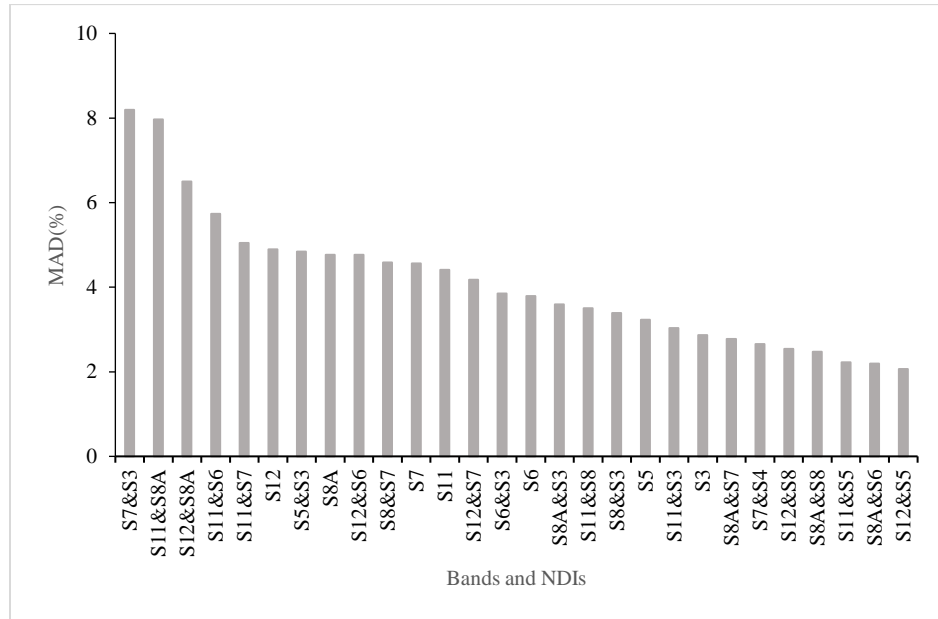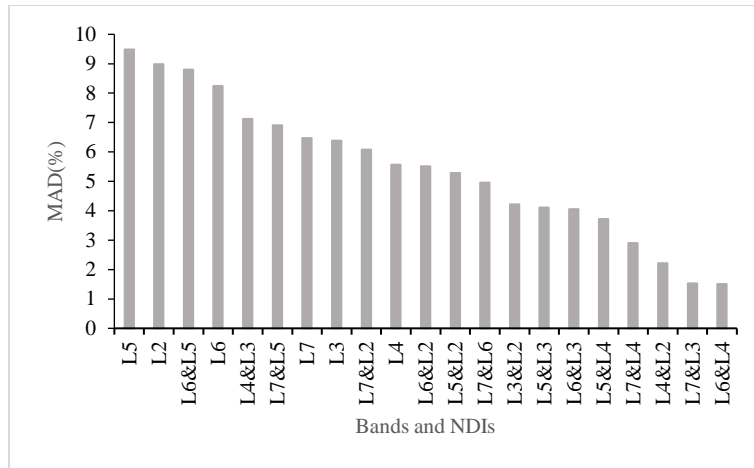
Figure 4-5. Variable importance in AGB estimation from Landsat 8 pixel values using RF regression. The model was developed using 500 ntree and 7 mtry. Higher MAD values indicate greater variable importance

To determine which spectral range has the best AGB estimation performance, we summarized the proportion of predictors within each spectral range (Visible, Red edge, NIR, and SWIR) that were in the most important 25% of the predictors (Figure 4-6). Using Sentinel-2 data, the SWIR bands contributed most for AGB estimation, followed by red-edge, NIR, and visible bands (Figure 4-6(a)). In the pseudo dataset model, the most important spectral range is NIR, followed by SWIR and visible (Figure 4-6(b)). In the Landsat 8 model, NIR is more important than visible and SWIR, which had the same percentage (Figure 4-6(c)).
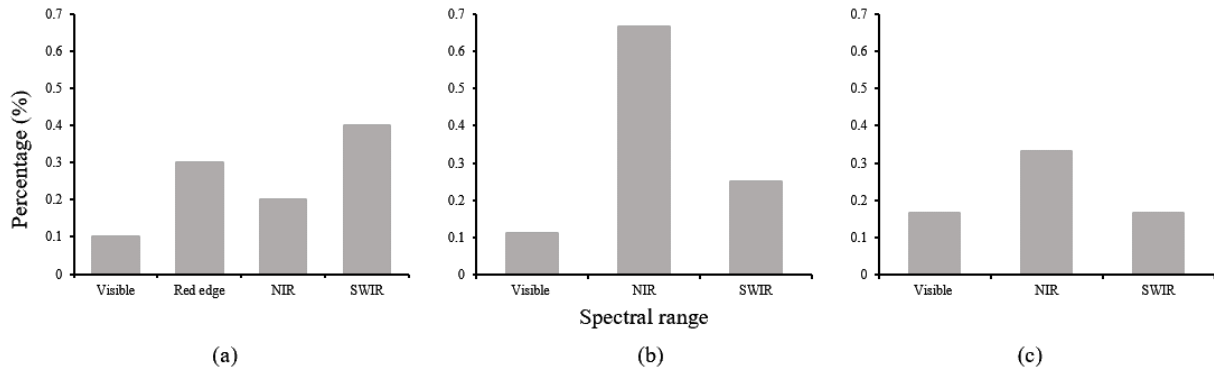
Figure 4-6. Proportion of predictors from each spectral range selected in the top 25% most important predictors: (a) Sentinel-2, (b) pseudo dataset, and (c) Landsat 8.

4.4.3. Comparison of full and reduced predictor models

RF AGB estimation models developed using all predictors were compared to models developed from a reduced set of predictors using Sentinel-2, pseudo dataset, and Landsat 8 inputs (Table 4-4). The full models used all available predictors while the reduced models used a selection of most important predictors based on backward variable selection. The reduced Sentinel-2 pixel-based model used the top 10 predictors shown in Figure 4-3, the majority of which were NDIs dominated by red-edge and SWIR bands. The pixel-based pseudo dataset model used the top 5 predictors shown in Figure 4-4, 80% of which included the NIR band. The pixel-based Landsat 8 model used the top 10 predictors shown in Figure 4-5, which included bands from across all parts of the spectrum. In the reduced neighborhood-based models, Sentinel-2 model used the three most important predictors, which were NDIs from the combination of NIR with green, red edge and SWIR bands; the pseudo dataset model used the four most important predictors, which were NDIs built from NIR in combination with visible and SWIR bands. Based on model R^2 and RMSE values, the Sentinel-2 model using all predictors

111

has better performance than the full models using the pseudo dataset predictors, while the Landsat 8 based model had the lowest performance in AGB estimation. The same trend also exists in the pixel-based reduced models and neighborhood mean full and reduced models. The pixel-based models outperformed the corresponding neighborhood mean models using the Sentinel-2 and pseudo datasets. In all cases, the reduced model returned higher R^2 value and lower RMSE value comparing with its corresponding full model. The use of the variable selection method reduced the number of predictors in the model and improved model performance.

Table 4-4. Comparison of full and reduced models using Sentinel-2, pseudo and Landsat 8 datasets

	Dataset	Variable Selection	Number of predictors	R^2	RMSE (Mg ha^{-1})
Pixel	Sentinel-2	Full	55	0.27	59.9
		Reduced	10	0.40	54.6
	Pseudo dataset	Full	21	0.24	61.3
		Reduced	5	0.31	58.4
	Landsat 8	Full	21	0.21	62.4
		Reduced	10	0.27	60.1
Neighborhood mean	Sentinel-2	Full	55	0.27	60.3
		Reduced	3	0.38	55.3
	Pseudo dataset	Full	21	0.24	61.4
		Reduced	4	0.28	59.6

4.5. Discussion

4.5.1. RF parameter tuning

Over the last two decades, the RF algorithm has received substantial attention due to its ability to solve multicollinearity and overfitting problems (Bourgoin et al., 2018; Zeng et al., 2019). The RF algorithm can also quantitatively measure the importance of predictors, which proved important in this study; regardless of the input data applied, models that used all available

predictors did not perform as well as those that were based on a subset of the most important predictors. The application of RF has been more popular in classification rather than regression focused studies, and there have been few studies applying RF for remote sensing AGB estimation. However, the robust nature of the algorithm makes it well suited for this area to provide non-redundant spectral information while improving regression accuracy (Adam et al. 2012).

There are two parameters that need to be tuned when using the RF algorithm: ntree and mtry. Unfortunately, there is no universal guidance for the selection of these two parameters and our analysis shows that the results are sensitive to parameter selection. The literature reports a range of ntree and mtry values, though these are often listed without an explanation of the values selected. For example, Karlson et al. (2015) reported they applied ntree of 1000 and mtry of the square foot of number of predictor variables. Hudak et al. (2012) used an ntree of 1000 and did not report their mtry value. In most cases, people focused more on the RF outcomes rather than the input parameters. Our results showed that the default ntree (500) and mtry (1/3 number of predictors) values used in the R software were a good starting place. However, our study results also indicated that the choice of ntree and mtry value could impact the RF outcomes, which is consistent with that reported by Mutanga et al. (2012). The default ntree value appears to include enough trees to capture sufficient outcome variability for the voting process. Conversely, while the default mtry value did produce a good outcome in general, this varied across different input datasets and selecting an optimal value for the mtry value setting may need more attention.

4.5.2. Band contributions

Our results showed that the red-edge bands available in the Sentinel-2 dataset are important for AGB estimation. After removing the red-edge bands to create the pseudo dataset, R^2 values dropped in both the full model and reduced models (Table 4-4). This model accuracy difference shows clear evidence of the additional information provided when the red-edge band is included in the analysis. Consistent with our results, Schuster et al. (2012) indicated that the incorporation of red-edge information can increase land use and land cover accuracy. Schumacher et al. (2016) also showed that red-edge indices and texture measures played an important role in wood volume estimation. The utility of the red-edge bands as compared to NIR and visible bands can be attributed to the fact that the red-edge region is insensitive to soil background and highly associated with properties of vegetation, such as chlorophyll content (Mutanga and Skidmore, 2004; Mutanga et al., 2012).

Our results also showed the SWIR bands had value for AGB estimation, which has been mentioned by prior studies in biomass estimation and in related areas (Dube et al., 2016; Lu, 2006). Verrelst et al. (2012) stated the most sensitive Sentinel-2 bands for LAI estimation were in the green and the SWIR range. Chrysafis et al. (2017) explored the correlation between growing stock volume and single Sentinel-2 bands. Among all the Sentinel-2 bands tested, the first SWIR band resulted in the highest correlated with growing stock volume and was associated with the highest linear regression R^2 value. This could be attributed to the fact that SWIR bands are sensitive to vegetation structures (Verrelst et al., 2012). However, while the SWIR bands contributed to the retrieval accuracy of biophysical parameters in our study as well as in others, they are less frequently chosen and applied than other parts of the spectrum. Moreover, these bands are often not included on some remote sensors, especially those on unmanned aerial

114

vehicles (UAVs) and on many of the high spatial resolution commercial sensors. Vegetation focused studies would benefit from incorporation of SWIR bands during the development of future generation sensors.

The model using Sentinel-2 data, retained a high proportion of red-edge bands in the top 25% of predictors. The model also included a lower proportion of the NIR bands in the most valued predictors compared to SWIR bands. On the contrary, when the pseudo dataset—without the red-edge bands—was used, a higher proportion of the NIR bands appear in the top 25% of predictors compared to the proportion of SWIR bands. The change in relative importance between NIR and SWIR bands could be attributed to the correlation among spectral bands that exists in various remote sensing datasets (Feilhauer et al., 2015; Sukawattanavijit et al., 2017), especially those with a high number of narrow spectral bands (Yue et al., 2017). Jia and Richards (1999) observed that neighboring spectral bands are more correlated than bands that are further apart. In Sentinel-2, the red-edge and NIR bands capture the spectral response from neighboring portions of the spectrum. The correlation between these regions may cause data redundancy, making the NIR bands less critical in the presence of red-edge bands.

Many research projects incorporate indices such as NDVI and other simple or normalized two-band ratios. However, there is no reason to believe the indices in common use are the optimal ones, particularly as new band passes are available. Verrelst et al. (2012) identified a three-band index that performed well for LAI estimation. Richter et al. (2012) tested hyperspectral band combinations using 2–10 bands for LAI retrieval. They concluded that the optimal number of bands ranged from 6–8. Richter et al. (2012) also concluded the importance of spectral regions for LAI retrieval was NIR, red edge, visible and SWIR, in descending order.

4.5.3. Sentinel-2 and Landsat 8 comparison

Sentinel-2 and Landsat 8 have similar orbits and fundamentally similar applications. However, Sentinel-2 has more spectral bands, larger swath width, finer spatial resolution, and with a two-satellite system, higher revisit frequency. Our results showed Sentinel-2 data can be applied to estimate AGB more accurately than Landsat 8. This appears to be attributed to both the additional red-edge bands as well as the finer spatial resolution. Our results were consistent with studies that compared Sentinel-2 and Landsat 8 in the field of land use and land cover classification (Forkuor et al., 2018).

We applied backward selection to progressively remove the variables with the least MDA until the model reached lowest RMSE. Table 4-4 indicates the number of top important predictors kept in the reduced models. The models that were reduced to include only the most important predictors were compared with full models that used all predictors. Higher R^2 and lower RMSE values highlight the improvement in model performance regardless of input dataset when the model was reduced to include only the most important predictors. This finding is in line with previous studies using the RF algorithm (Adam et al., 2014; Karlson et al., 2015). A possible explanation to the better results is that the reduced model eliminates noise propagating in the redundant data (Adam et al., 2014). Our study highlights the need to consider RF variable selection for use in similar tasks.

4.6. Conclusion

This study compared Sentinel-2 and Landsat data for AGB estimation. Our results showed that the finer spatial resolution and inclusion of red-edge bands in Sentinel-2 led to better performance than Landsat 8. The red-edge bands are crucial for estimating forest biophysical

parameters and adding red-edge bands to future Landsat missions could provide substantial value for vegetation-focused studies. Additionally, the value of the SWIR bands deserves more attention. The traditional and popular NDVI did not rate highly in AGB estimations compared to NDIs associated with red-edge and SWIR bands. While this study found value in two-band NDIs that included red-edge and SWIR, future research may also consider incorporation of these valuable spectral regions in other ways.

Our study also explored the difference between using models that incorporated all available variables with those that used backward variable selection to reduce the variables included in the model. Our research showed that the reduced models improved model performance compared with the full models, which suggests that variable selection may be an important consideration when RF regression is applied to similar tasks. Our best RF regression ntree and mtry values are consistent with the default values (ntree = 500 and mtry = 1/3 number of predictors) in temperate forest AGB estimation. While there was some variability in output as these parameters varied, our analysis suggests that applications of RF regression should prioritize model variable selection over exploration of RF parameters when time is limited.

4.7. References

Adam, E. M., Mutanga, O., Rugege, D., & Ismail, R. (2012). Discriminating the papyrus vegetation (Cyperus papyrus L.) and its co-existent species using random forest and hyperspectral data resampled to HYMAP. *International Journal of Remote Sensing*, *33*(2), 552–569. https://doi.org/10.1080/01431161.2010.543182

Adam, E., Mutanga, O., Abdel-Rahman, E. M., & Ismail, R. (2014). Estimating standing biomass in papyrus (Cyperus papyrus L.) swamp: Exploratory of in situ hyperspectral indices and random forest regression. *International Journal of Remote Sensing*, *35*(2), 693–714. https://doi.org/10.1080/01431161.2013.870676

Avitabile, V., Baccini, A., Friedl, M. A., & Schmullius, C. (2012). Capabilities and limitations of Landsat and land cover data for aboveground woody biomass estimation of Uganda. *Remote Sensing of Environment*, *117*, 366–380. https://doi.org/10.1016/j.rse.2011.10.012

Belgiu, M., & Drăguţ, L. (2016). Random forest in remote sensing: A review of applications and future directions. *ISPRS Journal of Photogrammetry and Remote Sensing*, *114*, 24–31. https://doi.org/10.1016/j.isprsjprs.2016.01.011

Boisvenue, C., Smiley, B. P., White, J. C., Kurz, W. A., & Wulder, M. A. (2016). Integration of Landsat time series and field plots for forest productivity estimates in decision support models. *Forest Ecology and Management*, *376*, 284–297. https://doi.org/10.1016/j.foreco.2016.06.022

Bourgoin, C., Blanc, L., Bailly, J.S., Cornu, G., Berenguer, E., Oszwald, J., Tritsch, I., Laurent, F., Hasan, A., Sist, P. & Gond, V. (2018). The potential of multisource remote sensing for mapping the biomass of a degraded Amazonian forest. *Forests*, *9*(6), 303. https://doi.org/10.3390/f9060303

Breiman, L. (2001). Random forests. *Machine Learning*, *45*(1), 5–32. https://doi.org/10.1023/A:1010933404324

Cao, L., Coops, N. C., Hermosilla, T., Innes, J., Dai, J., & She, G. (2014). Using small-footprint discrete and full-waveform airborne LiDAR metrics to estimate total biomass and biomass components in subtropical forests. *Remote Sensing*, *6*(8), 7110–7135. https://doi.org/10.3390/rs6087110

Chi, H., Sun, G., Huang, J., Li, R., Ren, X., Ni, W., & Fu, A. (2017). Estimation of Forest Aboveground Biomass in Changbai Mountain Region Using ICESat/GLAS and Landsat/TM Data. *Remote Sensing*, *9*(7), 707. https://doi.org/10.3390/rs9070707

Chrysafis, I., Mallinis, G., Siachalou, S., & Patias, P. (2017). Assessing the relationships between growing stock volume and sentinel-2 imagery in a mediterranean forest ecosystem. *Remote Sensing Letters*, *8*(6), 508–517. https://doi.org/10.1080/2150704X.2017.1295479

Delegido, J., Verrelst, J., Alonso, L., & Moreno, J. (2011). Evaluation of sentinel-2 red-edge bands for empirical estimation of green LAI and chlorophyll content. *Sensors*, *11*(7), 7063–7081. https://doi.org/10.3390/s110707063

Dube, T., Mutanga, O., & Ismail, R. (2016). Quantifying aboveground biomass in African environments : A review of the trade-offs between sensor estimation accuracy and costs. *Tropical Ecology*, *57*(3), 393–405.

Feilhauer, H., Asner, G. P., & Martin, R. E. (2015). Multi-method ensemble selection of spectral bands related to leaf biochemistry. *Remote Sensing of Environment*, *164*, 57–65. https://doi.org/10.1016/j.rse.2015.03.033

Filella, I., & Penuelas, J. (1994). The red edge position and shape as indicators of plant chlorophyll content, biomass and hydric status. *International Journal of Remote Sensing*, *15*(7), 1459–1470. https://doi.org/10.1080/01431169408954177

Forkuor, G., Dimobe, K., Serme, I., & Tondoh, J. E. (2018). Landsat-8 vs. Sentinel-2: examining the added value of sentinel-2's red-edge bands to land-use and land-cover mapping in Burkina Faso. *GIScience and Remote Sensing*, *55*(3), 331–354. https://doi.org/10.1080/15481603.2017.1370169

Frampton, W. J., Dash, J., Watmough, G., & Milton, E. J. (2013). Evaluating the capabilities of Sentinel-2 for quantitative estimation of biophysical variables in vegetation. *ISPRS Journal of Photogrammetry and Remote Sensing*, *82*, 83–92. https://doi.org/10.1016/j.isprsjprs.2013.04.007

Ghosh, S. M., & Behera, M. D. (2018). Aboveground biomass estimation using multi-sensor data synergy and machine learning algorithms in a dense tropical forest. *Applied Geography*, *96*(May), 29–40. https://doi.org/10.1016/j.apgeog.2018.05.011

Gleason, C. J., & Im, J. (2012). Forest biomass estimation from airborne LiDAR data using machine learning approaches. *Remote Sensing of Environment*, *125*, 80–91. https://doi.org/10.1016/j.rse.2012.07.006

Gonzalez, P., Asner, G. P., Battles, J. J., Lefsky, M. A., Waring, K. M., & Palace, M. (2010). Forest carbon densities and uncertainties from Lidar, QuickBird, and field measurements in California. *Remote Sensing of Environment*, *114*(7), 1561–1575. https://doi.org/10.1016/j.rse.2010.02.011

Horler, D. N. H., Dockray, M., & Barber, J. (1983). The red edge of plant leaf reflectance. *International Journal of Remote Sensing*, *4*(2), 273–288. https://doi.org/10.1080/01431168308948546

Hudak, A. T., Strand, E. K., Vierling, L. A., Byrne, J. C., Eitel, J. U. H., Martinuzzi, S., & Falkowski, M. J. (2012). Quantifying aboveground forest carbon pools and fluxes from repeat LiDAR surveys. *Remote Sensing of Environment*, *123*, 25–40. https://doi.org/10.1016/j.rse.2012.02.023

Immitzer, M., Atzberger, C., & Koukal, T. (2012). Tree species classification with Random forest using very high spatial resolution 8-band worldView-2 satellite data. *Remote Sensing*, *4*(9), 2661–2693. https://doi.org/10.3390/rs4092661

Ismail, R., & Mutanga, O. (2010). A comparison of regression tree ensembles: predicting Sirex noctilio induced water stress in Pinus patula forests of KwaZulu-Natal, South Africa. *International Journal of Applied Earth Observation and Geoinformation*, *12*, S45–S51. https://doi.org/10.1016/j.jag.2009.09.004

Jenkins, J. C., Chojnacky, D. C., Heath, L. S., & Birdsey, R. A. (2003). National-Scale Biomass Estimators for United States Tree Species. *Forest Science*, *49*(1), 12–35. https://doi.org/10.1093/forestscience/49.1.12

Jia, X., & Richards, J. A. (1999). Segmented principal components transformation for efficient hyperspectral remote-sensing image display and classification. *IEEE Transactions on Geoscience and Remote Sensing*, *37*(1), 538–542.https://doi.org/ 10.1109/36.739109

Karlson, M., Ostwald, M., Reese, H., Sanou, J., Tankoano, B., & Mattsson, E. (2015). Mapping tree canopy cover and aboveground biomass in Sudano-Sahelian woodlands using

Landsat 8 and random forest. *Remote Sensing*, *7*(8), 10017–10041. https://doi.org/10.3390/rs70810017

Kelsey, K. C., & Neff, J. C. (2014). Estimates of aboveground biomass from texture analysis of landsat imagery. *Remote Sensing*, *6*(7), 6407–6422. https://doi.org/10.3390/rs6076407

Knapp, N., Huth, A., Kugler, F., Papathanassiou, K., Condit, R., Hubbell, S. P., & Fischer, R. (2018). Model-assisted estimation of tropical forest biomass change: A comparison of approaches. *Remote Sensing*, *10*(5), 1–23. https://doi.org/10.3390/rs10050731

Korhonen, L., Hadi, Packalen, P., & Rautiainen, M. (2017). Comparison of Sentinel-2 and Landsat 8 in the estimation of boreal forest canopy cover and leaf area index. *Remote Sensing of Environment*, *195*, 259–274. https://doi.org/10.1016/j.rse.2017.03.021

Laurin, Gaia Vaglio, Balling, Johannes, Corona Piermaaria, Mattioli, W. (2018). Above-ground biomass prediction by Sentinel-1 multitemporal data in central Italy with integration of ALOS2 and Sentinel-2 data. *Journal of Applied Remote Sensing*, *12*(1). https://doi.org/10.1117/1.JRS.12

Liaw, A., & Wiener, M. (2002). Classification and Regression by randomForest. *R News*, *2*(3), 18–22. http://CRAN.R-project.org/doc/Rnews/

Liu, L., Coops, N. C., Aven, N. W., & Pang, Y. (2017). Mapping urban tree species using integrated airborne hyperspectral and LiDAR remote sensing data. *Remote Sensing of Environment*, *200*, 170–182. https://doi.org/10.1016/j.rse.2017.08.010

Lu, D. (2006). The potential and challenge of remote sensing-based biomass estimation. *International Journal of Remote Sensing*, *27*(7), 1297–1328. https://doi.org/10.1080/01431160500486732

Lumbierres, M., Méndez, P., Bustamante, J., Soriguer, R., & Santamaría, L. (2017). Modeling Biomass Production in Seasonal Wetlands Using MODIS NDVI Land Surface Phenology. *Remote Sensing*, *9*(4), 392. https://doi.org/10.3390/rs9040392

Mura, M., Bottalico, F., Giannetti, F., Bertani, R., Giannini, R., Mancini, M., Orlandini, S., Travaglini, D. & Chirici, G. (2018). Exploiting the capabilities of the Sentinel-2 multi spectral instrument for predicting growing stock volume in forest ecosystems. *International Journal of Applied Earth Observation and Geoinformation*, *66*, https://doi.org/10.1016/j.jag.2017.11.013

Mutanga, O., & Skidmore, A. K. (2004). Narrow band vegetation indices overcome the saturation problem in biomass estimation. *International Journal of Remote Sensing*, *25*(19), 3999–4014. https://doi.org/10.1080/01431160310001654923

Mutanga, Onisimo, Adam, E., & Cho, M. A. (2012). High density biomass estimation for wetland vegetation using worldview-2 imagery and random forest regression algorithm. *International Journal of Applied Earth Observation and Geoinformation*, *18*(1), 399–406. https://doi.org/10.1016/j.jag.2012.03.012

Pandit, S., Tsuyuki, S., & Dube, T. (2018). Estimating above-ground biomass in sub-tropical buffer zone community forests, Nepal, using Sentinel 2 data. *Remote Sensing*, *10*(4). https://doi.org/10.3390/rs10040601

Powell, S. L., Cohen, W. B., Healey, S. P., Kennedy, R. E., Moisen, G. G., Pierce, K. B., & Ohmann, J. L. (2010). Quantification of live aboveground forest biomass dynamics with Landsat time-series and field inventory data: A comparison of empirical modeling approaches. *Remote Sensing of Environment*, *114*(5), 1053–1068. https://doi.org/10.1016/j.rse.2009.12.018

Puliti, S., Saarela, S., Gobakken, T., Ståhl, G., & Næsset, E. (2018). Combining UAV and Sentinel-2 auxiliary data for forest growing stock volume estimation through hierarchical model-based inference. *Remote Sensing of Environment*, *204*, 485–497. https://doi.org/10.1016/j.rse.2017.10.007

R Development Core Team. (2008). *R: A Language and Environment for Statistical Computing*. Retrieved from http://www.R-project.org

Ramoelo, A., Cho, M., Mathieu, R., & Skidmore, A. K. (2015). Potential of Sentinel-2 spectral configuration to assess rangeland quality. *Journal of Applied Remote Sensing*, *9*(1), 094096. https://doi.org/10.1117/1.JRS.9.094096

Rhee, J., & Im, J. (2017). Meteorological drought forecasting for ungauged areas based on machine learning: Using long-range climate forecast and remote sensing data. *Agricultural and Forest Meteorology*, *237–238*(May), 105–122. https://doi.org/10.1016/j.agrformet.2017.02.011

Richter, K., Hank, T. B., Vuolo, F., Mauser, W., & D'Urso, G. (2012). Optimal exploitation of the sentinel-2 spectral capabilities for crop leaf area index mapping. *Remote Sensing*, *4*(3), 561–582. https://doi.org/10.3390/rs4030561

Rouse Jr, J., Haas, R., Schell, J., & Deering, D. (1974). Monitoring vegetation systems in the Great Plains with ERTS.

Schumacher, P., Mislimshoeva, B., Brenning, A., Zandler, H., Brandt, M., Samimi, C., & Koellner, T. (2016). Do red edge and texture attributes from high-resolution satellite data improve wood volume estimation in a semi-arid mountainous region? *Remote Sensing*, *8*(7), 1–19. https://doi.org/10.3390/rs8070540

Schuster, C., Förster, M., & Kleinschmit, B. (2012). Testing the red edge channel for improving land-use classifications based on high-resolution multi-spectral satellite data Testing the red edge channel for improving land-use classifications based on high-resolution multi-spectral satellite data. *International Journal of Remote Sensing*, *33*(17), 5583–5599. https://doi.org/10.1080/01431161.2012.666812org/10.1080/01431161.2012.666812

Sibanda, M., Mutanga, O., Dube, T., S Vundla, T., & L Mafongoya, P. (2018). Estimating LAI and mapping canopy storage capacity for hydrological applications in wattle infested ecosystems using Sentinel-2 MSI derived red edge bands. *GIScience and Remote Sensing*, *00*(00), 1–19. https://doi.org/10.1080/15481603.2018.1492213

Sukawattanavijit, C., Chen, J., & Zhang, H. (2017). GA-SVM algorithm for improving land-cover classification using SAR and optical remote sensing data. *IEEE Geoscience and Remote Sensing Letters*, *14*(3), 284–288. https://doi.org/10.1109/LGRS.2016.2628406

Tian, X., Yan, M., van der Tol, C., Li, Z., Su, Z., Chen, E., Li, X., Li, L., Wang, X., Pan, X. & Gao, L. (2017). Modeling forest above-ground biomass dynamics using multi-source data and incorporated models: A case study over the qilian mountains. *Agricultural and Forest Meteorology*, *246*, 1–14. https://doi.org/10.1016/j.agrformet.2017.05.026

Vafaei, S., Soosani, J., Adeli, K., Fadaei, H., Naghavi, H., Pham, T., & Tien Bui, D. (2018). Improving Accuracy Estimation of Forest Aboveground Biomass Based on Incorporation of ALOS-2 PALSAR-2 and Sentinel-2A Imagery and Machine Learning: A Case Study of the Hyrcanian Forest Area (Iran). *Remote Sensing*, *10*(2), 172. https://doi.org/10.3390/rs10020172

Verrelst, J., Muñoz, J., Alonso, L., Delegido, J., Rivera, J. P., Camps-Valls, G., & Moreno, J. (2012). Machine learning regression algorithms for biophysical parameter retrieval:

Opportunities for Sentinel-2 and -3. *Remote Sensing of Environment*, *118*, 127–139. https://doi.org/10.1016/j.rse.2011.11.002

Wang, M., Sun, R., & Xiao, Z. (2018). Estimation of Forest Canopy Height and Aboveground Biomass from Spaceborne LiDAR and Landsat Imageries in Maryland. *Remote Sensing*, *10*(2), 344. https://doi.org/10.3390/rs10020344

Yue, J., Yang, G., Li, C., Li, Z., Wang, Y., Feng, H., & Xu, B. (2017). Estimation of winter wheat above-ground biomass using unmanned aerial vehicle-based snapshot hyperspectral sensor and crop height improved models. *Remote Sensing*, *9*(7), 708. https://doi.org/10.3390/rs9070708

Zeng, N., Ren, X., He, H., Zhang, L., Zhao, D., Ge, R., Niu, Z. (2019). Estimating grassland aboveground biomass on the Tibetan Plateau using a random forest algorithm. *Ecological Indicators*, *102*, 479–487. https://doi.org/10.1016/j.ecolind.2019.02.023

Zhang, B., Zhang, L., Xie, D., Yin, X., Liu, C., & Liu, G. (2016). Application of synthetic NDVI time series blended from landsat and MODIS data for grassland biomass estimation. *Remote Sensing*, *8*(1), 1–21. https://doi.org/10.3390/rs8010010

Zheng, D., Rademacher, J., Chen, J., Crow, T., Bresee, M., Le Moine, J., & Ryu, S.R. (2004). Estimating aboveground biomass using Landsat 7 ETM+ data across a managed landscape in northern Wisconsin, USA. *Remote Sensing of Environment*, *93*(3), 402–411. https://doi.org/10.1016/j.rse.2004.08.008

Zhu, X., & Liu, D. (2015). Improving forest aboveground biomass estimation using seasonal Landsat NDVI time-series. *ISPRS Journal of Photogrammetry and Remote Sensing*, *102*, 222–231. https://doi.org/10.1016/j.isprsjprs.2014.08.014

5. Conclusions and future Work

5.1. Conclusions

This dissertation focused on the use of remotely sensed data in forest aboveground biomass estimation using remotely sensed data from several sources—i.e., Landsat, Sentinel-2, and lidar. Chapter 1 introduced the field and outlined the dissertation hypotheses. In this chapter, conclusions of the dissertation are presented by revisiting the hypotheses and offering ideas for future research.

Hypothesis 1: Lidar and Landsat data fusion enhances AGB estimation compared to single source approaches.

Chapter 2 investigated the performance of AGB estimation when using Landsat and lidar data sources individually and integrated. The results of our study showed that Landsat data explained the least AGB variation due to its inherent limitation in spatial, spectral and radiometric resolutions. Lidar was more accurate than Landsat in AGB estimation, with the best AGB estimation performance coming from the models that relied on integration of lidar and Landsat data.

Hypothesis 2: AGB estimation quality varies with application of multiple linear regression (MLR), Random Forest (RF) and Geographically Weighted Regression (GWR) approaches.

In Chapter 2, we also compared the performance of MLR, RF and GWR for estimating AGB. MLR has better performance than RF, which may be attributed to the normal distribution of AGB in the plots used for model training. GWR explicitly incorporates the location of model inputs, thus can capture spatial effects. GWR performed slightly better than MLR using Landsat

127

or lidar individually, but the best performance in AGB estimation came from MLR using integration of lidar and Landsat.

Hypothesis 3: Forest type influences the performance of AGB estimation using lidar and Landsat inputs.

The results presented in Chapter 2 also showed that forest type influences the performance of lidar and Landsat AGB estimation. Forest stand-specific models produced better estimations of hardwood and mixed AGB than the pooled models when Landsat data was used. Using lidar or an integration of lidar and Landsat, models for softwood and mixed forests outperformed the corresponding pooled model. Landsat performed better for AGB estimation in hardwood plots than in softwood plots in our study. Our study showed that estimating hardwood AGB was more difficult than softwood AGB when using airborne lidar derived variables. Landsat data is sensitive to forest horizontal expansion while lidar is superior at modeling forest vertical structure. Integration of Landsat and lidar data combines the advantages from both dataset and thus results tend to be better when the data sourced are fused.

Hypothesis 4: Lidar sampling can capture the majority of AGB variation explained by full lidar coverage.

In Chapter 3, we aimed to determine how samples of lidar could best be combined with forest inventory data and Landsat imagery to produce viable wall-to-wall maps of AGB. We compared systematic sampling and classification-based sampling strategies with AGB derived from full lidar coverage. Using under 25% of full lidar coverage, the RMSE from systematic strip sampling and classification-based sampling both had higher RMSE (by 24% or more) than the full model. There was no general trend in terms of the variability in AGB estimation

accuracy with changes in systematic sampling intervals and sampling pattern. While systematic lidar sampling can achieve promising AGB accuracy and is easy to implement, there were high levels of variability among systematic sampling strategies, which may have been linked to differences in forest condition. Classification-based lidar sampling provides a planning framework that is more readily transferable to new sites by guiding selection of lidar samples representative of the study site. By applying lidar sampling, we significantly reduced lidar acquisition and processing cost without a major compromise in accuracy.

Hypothesis 5: The increased spectral and spatial resolution of Sentinel-2 improves AGB estimation outcomes compared to Landsat 8.

Sentinel-2 and Landsat 8 have similar orbits and fundamentally similar applications. However, Sentinel-2 has more spectral bands, larger swath width, finer spatial resolution, and with a two-satellite system, higher revisit frequency. In Chapter 4, we compared the performance of Sentinel-2 and Landsat 8 for AGB estimation. Our results showed Sentinel-2 data can be applied to estimate AGB more accurately than Landsat 8. The advantage of Sentinel-2 for AGB estimation appears to be attributed to both the red-edge bands as well as the finer spatial resolution. By using a pseudo dataset, we were able to explore the contribution of these two components separately. Without the red-edge bands, model accuracy decreased by approximately 6%. Without the finer spatial resolution, accuracy was approximately 3% lower. Understanding the contribution of distinct characteristics of remotely sensed data is critical to strengthen their appropriate applications.

5.2. Future research directions

In this dissertation, we explored factors that impact the accuracy of temperate forest AGB estimation, such as site condition, statistical method applied, and remotely sensed data used. This dissertation strengthened understanding of remote sensing forest AGB estimation and may help direct effective applications of remote sensing in the future. However, there are still many areas of exploration that deserve consideration.

Plot measurements often serve as a source of ground reference for training and testing remote sensing AGB estimation models. A commonly applied method to acquire plot-level AGB is by aggregating tree-level AGB values estimated from allometric equations. This procedure introduces many sources of uncertainty including tree measurements, allometric models, and misregistration between plot or tree location and remote sensing data (Chen et al., 2015; Yang et al., 2015). Although in this dissertation, we applied field inventory data for model training and testing, we do not account for these uncertainties, which may impact the reported model fit. Procedures to quantify uncertainty have been proposed in publications using statistical analysis (Breidenbach et al., 2013; Chave et al., 2004; Holdaway et al., 2014). For people whose statistical background knowledge is not strong enough to repeat the published uncertainty studies, a standardized procedure that is readily applicable would facilitate its usage for forest managements.

The contrast of red and near infrared vegetation reflectance has been widely applied in developing the two-band vegetation indices commonly applied (Baret and Guyot, 1991; Xue and Su, 2017). Despite being widely used, the limited reflectance bands utilized by the most popular indices might miss critical information. Although algorithms like principal component analysis

aim to condense non-correlated information, such techniques require calculation of complex coefficient matrix and may not be convenient to utilize, thus are not as popular as more simple vegetation indices. In Chapter 4, we presented the promising results using two-band vegetation indices developed from red-edge and shortwave infrared (SWIR) bands for AGB estimation. With greater access to the red-edge bands, in particular through the Sentinel-2 satellite, this provides an area of investigation that should receive attention in the future. Further studies should explore the value of new vegetation indices using three or more bands from the red-edge and SWIR spectral regions.

This dissertation showed that remote sensing data from various sources performed differently depending on ground conditions. In Chapter 2, we showed that Landsat and lidar variables perform differently depending on forest type and forest AGB range. Generally, with more data and higher resolutions, higher accuracies are more likely. Previous studies have demonstrated that lidar sampling can be used to support AGB estimation. In Chapter 3, we presented a method for using freely available Landsat data to capture variation in site conditions in order to plan acquisition of lidar samples that can be used to calculate AGB with accuracy levels that approach that from using full lidar coverage. The higher resolution Sentinel-2 data is now widely available, and with the increase in unmanned aerial vehicles, even more data will be accessible in the future. With the evolution of remote sensing platforms, the cost of data acquisition and storage will likely drop significantly in the future, but data processing cost will increase with data size. Therefore, developing tools to appropriately and efficiently apply remote sensing data is going to become even more important and exploring the strengths and weakness of remote sensing data in different applications is necessary. We must invest effort in order to achieve an optimal balance between cost and information needs.

5.3.　References

Baret, F., & Guyot, G. (1991). Potentials and limits of vegetation indices for LAI and APAR assessment. *Remote Sensing of Environment*, 35(2–3), 161–173. https://doi.org/10.1016/0034-4257(91)90009-U

Breidenbach, J., Antón-Fernández, C., Petersson, H., McRoberts, R. E., & Astrup, R. (2013). Quantifying the model-related variability of biomass stock and change estimates in the Norwegian National Forest Inventory. *Forest Science*, 60(1), 25–33. https://doi.org/10.5849/forsci.12-137

Chave, J., Condit, R., Aguilar, S., Hernandez, A., Lao, S., & Perez, R. (2004). Error propagation and scaling for tropical forest biomass estimates. Philosophical Transactions of the Royal Society of London. *Series B: Biological Sciences*, 359(1443), 409–420. https://doi.org/10.1098/rstb.2003.1425

Chen, Q., Laurin, G. V., & Valentini, R. (2015). Uncertainty of remotely sensed aboveground biomass over an African tropical forest: Propagating errors from trees to plots to pixels. *Remote Sensing of Environment*, 160, 134–143. https://doi.org/10.1016/j.rse.2015.01.009

Holdaway, R. J., McNeill, S. J., Mason, N. W., & Carswell, F. E. (2014). Propagating uncertainty in plot-based estimates of forest carbon stock and carbon stock change. *Ecosystems*, 17(4), 627–640. https://doi.org/ 10.1007/s10021-014-9749-5

Xue, J., & Su, B. (2017). Significant remote sensing vegetation indices: a review of developments and applications. *Journal of Sensors*, 2017. https://doi.org/10.1155/2017/1353691

Yang, Y., Yanai, R. D., Fatemi, F. R., Levine, C. R., Lilly, P. J., & Briggs, R. D. (2015). Sources of variability in tissue chemistry in northern hardwood species. *Canadian Journal of Forest Research*, 46(3), 285–296. https://doi.org/10.1139/cjfr-2015-0302

Vita

Name   Siqi Li

Date and Place of Birth   February 2, 1991; Shijiazhuang, China

Education:

Name and Location	Dates	Degree
SUNY-ESF, Syracuse, NY	09/2015–Present	Ph.D.
SUNY-ESF, Syracuse, NY	02/2017–Present	M.P.S.
Northeast Forestry University	09/2013 – 07/2015	M.S.
Northeast Forestry University	09/2009 – 07/2013	B.S.

Employment:

Employer	Dates	Job Title
SUNY-ESF, Syracuse, NY	09/2015–Present	Graduate Assistant
GroundPoint Technologies, Marcellus, NY	05/2018 – 05/2019	GIS Analyst
Syracuse University	05/2017–08/2017	GIS Analyst
Northeast Forestry University, Harbin, China	09/2013 – 07/2015	Graduate Assistant

Publications:

Zhao, Y. H., Li, S. Q., Zhen, Z., Li, F. R., & Wei, Q. B. (2016). Estimation and spatial-temporal pattern of forest aboveground biomass and NPP in Heihe Region, Heilongjiang Province, China. *The Journal of Applied Ecology*, *27*(10), 3070-3080.